Investigating promotion and poisoning using the Harris functional

Humphreys, Stuart

Award date:
2001

Awarding institution:
University of Bath

INVESTIGATING PROMOTION AND POISONING USING THE HARRIS FUNCTIONAL

Submitted by Stuart Humphreys
for the degree of
Doctor of Philosophy
of the University of Bath
2001

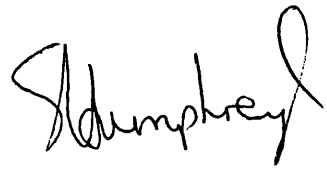

ProQuest LLC
789 East Eisenhower Parkway
P.O. Box 1346
Ann Arbor, MI 48106-1346

Abstract

Total energy pseudopotential methods, based on density functional theory (DFT), have become a powerful technique to describe the interaction of simple adsorbates (including dissociating molecules) with metallic surfaces. For surface catalytic systems, the primary interest is often the *change* or *control* of the rate limiting step (very often a dissociation barrier) for a reaction. This can also be investigated by total energy calculations. However, the main disadvantage of using first principles calculations is the lack of interpretability, i.e. *explaining* either the origin of a dissociation barrier, or the change in a dissociation barrier, is difficult from just the bare total energy calculations.

This thesis presents the theory and computational procedure to increase the interpretability of a DFT total energy calculation, in the context of co-adsorption. The method has been tested on the H_2/Cu(111) system where the aim was to explain the origin of any changes to the H_2 dissociation barrier due to co-adsorption of either K, O or H atoms.

The theory is based on DFT and uses a Harris functional approach rather than the standard Kohn-Sham functional. In essence, we used the Kohn-Sham self-consistent calculations to calculate any changes in the dissociation barrier in the presence of the co-adsorbates, then applied Harris functional DFT to quantitatively interpret the results in order to explain the observed changes. Although the method can be applied to co-adsorption in general, certain physical constraints must be applied to any system under investigation.

The method has the potential to highlight new mechanisms that might underpin the interaction of two species on a surface, and also substantiate existing models that have been put forward.

Acknowledgements

I would first like to thank my supervisor, David Bird, for the guidance and support he has shown over the course of my PhD. His knowledge, enthusiasm and speed of thought has been an inspiration.

Secondly, I would like to thank all my friends, both at Bath and elsewhere, for their support and sarcasm over the past few years.

Finally, all those who had to endure the proof reading of various sections of this thesis also deserve an acknowlegement of thanks.

Contents

Chapter 1

Introduction

1.1 Aims and motivations

One of the fundamental aims in surface science is to understand how and why molecules both break up and recombine on surfaces. The molecule-surface interaction plays host to a wealth of chemical reactions and has been the subject of research spanning decades, both theoretical and experimental. Despite the fundamental scientific research that these studies represent, one must ask the question : can the experimental and theoretical methods of surface physics provide a useful account of real-life surface reaction processes, for instance the synthesis of ammonia and methanol or the reduction of noxious emissions from car exhausts? Although, with enough persistence, it might be possible to develop the theory to explain a given result or observation, the real power comes in formulating general principles which provide qualitative insight and lead to quantitative predictive power.

The three examples given above of real-life commercial surface reaction processes are based on the phenomenon called heterogeneous catalysis. In general, heterogeneous catalysis represents a complex process involving many steps encompassing a variety of surface phenomena, such as physisorption, atomic and molecular chemisorption, surface diffusion and associative desorption of a product to name but a few (Zangwill, 1988). The purpose of the surface is to confine the gaseous reactants to a two-dimensional space in order to increase the probability for collision and reaction, producing a sought-after reaction product which can then desorb from the surface and be collected.

The action and efficiency of catalysts in general can depend quite sensitively on the presence of **poisons** and **promotors** (King, 1993; Kiskinova, 1992; Somorjai, 1994). These are chemical additives that retard or promote specific reactions, respectively, relative to the behaviour of the pristine catalyst. As unwanted competing reactions often accompany any particular desirable reaction one seeks to catalyse, the addition of a poisoning agent that suppresses one or more of these processes is desirable. Alternatively, by promoting, say, the rate-limiting step in a catalytic process, the catalyst's performance will be enhanced. As the rate-limiting step in many catalytic processes is the dissociation of small molecules (Mortensen, 1988), the promotion and poisoning of dissociation reactions has been one of the central research areas of surface science during the past few decades. Although many experimental accounts are available, the theoretical literature is scarce.

Currently, the role of catalytic promoters and poisons is not well understood at a fundamental level. This is due to the lack of interpretability that can be extracted from both the experimental and computational work carried out to investigate these systems. In this work, a computational method has been developed and tested, enabling

a quantitative interpretation of the effect of promoters and poisons. The method can be used as a computational tool to investigate co- adsorption in general. The method establishes quantitatively the contributions from individual mechanisms that underpin the interaction of two species adsorbed on a solid surface. Improving our interpretation of the promotion and poisoning of molecular dissociation could have a significant effect on future studies of catalytic systems, including the selective *modification* of a catalytic surface to enhance a given reaction.

In the next section the dominant theoretical method currently available for handling large, complex adsorbate systems is discussed - plane-wave pseudopotential total energy calculations (Payne, 1992), which have become ubiquitous in many fields of theoretical condensed matter physics. Although these first principles calculations are able to calculate the extent to which two adsorbates interact on a surface, they can't show quantitatively which processes contribute to the overall interaction. In other words, establishing how much of the total interaction is due to, for example, direct electrostatic processes or indirect substrate-mediated processes cannot be achieved from the large-scale calculations alone. This underlines why promotion and poisoning reactions are not well understood and hence the need for a new method in order to increase our interpretation and understanding of these processes.

1.2 Total energy pseudopotential methods

The rapid growth in available computing power, and the development of efficient and fast methods has increased the range of problems addressable using *ab initio* methods. Plane-wave pseudopotential total energy calculations provide a flexible and powerful tool

for handling large, complex systems theoretically. They are not limited to crystalline materials, since they are powerful enough to handle other structures (surfaces, adsorbates, isolated atoms) using the *supercell*, see section 2.7, method.

Total energy pseudopotential methods also allow the atomic forces within a lattice to be calculated efficiently, so have become the standard method for structural optimisation. However, an important deficiency of the pseudopotential approach is that although it describes the interaction between atomic nuclei, the description of electrons near atomic nuclei is incorrect (no core electrons are included and the valence electrons have a different structure in this region), see section 2.6. But if one is interested in the interaction of an adsorbate with a surface or the interaction between two adsorbates, it is essentially the valence, or bonding, electrons that are significant to the interaction, the core electrons are therefore *frozen* to the free atom states. This is an approximation and core electrons of atoms have been shown to relax differently when placed in different surface environments (Zangwill, 1988) and therefore can have a role to play in surface studies. But inclusion of core electrons into total energy calculations is extremely demanding computationally.

In adsorption theory, total energy pseudopotential calculations are predominantly based on *density functional theory* (DFT) (Hohenberg, 1964; Dreizler, 1990; Parr, 1989), see section 2.3. DFT provides an extremely useful view of the problem of many interacting electrons in an external potential, which in the case of a surface with adsorbates is solely given by the position and charges of the nuclei. Calculations can now be routinely performed for adsorbate systems consisting of hundreds of atoms.

The quantities of interest that can be extracted from a DFT total energy pseudopotential calculation are essentially the total energy of the system, the ground state electronic charge density and the density of states (DOS) projected onto individual atoms or orbitals.

Although this has given considerable insight into molecule surface interactions, a correct implementation to quantitatively compare individual systems, for example the difference in the energy barrier to dissociation for a diatomic molecule above either a clean or pre-doped surface (i.e. promotion and poisoning), has not, as far as it is known to date, been done. It is a straightforward matter to calculate the *difference* in activation barrier from one system to the next, however identifying the contribution to these differences from underlying mechanisms is difficult, and crucial if our understanding of catalytic promotion and poisoning reactions is to increase.

The crux of the work in this thesis has been to manipulate the general expressions of DFT in order to derive an interpretable expression which can be used to study the interaction of two species above a solid surface. This has been achieved by applying DFT within a **Harris** (Harris, 1985) functional framework as opposed to the standard Hohenberg-Kohn energy functional (Hohenberg, 1964). Certain physical constraints must also be applied to the comparisons that are being made between different systems. Chapters 3, 4 and 5 discuss the derivation and computational procedure in detail. In chapter 2, the basic principles of DFT are outlined along with the method of calculating the total energy in a pseudopotential framework for an adsorbate system. These first principles calculations provide the basic results for the model systems that have been used in this work to investigate promotion and poisoning. Then, by implementing the methods and results from chapters 3, 4 and 5, it is shown how a quantitative interpretation of the first principles calculations can be achieved.

1.3 Investigating diatomic promotion and poisoning

The fundamental process addressed in this work is the dissociative chemisorption of H_2 above the Cu(111) surface. This system was chosen for its simplicity and because for many years it has been used, by both experimentalists and theorists, as a benchmark for testing models of the gas-surface interaction (Hammer, 1994). The close packed (111) surfaces are typically chosen to be model systems for gas-surface studies. They are generally more stable than the more open surfaces which are often close to a structural instability and sometimes reconstruct when clean (Scheffler, 1999). Also any role *d* electrons might play in promotion and poisoning could be investigated by choosing Cu as opposed to an *sp* metal such as Al.

In order to address promotion or poisoning of H_2 dissociation on Cu(111), the critical quantity is the *energy barrier* the molecule must overcome in order to dissociate before binding to the surface as two individual atoms. If a pre-adsorbed species has the effect of lowering the energy barrier to dissociation then it is acting as a promoter, whereas if it raises the barrier it is acting as a poison. The promoting and poisoning effect on the reactivity of a catalyst has been studied extensively in experimental surface science for selected model catalyst systems (Brown, 1991; Ertl, 1981; Hayden, 1991; Li, 1989; Resch, 1993) . It has been found that, in general, electropositive adsorbates (such as K) tend to act as promoters, while electronegative adsorbates (such as O) are poisons. However, this picture breaks down for hydrogen dissociation, see section 1.8. The pre-adsorbates chosen for this work were O, K and H atoms. O and K were chosen as they represent examples of an electronegative and electropositive atom respectively. The effect of H atoms on the surface would assess whether H_2 could undergo a self-promotion or poisoning reaction on Cu(111). Self promotion and poisoning reactions have the potential to be significant when

ever a diatomic molecule dissociates on a surface to bind individually as two separate atoms. The dissociated atoms may then interact with subsequent incoming molecules during dissociation. To date there has been no previous theoretical work on the promotion and poisoning of H_2 dissociation over Cu(111).

The promoting and poisoning effect of O, K and H on H_2 dissociation on Cu(111) was investigated using the following recipe:

- DFT total energy pseudopotential calculations were carried out to determine the energy barrier to dissociation for H_2 on clean Cu(111) to confirm agreement with previous work.
- Next, DFT total energy pseudopotential calculations were carried out to determine any change in the barrier height to dissociation when the Cu(111) surface is pre-doped with either O, K or H. This was carried out as a function of the distance between the atomic adsorbate and dissociating molecule.
- Using the Harris functional DFT developed in chapters 3, 4 and 5, the next step was to investigate the origin of any calculated change in the dissociation barrier. We show that the terms within the governing expression for the change in the dissociation barrier, using Harris functional DFT, are not only interpretable but also computable.
- From the results of applying Harris functional DFT, the final step was to investigate whether existing models are relevant and also look for the signature of new models and mechanisms that by be underpinning the interaction on the surface.

On a given surface there are many different sites available for an approaching molecule

to dissociate over, all of which could harbour different barriers to dissociation. There are also many different sites where a pre-adsorbate atom could be adsorbed on the surface and at varying concentrations on the surface. Ideally all these different permutations of interaction between molecule and atom should be investigated in order to identify fully the mechanisms underpinning the interaction.

Total energy calculations go some way to overcoming this difficulty in that atoms can be placed at will on the surface and so in principle all these permutations could be investigated, if one had the time. Experimentally, it is much harder to control the conditions on the surface, despite the advances that have been made in ultra high vacuum equipment (UHV). Therefore experimental investigations into promotion and poisoning reactions can lead only to broad conclusions in terms of the underlying mechanisms involved.

1.4 First principles calculations for H_2 dissociation

In recent years tremendous progress has been made through first principles studies of the statics and dynamics of adsorption and dissociation on metal surfaces. In this section an overview is given of the key results, with particular reference to H_2 dissociation on Cu(111). The four important results that have come from first principles calculations based on density functional theory are (Bird, 1996):

- The presence or absence of an activation (or dissociation) barrier. Current *ab initio* calculations have predicted barriers to an accuracy of order 0.25eV as compared with experiment (Hammer, 1997);

- The generation of multi-dimensional potential energy surfaces (PES) upon which the dynamics of molecular dissociation can be calculated;
- The use of gradient-corrected density functionals to describe the effects of exchange and correlation (in particular the generalised gradient approximation, GGA, see section 2.5) are crucial to obtain accurate energetics for molecule-surface systems;
- Interpretation of the PES in terms of the underlying electronic structure. A lot of progress has been made here by projecting the DOS onto different atoms and orbitals within a system, and then looking at differences from one system to the next.

These four points are illustrated by looking at the work on the system relevant to this thesis, the H_2/Cu(111) system. The purpose is to give the reader an insight into the complex nature of one of the simplest molecule-surface reactions, H_2 dissociation. The knowledge will form a good basis for the more general discussion on promotion and poisoning models, which will follow.

When an H_2 molecule (or any molecule for that matter) dissociates on a static metal surface several inter-atomic coordinates usually vary simultaneously. To understand the process, therefore, we need to understand how the energy of the system varies with several coordinates. The total energy as a function of all the coordinates of the system defines a potential energy surface for the reaction (Darling, 1995). Because total energy DFT calculations give the ground state properties of a system, only the ground state PES is calculated, that is electronic excitations are ignored. Although electronic excitations could have an important role in inhibiting or promoting a dissociation reaction, the ground state PES is still a good starting point for a discussion of a reaction.

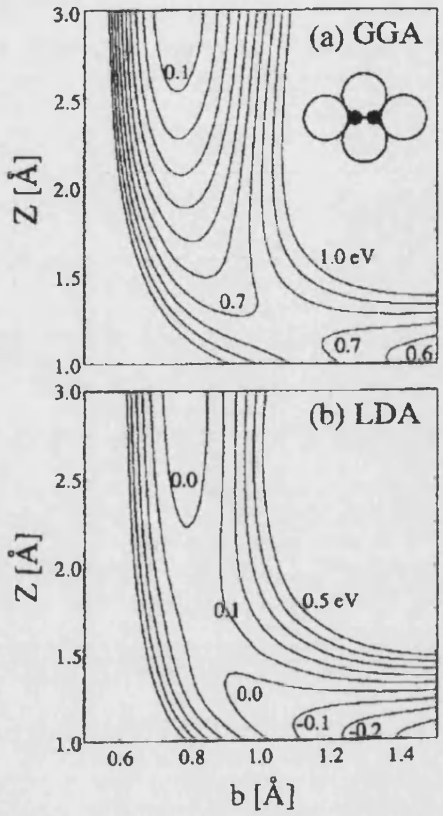

Figure 1.1: A cut through the 6D PES for H_2 dissociation over Cu(111) : (a) calculated with the GGA and (b) LDA. Only (a) conforms with experiment. The insert shows the geometry (Hammer 1994).

Figure 1.1 shows a section of the PES for an H_2 molecule dissociating on a Cu (111) surface (Hammer 1994), calculated within both the *local density approximation* (LDA) and the *generalised gradient approximation* (GGA), see section 2.5. In the calculations, the molecule is kept parallel to the surface and centred over the bridge as shown in the insert. This is the minimum barrier configuration for H_2 above the Cu(111) surface (Hammer, 1994). The PES is displayed as a function of the molecular bond-length, b, and the molecular centre of mass distance, Z, above the Cu surface. In such a PES, the initial and final states are (local) minima - these states are locally stable forms of the system. In the case of H_2 dissociating on Cu(111), the initial state is where the molecule is far away from the surface and the final state is the minimum in the lower right corner in the figure

where Z is small and b is large: the two atoms have separated and are bound close to the surface. The two minima are separated by a barrier, the height of which is the activation energy of the process. The barrier position is also known as a saddle point in the PES and represents a flat region of the PES with respect to the particular co-ordinates being considered.

Numerous experimental investigations (Anger, 1989; Berger, 1989; Rettner, 1992) have established that the dissociation of H_2 over Cu(111) is an activated process. Comparing the LDA and GGA barriers in Figure 1.1 provides a good illustration of the success of utilising GGA expressions within DFT total energy calculations, to describe the effects of exchange and correlation.

The barrier for dissociation depends strongly on the point of impact in the unit cell and the orientation of the incoming molecule (the centre of mass co-ordinates X and Y, along the $[11\bar{2}]$ and $[\bar{1}10]$, the azimuthal angle, ϕ, and the polar angle, θ, of the molecule relative to the surface), see Figure 1.2.

Figure 1.3 shows the variation of the barrier in the (X,Y) plane for two values of ϕ. It is clear that there is a strong variation of the barrier height in these three molecular degrees of freedom. The sensitivity of the H_2-metal interaction energy with respect to molecular rotations strongly suggests that *steering* of the incoming H_2 molecule into energetically favourable orientations is very effective. Usually rotations suppresses sticking (dissociation), though this phenomena is more important for the cartwheel, θ, rotations than the helicopter, ϕ, rotations. For a system with an activation barrier in the exit channel, such as H_2/Cu(111), helicopter rotations seem to favour sticking (Darling, 1995).

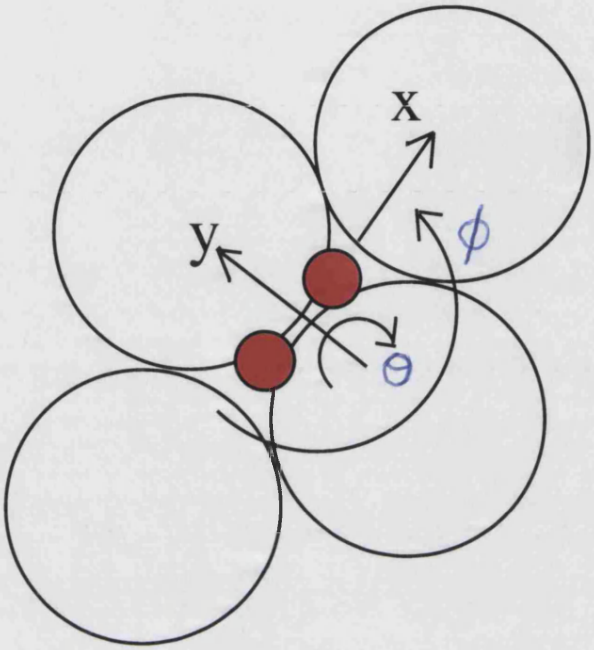

Figure 1.2: Plan view of a (111) surface showing surface atoms (large open circles), a hydrogen molecule (red atoms) dissociating about a bridge site. The four co-ordinates θ, ϕ, X and Y are indicated. These, coupled with the Z and d co-ordinates, are the six which are required to describe the position of an H_2 molecule above a static surface.

Figure 1.1 also suggests another means to promote dissociation. Because the barrier exists at an H_2-substrate distance not far from the eventual dissociated atom chemisorption bond length, it is predominantly the molecular bond length stretching apart that will overcome the rate-limiting barrier. This is called a transition state lying in the 'exit region'. Therefore it pays to excite the molecule *vibrationally* (Rettner, 1992; Berger, 1990) to assist sticking.

Having calculated the first principles potential energy surface, one can proceed to investigate the dynamics of the H_2 - metal interaction. The strong dependence of the PES on all degrees of freedom makes the dynamics quite complicated, and it is only recently that it has been understood in some detail. For a detailed discussion of the dynamics of the H_2 dissociation process, the reader is referred to the review by Darling

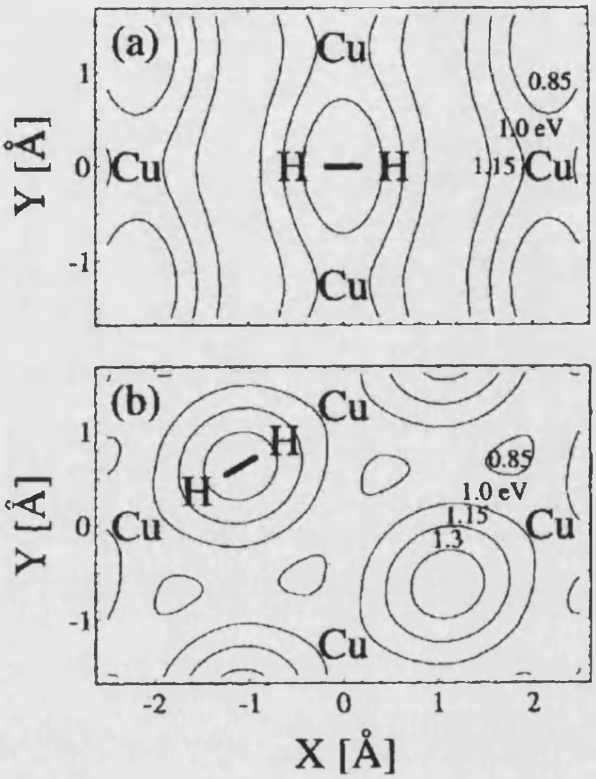

Figure 1.3: The barrier height as a function of X,Y. The 'Cu' marks the atomic positions in the Cu(111) surface. (a)ϕ=0. A molecule is depicted in the optimum reaction geometry, perpendicular to the Cu-Cu bridge. (b) $\phi=\pi/6$. A molecule is shown in the worst case, dissociation parallel with the bridge. (Hammer 1994)

and Holloway (1995).

Typically, the dynamics of the atoms are treated classically by solving Newton's equations of motion, but the underlying PES and the forces acting on the atoms should be calculated in an *ab initio* density functional framework. This is called *ab initio* molecular dynamics.

However, when the moving nuclei are hydrogen atoms, as in our discussion, it has been shown (Kinnersley, 1996) that it is also necessary to treat the nuclei as quantum particles. For such problems a rather involved high dimensional *ab initio* quantum dynamics method has been implemented (Gross, 1995) which is probably the most advanced approach to

date. Although 2D elbow plots of the PES can give insight into the dissociation properties, a full treatment of the dynamics requires knowledge of the 6D PES, which takes into account the lateral corrugation of the surface and rotations of the molecule both parallel and perpendicular to the surface.

1.4.1 Summary

In the previous section, some of the key points from first principles calculations on H_2 dissociation were stated. The underlying PES underpins the dynamics of the dissociation process revealing the potential for many different barriers on a metal surface, depending on the impact parameters and angles. This multi-dimensional character of H_2 sticking on metals causes a wealth of effects and is most likely to appear strongest for dissociation in the exit region of a PES. Here, final state properties of the dissociated product are significant, i.e. the characteristics of the PES reflect greatly the atomic chemisorption properties of atomic hydrogen (Wilke, 1995). Generally, the energetically most favourable orientation of the molecular axis optimises the H-surface bond strength of both H atoms of the H_2 molecule.

To address promotion and poisoning, it is tempting to focus on the changes in the PES when H_2 dissociates over a pre-doped surface. Although this may be informative in that changes in the height and position of barriers can be determined, it will not answer the question of why the barrier height has changed, indeed the question of why there is a barrier in the first place in Figure 1.1 cannot be answered from observation of the PES alone. To answer these questions we must appeal to the underlying electronic structure of the system, for both the surface and the approaching molecule, plus the induced changes that result during adsorption and dissociation.

1.5 Origin of the H_2/Cu(111) dissociation barrier

1.5.1 Introduction

In this section, the properties of the transition state for H_2 dissociation on Cu(111) are discussed in terms of the underlying electronic structure. In addition to the accurate DFT calculations, it has been crucial to develop simple models which enables an understanding of the large-scale calculations and experiments. DFT also provides a theoretical basis for such models as will be discussed in chapter 3. Most intuitive arguments about bonding in chemistry are based on changes in the one-electron spectrum - the formation of bonding and antibonding states (Hoffman, 1988). Within a covalent or tight-binding framework, this model is extremely intuitive. For example, from the filling of the bonding and anti-bonding states it is possible to gauge the stability of the chemical bond, plus simple perturbative methods can be used to calculate the energy change in forming the bond.

Figure 1.4 shows schematically the interaction between an adsorbate, characterised by the valence level E_a, and the localised d band of a transition metal surface to produce a bonding and anti-bonding state. This simple model has been used to describe the interaction of a whole range of atomic and molecular adsorbates with the d band of transition metals (Hammer, 1995). Depending on the energy of the adsorbate level and the 'filling' of the metal d band, the anti-bonding states can also have a degree of occupancy if the Fermi level of the adsorbate system cuts through or is above the level of the anti-bonding states. The overall filling of these states will determine the strength of the surface bond with the d states. Because the d band plays a pivotal role in the reactivity of transition metals, the simple model presented here has become an extremely powerful tool to understand the adsorption chemistry of transition metals.

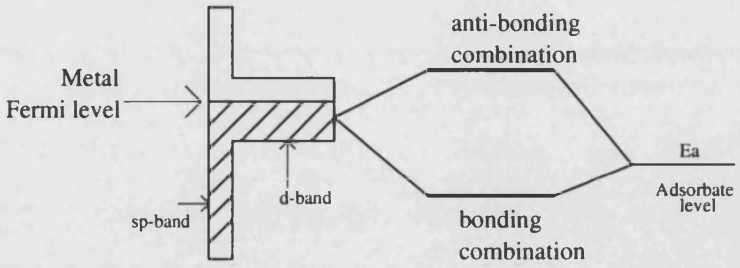

Figure 1.4: Schemtaic view of the interaction of an adsorbate with a transition metal surface. The density of states for the transition metal shows the broad *sp* band and localised *d* band. The filling of the *d* band varies from one metal to the next.

In the context of DFT total energy calculations, although the sum of the one-electron eigenvalues does enter the expression for the total energy through the kinetic energy term, see equation (2.12), there are other equally important terms. Direct calculations show that usually the total energy of a system is very far from given by the one-electron sum alone (Hammer, 1997) and caution must be taken when applying arguments based on one-electron energies. A possible solution has been devised based on the effective medium theory and the reader is referred to various articles (Jacobsen, 1996; Hammer, 1997; Nørskov, 1980; Jacobsen 1988; Häkkinen, 1989) for the background. The details are not important at this stage. Moreover, the analysis of promotion and poisoning presented in chapter 3 provides the full DFT background that supports the results set out in section 1.5.2.

1.5.2 Hammer - Nørskov model

Within the framework of the effective medium theory, it can be shown that the difference in interaction energy of an adsorbate in two surroundings can be written (Hammer, 1995):

$$\delta E_{ads} = \delta \int^{E_f} E n_{ads}(E) dE + \delta E_{es} \tag{1.1}$$

where the first term is the difference in the sum of the induced one-electron energies for the adsorbate in both surroundings and the second is the difference in the electrostatic energy of the adsorbate in the two surroundings. We now want to look at whether equation (1.1) be used to help understand the transition state for H_2 over Cu(111) and the possible substrate- mediated promotion and poisoning of the reaction. First, the key steps in the H_2/Cu(111) interaction are described (Scheffler, 1999):

- When the H_2 molecule approaches the Cu(111) surface the molecular wavefunction begins to overlap with the metal surface charge density, which, for a semi-infinite surface, this will mean a continuum of states.
- For the H_2 molecule, it is the bonding σ_g and antibonding σ_u^* states that interact with the surface electronic states, which for Cu(111) comprise *sp* and *d* electrons.
- The mixing with the *sp* band is shown to broaden such molecular states in line with the so-called Newns-Anderson model (Newns, 1969). Then the interaction of these new resonance states with the narrower *d* band (i.e. it has been argued that adsorption is a two stage process) determines two bonding states, $\sigma_g - d$, $\sigma_u^* - d$ and two antibonding states, $(\sigma_g - d)^*$, $(\sigma_u^* - d)^*$.

Experiments and first principles investigations have shown that for Al(111), the free electron like *sp* surface gives rise to a considerable barrier for dissociation of the order 0.5eV (Hammer 1993). It is assumed that this part of the interaction on transition metals, in general, is approximately the same and of the order 0.5eV (Hammer, 1997). Therefore the overall size of the activation barrier over transition metals (and hence the differences from one metal to the next) is governed by the interaction with the metal *d* states.

Equation (1.1) can now be applied to investigate, at least semi- quantitatively, the interaction of the H_2 molecular resonances with the Cu(111) *d* band, if it is assumed that the presence of the *d* band in Cu(111) constitutes the *change of environment* for the H_2 molecule compared with that of an *sp* metal. If the interaction is sufficiently weak, a simple perturbation expression can be written down for the contribution to the induced one-electron sums of equation (1.1) from the energy gain due to hybridisation of the H_2 molecular resonances with the surface *d* states:

$$\Delta E \approx \frac{V^2}{\epsilon_d - \epsilon_\sigma} \tag{1.2}$$

and similarly for the σ_u^* state.

Within this model the electrostatic term in equation (1.1) is assumed negligible.

In equation (1.2), V (which is calculated within the effective medium framework (Hammer, 1995)) represents the overlap matrix element between the surface *d* band in the vicinity of the H_2 molecule and either the bonding or antibonding molecular resonance, and ϵ_d, ϵ_{σ_g} and $\epsilon_{\sigma_u^*}$ are the energies of the centre of the surface *d* band, the H_2 bonding resonance and the H_2 antibonding resonance respectively.

The analysis can now be made more general by defining as an approximate reactivity measure, ΔE_{ts}, the *total* energy difference due to the coupling to the *d* bands of a transition metal:

$$\Delta E_{ts} = -2\frac{V^2}{\epsilon_{\sigma_u^*} - \epsilon_d} - 2(1-f)\frac{V^2}{\epsilon_d - \epsilon_{\sigma_g}} + \alpha V^2. \tag{1.3}$$

Here, the first term describes the energy gain due to the hybridisation between the σ_u^* and the *d* states (the factor of two is for spin). The second term is the corresponding $\sigma_g - d$ interaction with an extra factor $(1-f)$ because the filling f of the antibonding

state, $(\sigma_g - d)^*$, varies from one metal to the next and is assumed to equal the filling of the d band of the bare metal in question (Hammer, 1997). The last term is the repulsion due to the orthogonalisation of both the molecular resonances to the metal d states. This reactivity measure is clearly approximate, however the basic idea to explicitly include the direct covalent interaction between the molecular resonance states and the metal d band is what makes this measure powerful compared to reactivity theories that rely on the properties of the unperturbed metal states.

For the case of the noble metals, such as Cu, with full d bands, the model is particularly simple in that the second term in equation (1.3) is dropped, due to Cu having full d bands, i.e. with $f = 1$. Calculations have shown that there is excellent correlation between H_2 activation barriers calculated from first principles and the approximate reactivity measure ΔE_{ts} for a range of transition metals and alloys (Hammer, 1997). Based on the above analysis, it is now possible to identify which electronic factors are the most important in determining the barrier height of H_2 dissociation on Cu(111). The conclusions for Cu and other late and noble transition metals are that the $\epsilon_{\sigma_u^*} - d$ term and the αV^2 terms dominate due to the $(1 - f)$ factor associated with the ϵ_{σ_g} interaction.

In conclusion, arguments based on the effective medium theory have produced an approximate expression, equation (1.1), for the difference in interaction energy for an adsorbate, in this case an H_2 molecule, on either a *sp* or transition metal surface. Because the interaction with the *sp* metal is assumed to be the same as the interaction with the *sp* states over a range of transition metal surfaces, it is the subsequent mixing with the d band which governs the overall height of the H_2 dissociation barrier and this can be investigated through simple perturbative arguments, based on bonding and anti-bonding levels, involving the relevant electronic states.

1.6 Indirect mechanisms for promotion and poisoning

For H_2 on Cu(111), the molecule and surface are interacting significantly at the transition state, and consequently there are two kinds of interaction that can take place with a pre-adsorbed atom which could affect the size and position of the barrier, namely a direct or indirect interaction. An indirect, or substrate-mediated interaction, would represent a change in the local surface electronic structure in the vicinity of the approaching H_2 molecule, caused by a pre-adsorbed atom. A direct interaction would take the form of either a direct orbital overlap between molecule and atom or a direct electrostatic interaction between both species (Mortensen, 1998).

1.6.1 Hammer - Nørskov model

Equation (1.1) can also be applied to investigate the difference in adsorption properties for an H_2 molecule dissociating over a clean or pre-doped surface. Because equation (1.3) is a measure of the reactivity of H_2 dissociation, i.e. at the transition state, a mechanism for substrate mediated promotion and poisoning becomes apparent. The interaction between an adsorbed atom and the metal surface will tend to broaden the local density of d states on the surrounding surface atoms, relative to that of the clean surface, due to the direct covalent interaction with the adsorbate states. In turn, this broadening leads to a down-shifting of the d band centre in order to preserve the local d charge (Bird, 1998). According to equation (1.3), a lowering of ϵ_d results in a reduction in the magnitude of the stabilising effect of the $d - \sigma_u^*$ interaction. This would represent a substrate-mediated poisoning effect from the pre-adsorbed atom. It is expected that

this sort of promotion and poisoning mechanism is applicable for interaction where the pre-adsorbed atom and dissociating molecule share surface atoms, see Figure 1.5, where adsorbates 1 and 3 represent this kind of interaction with the dissociating molecule, which is represented by the large red atoms.

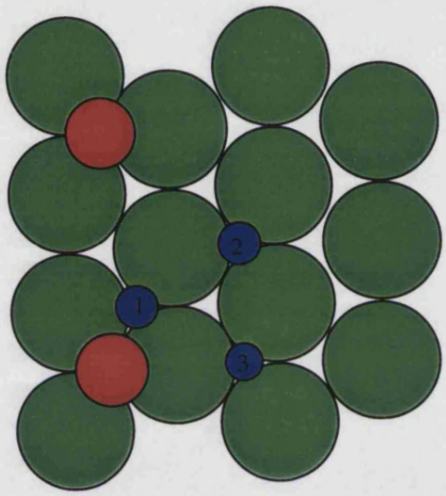

Figure 1.5: Surface showing two different co-adsorbates at varying range from each other.

1.6.2 Models based on work function changes and population and depopulation of surface states

According to the model of H_2 adsorption given earlier, the interaction of the molecular states with the metal *sp* band causes an orthogonalisation energy cost as the Pauli exclusion principles forces the kinetic energy of the electrons to rise steeply, the Pauli repulsion. A rapid fall-off of the surface charge density implies a late onset of this repulsion for an incoming molecule. For molecules such as H_2, a reduced Pauli repulsion at the barrier could result in a lowering of the barrier. Assuming that the electrons leak out further into the vacuum, if the work function is small, while a large work function confines

the electrons close to the surface, Brown *et al* (1991) were able to explain the poisoning effect of low alkali-metal coverage and the promoting effect of oxygen by the associated work function change. The strong poisoning effect of low alkali-metal coverage for H_2 dissociation on Pt(111) (Brown, 1991) and on Ni(111) (Resch, 1993) can be described reasonably well in this model.

Another mechanism that has been put forward to account for promotion and poisoning that has been reported in the experimental literature, involves *surface states* (for a complete review, see Bertel (1995, 1996)). Surface states are localised electronic states that leak furthest out from a surface and are known to exist at the surfaces of many metals, alloys and semiconductors (Davidson, 1992). Many transition metals, with the exception of Pd, exhibit a Schockley surface state in the centre of the surface Brillouin zone (SBZ) with an energy close to the Fermi level. The key point is that effects due to these Schockley surfaces states will tend to be long ranged because a surface state band in the centre of the SBZ will tend to have a long Fermi wavelength (Bird, 1998).

Promotion and poisoning can then be understood in terms of a depletion or filling of the surface state band; an electronegative adsorbate will tend to deplete the band, thus reducing the onset of the Pauli repulsion between the molecular states and the metal *sp* band. This will tend to promote dissociation as the molecule can approach closer to a surface where the attractive branch of the chemisorption potential will be stronger. The opposite is true for electropositive adsorbates (Bertel, 1995). This model strongly supports the non-activated dissociation pathways on Pd(100) which has an unoccupied surface state band and the correlation between the oxygen-induced surface state energy shift and the promotion of H_2 dissociation on Ni(111) (Resch, 1993; Passek, 1993). It has also been shown that K doped Pd(110) has no electronic effect on the sticking coefficient of H_2

(Resch, 1994), indicative of an initially empty surface state band remaining unoccupied.

The work function and surface state models have been applied to explain, quite convincingly, a number of experimental results. Both models tend to support longer range interaction between adsorbates on a surface, which will most likely contribute to the *sp* changes to the eigenvalue sums in equation (1.1). However, without a quantitative model for the role of *sp* electrons which can be directly compared with first principles calculations, the full picture for this part of the interaction is still unclear.

1.7 Direct mechanisms for promoting and poisoning

In this section, electrostatic interactions between adsorbates are discussed along with interactions arising from direct orbital overlap. Electrostatic interactions are important when an adsorbate A, induces a dipole moment μ (on the clean surface) that interacts with another adsorbate X that induces an electric field ϵ. To lowest order in a multi-pole expansion, the electrostatic interaction energy will be

$$\Delta E = -\epsilon\mu. \tag{1.4}$$

The value of ϵ is taken at the position of the adsorbate A. This model has been shown to correlate well with the interaction energy of N_2, in its transition state on the Ru(0001) surface, at varying distances from either Na or Cs adsorbates, as compared with first principles calculations (Mortensen, 1998). Both Na and Cs are found to lower the activation barrier for N_2 dissociation, due to (in terms of this model) the induced negative electric field from the alkali metal (and corresponding negative work function change) and

the negative dipole moment of the N_2 in its transition state. In this model, the size of the interaction depends on the adsorbate-adsorbate distance and is stronger for the alkali metals than electronegative elements, such as S and O, which in general produce smaller electric fields and smaller changes in the work function.

Direct orbital overlap of a pre-adsorbate species and dissociating molecule is another direct interaction that could affect the transition state. It would be expected that this sort of interaction would be repulsive. This argument was put forward to explain the Sulphur-induced poisoning of the H_2/Pd(100) system (Wilke, 1995). In figure 1.5, atom 1 would represent an adsorbate atom likely to have a direct orbital overlap with the dissociating molecule (large red atoms).

The models outlined so far, whether indirect or direct, have been used to explain previous work on diatomic promotion and poisoning, both experimental and theoretical. Only an overview has been given, but this is sufficient to convey the general ideas and arguments that are being used today. The level of success that these models have had is considerable, but validating models is nevertheless extremely difficult without quantitative evidence to support them. This has certainly been the case to date. However, the analysis presented in chapters 3, 4 and 5 does allow models such as the ones described above to be tested quantitatively.

In the final section below, a brief account is given on previous experimental work on the promotion and poisoning of H_2 dissociation.

1.8 Experimental work on the promotion and poisoning of H_2 dissociation

First, it is important to stress the limitations of what can be inferred from experiment. It is certainly possible to determine changes in dissociation barrier directly from graphs showing the uptake of hydrogen as a function of the incident translational energy on an adsorbate-covered surface. In general, however, the multidimensional character of the underlying PES dictates different barriers across the surface and the resulting effect on individual barriers from pre-adsorbed atoms is unclear. For example, to conclude that the position of the lowest barrier on the clean surface coincides with the lowest barrier position on the doped surface is clearly an assumption. The coverage of the co-adsorbates in the experiments is generally in the range of $\theta = 0$ to $\theta = 0.3$, i.e. quite low ($\theta = 1$ corresponds to one adsorbate atom to one surface atom), and in light of the long range interaction reported on, for example, the Pt(111) surface (Brown, 1991), a range of surface sites can be influenced by the presence of the adatom. Limitations such as these make understanding the mechanisms behind adsorbate-adsorbate interactions extremely difficult. Ideally, one would like to gauge not only the change in dissociation barrier but also any change in the *position* of the barrier. For these studies we have to resort to first principles investigations where adsorbates on the surface can be placed at will, new activation barriers established for different surface sites and ultimately new PES's generated. In the next section, therefore, only an overview is given of the results for H_2 dissociation. This thesis is primarily interested in computational methods and underlying mechanisms and to this end the experimental literature does not provide many answers.

Many experiments have focused on the interaction of alkali metals by studying the effect

of pre-adsorbed K on H_2 dissociative adsorption. On the Pt(111) (Brown, 1991) surface the effect of K was to increase both the desorption barrier and the activation barrier to dissociative adsorption. The effect of raising the barrier appeared to be long range with each K atom effectively blocking dissociation over an area of between 70 and 430Å^2. The effect of K on Fe(111) and Fe(100) (Ertel, 1981) was also to reduce the sticking probability of H_2 and induce states with apparent higher barriers to desorption as confirmed by TPD curves. In the case of W(100) (Li, 1989), which is characterised by non-activated adsorption on the clean surface, the effect of either Cs or K was to make dissociation activated, and an exponential decrease in the initial sticking probability with alkali coverage was observed. On Pd(111) (Bertel, 1995) and Ni(111) (Resch, 1993), the effect of pre-adsorbed K was to poison H_2 dissociative adsorption. When the Cu(110) surface was studied the adsorption of H_2 on the Cu(110)-K(1$\times$ 2) surface was characterised by an increased desorption energy, in line with the above findings, but a decrease in the activation energy to dissociative adsorption as verified by measurements of the sticking coefficient (Hayden, 1991). Oxygen was found to act as a promoter on Ni(111) up to a coverage of one eighth of a monolayer, and as a poison at higher coverage (Resch, 1993)

It appears from the above results that, with the exception of the Cu(110) surface, electropositive elements tend to inhibit hydrogen adsorption and that perhaps electronegative elements promote adsorption. Explanations of these effects have only recently started to emerge in line with advances in first principles calculations.

1.9 Conclusion

These are the main conclusions to be taken from this introduction into diatomic promotion and poisoning:

- Promotion and poisoning reactions have been studied experimentally for many years; however, what can be interpreted is extremely limited.
- First principles calculations go some way to understanding these processes in that atoms and molecules can be placed at will on a surface and the resultant interaction energies calculated to a reasonable accuracy.
- First principles calculations, however, are limited in terms of the quantitative interpretation. This has been the motivation to develop the theory and computation to overcome this.
- A simple model based on one-electron sums, equation (1.1), has been used to investigate the transition state for H_2 on Cu(111), as well as other systems. This model can be extended to investigate promotion and poisoning, albeit only as a broad interpretative tool. The work presented now shows how DFT, in the context of a total energy pseudopotential calculation, can be used to derive an equation of the same form as equation (1.1), where each term can be represented explicitly and calculated, thus providing a much more powerful tool for investigating the origin of promotion and poisoning.

To summarise what is to follow:

Chapter 2 discusses the DFT total energy calculations used in this work.

Chapters 3, 4 and 5 discuss in detail the Harris functional derivation and implementation.

Chapter 6 presents the results of the self consistent DFT calculations of the promotion and poisoning of the H_2/Cu(111) system.

Chapter 7 uses the Harris functional analysis to interpret the self consistent results of chapter 6.

Chapter 2

First principles calculations

2.1 Introduction

In this chapter the first principles total energy calculations are discussed. These calculations provide the basic results for the Harris functional analysis developed in chapters 3, 4 and 5. The chapter is laid out in the following way:

- First an overview of density functional theory, the basic framework of theory for all the calculations and theory in this thesis, is presented. Application to metallic systems relevant for the work on Cu is also highlighted.
- Then an overview of two of the approximations used in DFT total energy calculations is given. In particular, coping with exchange and correlation for a many electron system and the pseudopotential approximation is discussed.
- Next, applying the basic theory in order to carry out a total energy calculation for

an adsorbate system is discussed. The focus here is on choice of basis set, periodic boundary conditions, supercells and FFT grids. The advantages and limitations of this method of implementation are also addressed.

- Finally, utilising a mixed basis set within a DFT total energy calculation is discussed. The significance of this will become clear in chapters 5 and 7.

In principle, all knowledge about a system of atoms can be obtained from the quantum mechanical wave function. This is obtained (non-relativistically) by solving the Schrödinger equation of the complete many electron system. However in practice, solving such an N-body problem proves to be impossible. For this reason it is necessary to use density functional theory developed by Kohn and Sham (Kohn, 1965) based on the theory of Hohenberg and Kohn (Hohenberg, 1964), which, in principle, is an exact ground state theory.

Atomic units are employed throughout this thesis, i.e.:

$$\hbar = m_e = e = 1, \tag{2.1}$$

where m_e is the mass of the electron, e is the charge on the electron and $\hbar$ is Plank's constant divided by 2π.

2.2 The Born-Oppenheimer approximation

The forces on both electrons and nuclei due to their electric charge are of the same order of magnitude, and so the changes which occur in their momenta as a result of these forces

must also be the same. One might, therefore, assume that the actual momenta of the electrons and nuclei are of similar magnitude. In this case, since the nuclei are so much more massive than the electrons, they must accordingly have much smaller velocities. Thus it is plausible that, on the typical time-scale of the nuclear motion, the electrons will very rapidly relax to the instantaneous ground state configuration. When solving the time-independent Schrödinger equation it can therefore be assumed that the nuclei are stationary, thus solving for the electronic ground state first and then calculating the energy of the system in that configuration, and subsequently solving for the nuclear motion. This separation of electronic and nuclear motion is known as the Born-Oppenheimer approximation (Born, 1927).

In all the total energy calculations in this thesis the ground state electronic charge density is solved for a given static configuration of ion cores.

2.3 Density functional theory

Hohenberg and Kohn proved that the total energy of a system including the energy of the many body effects of electrons (exchange and correlation) in the presence of a static external potential (for example, atomic nuclei) is a unique functional of the charge density (Hohenberg, 1964). The minimum value of the total energy functional is the ground state energy of the system. The electronic charge density which yields this minimum is then the exact ground state charge density.

It was then known by Kohn and Sham (Kohn, 1965) that is was possible to replace the many electron problem by an exactly equivalent set of self consistent one electron

equations. The total energy functional can be written as a sum of several terms:

$$\begin{aligned} E[n(\mathbf{r})] &= T[n(\mathbf{r})] + \int n(\mathbf{r}) V_{ion}(\mathbf{r}) d\mathbf{r} + \frac{1}{2} \int \int \frac{n(\mathbf{r}) n(\mathbf{r}')}{|\mathbf{r} - \mathbf{r}'|} d\mathbf{r} d\mathbf{r}' \\ &+ E_{xc}[n(\mathbf{r})] + E_{ion} \end{aligned} \tag{2.2}$$

for a fixed set of atomic nuclei at $\mathbf{R}_i$. The first term is the kinetic energy of the system of electrons with density $n(\mathbf{r})$. The second and third terms are the classical Coulomb interaction between electrons and ions and between electrons and other electrons respectively, both of which are simple functions of the electronic charge density $n(\mathbf{r})$. $E_{xc}[n(\mathbf{r})]$ is the energy of exchange and correlation for an interacting system. There is no simple expression for the exchange and correlation - this will be considered in section 2.5. E_{ion} is the total electrostatic interaction energy between the static ion cores.

According to the Hohenberg and Kohn theorem, the total energy functional given by equation (2.2) is stationary with respect to variations in the ground state charge density, that is, it is subject to the condition:

$$\int \delta n(\mathbf{r}) \{ \frac{\delta T[n(\mathbf{r})]}{\delta n(\mathbf{r})} + V_{ion}(\mathbf{r}) + \int \frac{n(\mathbf{r}')}{|\mathbf{r} - \mathbf{r}'|} d\mathbf{r}' + \mu_{xc}(\mathbf{r}) \} = 0 \tag{2.3}$$

where $\mu_{xc}(\mathbf{r})$ is the functional derivative of the exchange-correlation energy with respect to the electronic charge density. There is also the requirement that a variation in the charge density leaves the particle number:

$$N = \int n(\mathbf{r}) d\mathbf{r} \tag{2.4}$$

unchanged. This can be ensured by the condition:

$$\int \delta n(\mathbf{r}) d\mathbf{r} = 0. \tag{2.5}$$

Applying the condition of constant particle number to equation (2.3) gives the result:

$$\frac{\delta E[n(\mathbf{r})]}{\delta n(\mathbf{r})} = \frac{\delta T[n(\mathbf{r})]}{\delta n(\mathbf{r})} + V_{ion}(\mathbf{r}) + \int \frac{n(\mathbf{r}')}{|\mathbf{r} - \mathbf{r}'|} d\mathbf{r} + \mu_{xc}(\mathbf{r}) = \nu \tag{2.6}$$

where, ν, is the Langrange multiplier associated with the requirement of constant particle number. Comparing this to the corresponding equation for a system with an effective potential, $V_{eff}(\mathbf{r})$, but without electron-electron interactions results in:

$$\frac{\delta E[n(\mathbf{r})]}{\delta n(\mathbf{r})} = \frac{\delta T[n(\mathbf{r})]}{\delta n(\mathbf{r})} + V_{eff}(\mathbf{r}) = \nu \tag{2.7}$$

It can be seen that the mathematical representations are equivalent provided that:

$$V_{eff}(\mathbf{r}) = V_{ion}(\mathbf{r}) + \int \frac{n(\mathbf{r}')}{|\mathbf{r} - \mathbf{r}'|} d\mathbf{r} + \mu_{xc}(\mathbf{r}). \tag{2.8}$$

The effect of this is to allow an indirect variation in $n(\mathbf{r})$ through variation in the Kohn-Sham single particle orbitals, ψ_i, where the kinetic energy can be expressed in terms of the single particle states as:

$$T = \sum_{i=1}^{N} \frac{1}{2} \int \psi_i^*(-\nabla^2)\psi_i d\mathbf{r}. \tag{2.9}$$

It then follows that the solution can be found by solving the Schrödinger equation for

non-interacting particles moving under the influence of an effective potential $V_{eff}(\mathbf{r})$:

$$\{-\frac{1}{2}\nabla^2 + V_{eff}(\mathbf{r})\}\psi_i(\mathbf{r}) = \epsilon_i\psi_i(\mathbf{r}) \tag{2.10}$$

which gives the charge density:

$$n(\mathbf{r}) = \sum_{i=1}^{N} \psi_i^*(\mathbf{r})\psi_i(\mathbf{r}). \tag{2.11}$$

and the kinetic energy as:

$$T[n(\mathbf{r})] = \sum_{i=1}^{N} < \psi_i| - \frac{1}{2}\nabla^2|\psi_i > = \sum_{i=1}^{N} \epsilon_i[V_{eff}[n(\mathbf{r})]] - \int V_{eff}[n(\mathbf{r})]n(\mathbf{r})d\mathbf{r}. \tag{2.12}$$

The minimum of the Kohn-Sham energy functional, equation (2.2), leads to the ground state charge density of the electronic system with ions at the fixed positions $\mathbf{R}_i$, and is equivalent to the self consistent solutions to equations (2.8), (2.10) and (2.11). It is only this minimum which has any physical meaning, therefore the path by which this minimum is found is unimportant.

2.4 Metallic systems

The main difference between metals and insulators from the technical point of view is that the number of occupied bands in a metal is not the same at different $\mathbf{k}$ points in the first Brillouin zone. For an insulator this is not the case as a large band gap extends across the whole of the first Brillouin zone. The number of occupied bands for insulators is calculated as one half the total number of valence electrons due to two electrons of opposite spin allowed in each band, but this approach is not suitable for metals. Partial

occupancies are introduced to eliminate discontinuous changes in total energy that are created when an energy band crosses a Fermi level during the energy minimisation. It is usual therefore to make a finite-temperature formalism for the electronic system, smearing the Fermi surface. An artificial electronic temperature is then introduced by adding this gaussian-like smearing to each energy level.

In effect therefore it is the *free* energy of the system that is being minimised to find the equilibrium ground state (Gillan, 1989; White, 1995). The free energy, F, contains an extra entropy term in addition to the usual energy functional, E, and becomes:

$$F = E - T\sum_i A(f_i) \tag{2.13}$$

where $A(f_i)$ is the entropy function, f_i the occupancy of the ith Kohn-Sham eigenstate, T the electronic temperature and E is now the finite-temperature generalisation of equation (2.2):

$$\begin{aligned} E &= \sum_{i=1}^{N} \frac{1}{2} f_i \int \psi_i^*(-\nabla^2)\psi_i d\mathbf{r} + \int V_{ion}(\mathbf{r})n(\mathbf{r})d\mathbf{r} \\ &+ \frac{1}{2}\int\int \frac{n(\mathbf{r})n(\mathbf{r}')}{|\mathbf{r}-\mathbf{r}'|} d\mathbf{r}d\mathbf{r}' + E_{xc}[n(\mathbf{r})] + E_{ion}. \end{aligned} \tag{2.14}$$

The charge density is now defined as:

$$n(\mathbf{r}) = 2\sum_i f_i |\psi_i(\mathbf{r})|^2. \tag{2.15}$$

The choice of entropy function need not be the usual configurational entropy (leading to the Fermi-Dirac distribution). It is most conveniently determined by choosing an electron distribution (or occupation) function $f(x)$ (where $x = (\epsilon - E_F)/kT$, ϵ is the energy, E_F

the Fermi level and k the Boltzmann constant) from which the function $A(f_i)$ is (White, 1995):

$$A(f_i) = \int_0^{f_i} x(f)df = \int_{-\infty}^{x(f_i)} \frac{df}{dx}dx. \tag{2.16}$$

For $f(x)$ we use a spline of Gaussians:

$$f(x) = \frac{1}{2}e^{1/2}e^{-(x+1/2)^2} \tag{2.17}$$

for $x < 0$ and

$$f(-x) = 1 - f(x). \tag{2.18}$$

This has the advantage over the Fermi-Dirac distribution of occupancies falling off more quickly with energy, so fewer bands need to be included in the calculation. Once the equilibrium free energy has been obtained, it has been shown (Gillan, 1988) that the zero-temperature energy may be estimated (within an error of $O(T^3)$) as the average of the finite-temperature energy E and free energy F. The total energy for metals is corrected for the fact that it now includes an artificial electronic entropy function. This correction is possible since there exists an analytical form for the dependence of the total energy on the smearing width, T, i.e. the electronic temperature.

In first principles total energy calculations for metals the number of bands has to be slightly higher than would be required for an insulator. The norm is to add between 6 to 10 bands, but fewer or more may be required depending on the size of the system. This is discussed further in chapter 6 where the details of the first principles calculations for this work are discussed.

2.5 Exchange and correlation

The most difficult problem in any electronic structure calculation is the need to take account of the effects of the electron-electron interaction (Payne, 1992). Electrons repel each other due to the Coulomb interaction between their charges. The Coulomb energy of a system can be reduced by keeping the electrons spatially separated (i.e. the correlation energy). The wavefunction of a many-electron system must also be anti-symmetric under exchange of any two electrons because the electrons are fermions. This produces a spatial separation between electrons that have the same spin and thus reduces further the Coulomb energy of the system - the exchange energy.

The exchange-correlation energy functional, $E_{xc}[n(\mathbf{r})]$, is not known, and some approximation must be made to perform actual calculations. The simplest method of describing the exchange-correlation energy of an electronic system is to use the local-density approximation (LDA) (Ceperley, 1980; Perdew, 1981). In the LDA the exchange-correlation energy of an electronic system is constructed by assuming that the exchange-correlation energy per electron at a point $\mathbf{r}$ in the electron gas, $\epsilon_{xc}(\mathbf{r})$, is equal to the exchange-correlation energy per electron in a homogeneous electron gas that has the same density as the electron gas at point $\mathbf{r}$. Thus:

$$E_{xc}[n(\mathbf{r})] = \int \epsilon_{xc}(\mathbf{r}) n(\mathbf{r}) d^3\mathbf{r} \tag{2.19}$$

$$\frac{\delta E_{xc}[n(\mathbf{r})]}{\delta n(\mathbf{r})} = \frac{\delta [n(\mathbf{r})\epsilon_{xc}(\mathbf{r})]}{\delta n(\mathbf{r})} \tag{2.20}$$

with

$$\epsilon_{xc}(\mathbf{r}) = \epsilon_{xc}^{hom}[n(\mathbf{r})]. \tag{2.21}$$

The exchange-correlation energy for the homogeneous electron gas can be found accurately using Quantum Monte Carlo methods. Using these results accurate parameterisations can be constructed, and many parameterisations are available in the literature (Perdew, 1981; Vosko, 1980; Ceperley, 1980). The LDA assumes that the exchange-correlation energy functional is purely local and ignores, in principle, corrections to the exchange-correlation energy at a point **r** due to nearby inhomogeneities in the electron density. Despite the inexact nature of the approximation the LDA has been extremely successful in predicting adsorption geometries, vibrational properties and surface diffusion barriers in simple adsorption systems (Hammer, 1997). However, comparisons of calculations for H_2 dissociation on Cu(111) and Al(110) (Hammer, 1994) with molecular beam experiments indicate that the LDA barriers are too low (see Figure 1.1) and puts into question the validity of the LDA for activation barrier studies.

An approximation that goes beyond the LDA using a nonlocal exchange-correlation functional is the generalised gradient approximation (GGA) (Perdew, 1992; Becke 1988). The GGA takes into account nearby inhomogeneities in the electron density by considering the gradient expansion of the electron density. The generalised gradient correction has been shown in a number of studies to consistently improve binding energies of atoms and molecules (Brivio, 1999). In fact, it has become clear over recent years that gradient-corrected density functionals (in particular the generalised gradient approximation) are crucial to obtain accurate energies for molecule-surface systems. However, it remains an open question as to exactly how accurate the calculated potential energy surfaces are, even when gradient corrections are employed, and it is very difficult to make a direct and detailed comparison between theory and experiment.

2.6 The pseudopotential approximation

In this section, the important features of the pseudopotential approach to total energy calculations are given. The external potential in the case of a surface with adsorbates is solely given by the position and charges of the nuclei.

Solving equation (2.10) for the Kohn-Sham eigenstates and eigenvalues at each **k** point in the 1st Brillouin zone results in the band structure of the electrons in the periodic lattice of atomic nuclei. For an all-electron calculation, with $V_{ext}(\mathbf{r})$ the sum of the potentials of the nuclei, this requires an exorbitantly large number of basis states (for example plane waves in the case of the total energy calculations in this work). This is a consequence of the rapid oscillations in the wave functions near the nucleus, caused by the depth of the potential in this region responsible for binding the core states. This makes the plane wave basis set completely unsuitable for electronic structure calculations involving nuclear potentials.

A solution to this problem is provided by the *pseudopotential* approximation (Cohen, 1970; Bachelet, 1982) which allows convergence of the total energy to be achieved with a considerably smaller number of plane waves. Physical properties of the lattice are dominated by the high energy valence electrons, which propagate freely throughout the lattice, whereas the core electrons show very little interaction between atoms. For the study of adsorbate systems, one is generally interested in bonding and chemical reactivity where the valence electrons are of primary interest.

The pseudopotential approximation replaces the all-electron system in the potential of a lattice of nuclei with a related system of solely valence electrons in a potential consisting of a lattice of pseudopotentials centred at each atomic site. The pseudopotential should

satisfy the conditions that:

- The eigenvalues in the pseudopotential system are the same as the eigenvalues of the valence electrons in the all-electron system.
- The eigenfunctions in the pseudopotential system are the same as the eigenfunctions of the all-electron system in the region between atoms (where core states are not significant) and smoothly varying (node-less) near atomic sites.

Another way to view this is that the pseudopotential reproduces the valence electron scattering properties of the nucleus+core electrons outside a certain radius, r_c. Provided a pseudopotential can be found that satisfies these criteria, far fewer plane waves will be required to solve the secular equation for the lattice, see equation (2.10), since node-less pseudo-wave functions are smooth near the atomic sites, and the core states are not present.

An important aspect of the pseudopotential is the *transferability* property, which means that knowledge of states in the core regions of the lattice is not required from one system to the next. If the radial Schrödinger equation for a given potential is solved at an energy ϵ_l to give a solution $\phi_l(r)$, then this solution satisfies the identity:

$$-2\pi[(r\phi_l)^2\frac{d}{d\epsilon_l}\frac{d}{dr}\ln\phi_l] = 4\pi\int_0^R \phi_l^2 r^2 dr, \tag{2.22}$$

or that the energy dependence of the radial logarithmic derivative of $\phi_l(r)$ at radius R depends to first order on the charge within R associated with $\phi(r)$. If the pseudopotential is constructed such that the charge enclosed within r_c for both the pseudo-wave functions and all-electron wave functions is the same, then equation (2.22) states that the variation

of the scattering properties (the radial logarithmic derivative is directly related to the scattering phase shift (Schiff, 1955)) of the two potentials are equal to first order in energy. Provided this agreement to first order is sufficient then a potential that produces the valence states of a free atom will accurately reproduce the states for an atom involved in bonding. This requirement that the charge associated with ϕ_l within r_c is conserved is referred to as *norm conservation.* A brief description of the prescription to find a norm conserving pseudopotential is given below.

Firstly, a self consistent all-electron atomic calculation for the atom of interest is performed within the framework of the LDA or GGA, resulting in a self consistent potential for the free atom. The eigenstates of this potential are then divided into core and valence states, and the valence states alone are used to construct the pseudopotential. Close to the core (within the radius r_c) the valence eigenfunctions are replaced with a smooth, nodeless function that conserves the charge associated with each eigenfunction within r_c (The details of this smooth function for the pseudopotentials used in our calculations can be found in the paper by Trouiller and Martins (Trouiller, 1991), whose generation scheme for norm conserving pseudopotentials has become ubiquitous). The Schrödinger equation is then inverted for each of these pseudo atomic valence states at the appropriate eigenenergies (this potential is different for each state within r_c). This l dependent potential (where l is the angular momentum quantum number) is then 'unscreened' to remove the Coulomb and exchange-correlation interactions associated with the pseudo states. This yields an l dependent 'ionic' potential, $V_{l,ion}(r)$, which, when used in place of the nuclear potential for an atomic calculation, yields the same valence eigenvalues and valence eigenstates identical to the all-electron eigenstates outside the core region, but with a different, node-less structure inside the core radius. Because the solutions are norm conserving the potential is transferable - the scattering properties of the potential

are reproduced to first order at energies differing from the eigenenergies of the free atom.

All components of $V_{l,ion}(r)$ at large r (i.e. outside the radius r_c) reduce to the Coulombic potential, Z/r, becoming independent of l. It is thus expedient to express the pseudopotential as a *local* potential (i.e. one that only depends on the distance from the nucleus) plus a few l-dependent, short ranged 'corrections'. A pseudopotential that uses a different scattering function in each angular momentum channel is a nonlocal pseudopotential.

2.6.1 Kleinman-Bylander pseudopotentials

An efficient way of incorporating pseudopotentials into plane wave total energy calculations is to use the scheme of Kleinman and Bylander (Kleinman, 1982). By expressing the pseudopotential in a particular form they were able to evaluate the contribution to the total energy from the electronic interaction with the pseudopotentials very efficiently. The method has become standard practice throughout the literature and was used throughout our calculations. The Kleinman-Bylander pseudopotential has the form:

$$V_{KB} = V_{loc} + \sum_{lm} \frac{|\delta V_l \phi_{lm} >< \phi_{lm} \delta V_l|}{< \phi_{lm}|\delta V_l|\phi_{lm} >} \tag{2.23}$$

where $|\phi_{lm} >$ are the pseudo-atomic eigenstates (calculated during the generation of the corresponding pseudopotential), V_{loc} is an arbitrary local potential and δV_l is defined by:

$$\delta V_l = V_{l,NL} - V_{loc} \tag{2.24}$$

where $V_{l,NL}$ is the l angular momentum component of a non-local pseudopotential. The choice of local potential is arbitrary, and in general the sum over l is truncated at a small value (e.g. $l = 2$).

The pseudopotentials for Cu, K and O, used in the first principles calculations in this work, were all constructed using the Trouiller-Martin formalism (Trouiller, 1991). The pseudopotentials for the H atoms were the bare Coulombic potentials $(1/r)$.

In the next section the application of the theory developed above to performing actual total energy calculations for surface systems is discussed.

2.7 CASTEP/CETEP

The DFT total energy pseudopotential calculations for this work were carried out using the Cambridge Edinburgh Total Energy Package (CETEP), which is the parallel version of the CASTEP package and capable of handling larger systems than its serial counterpart. CASTEP has become ubiquitous for performing electronic relaxation to the ground state for metals, insulators and semiconductors and is used by many groups throughout the UK. It can also calculate forces acting on atoms and the stress on the unit cell of a system. The atomic forces can be used to find the equilibrium structure or to perform molecular dynamics simulations.

CASTEP is based on a *supercell* method, whereby all studies must be performed on a periodic system, even when the periodicity is artificial. For a surface system, the semi-infinite substrate is indeed periodic in the plane of the surface and is therefore represented by a periodic array of extended, two-dimensional slabs. However, there is

no natural periodicity in the direction perpendicular to its two surfaces. 3D periodicity is recovered by repeating the slabs in this direction, adding a vacuum region in between them. In this way a 3D periodic unit cell is defined, the supercell, containing the unit cell of a slab and a vacuum region, which is repeated over all space. Study of adsorbates is also possible by placing them within the supercell, so becoming a periodic array of adsorbates. The side view of a supercell used for a surface calculation is shown in Figure 2.1. The advantage of the supercell approach is that it allows standard momentum-space techniques in calculating the total energy. Bloch's theorem allows each wave function to be written as a sum of plane waves, which, as stated in the discussion on the pseudopotential approximation, is an expedient basis set for pseudopotential calculations (Payne, 1992).

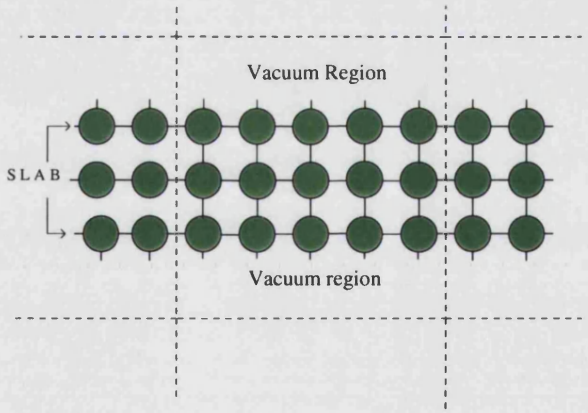

Figure 2.1: Schematic side view of a supercell containing a three layer slab and a vacuum region. The supercell is repeated throughout all space.

In effect, therefore, one calculates the total energy per unit cell of a crystal containing an array of adsorbates. The ionic positions are periodically repeated, so that if there is an ion at position $\mathbf{R}$ then there are periodic images at $\mathbf{R} + \mathbf{t}$ for all translation vectors $\mathbf{t}$ of the superlattice. The electron-ion potential $V_{ion}(\mathbf{r})$ has the symmetry of the superlattice

$$V_{ion}(\mathbf{r} + \mathbf{t}) = V_{ion}(\mathbf{r}). \tag{2.25}$$

The density $n(\mathbf{r})$ and hence the effective potential $V_{eff}(\mathbf{r})$, see equation (2.8), have the same symmetry. Then by Bloch's theorem the wavefunctions Ψ_i must satisfy:

$$\Psi_i(\mathbf{r}+\mathbf{t}) = e^{i\mathbf{k}.\mathbf{t}}\Psi_i(\mathbf{r}) \tag{2.26}$$

where $\mathbf{k}$ is a wavevector in the first Brillouin zone of the superlattice. The wavefunctions can thus be classified according to the wavevector $\mathbf{k}$ and $\psi_{\mathbf{k}i}(\mathbf{r})$ is the wavefunction for the ith band at wavevector $\mathbf{k}$. When a plane wave basis set is used to expand the wavefunctions, they become:

$$\Psi_{\mathbf{k}i}(\mathbf{r}) = \frac{1}{\Omega^{1/2}}\sum_{\mathbf{G}} C_{\mathbf{k}i\mathbf{G}} e^{i(\mathbf{G}+\mathbf{k}).\mathbf{r}} \tag{2.27}$$

where Ω is the volume of the supercell and $\mathbf{G}$ are the reciprocal lattice vectors of the superlattice. By the use of Bloch's theorem, the problem of the infinite number of electrons has now been mapped onto the problem of expressing the wavefunction in terms of an infinite number of reciprocal space vectors within the first Brillouin zone of the periodic cell, $\mathbf{k}$. This problem is dealt with by first sampling the Brillouin zone at special sets of $\mathbf{k}$ points (Monkhorst, 1976). The density $n(\mathbf{r})$ in principle involves an integral of the $|\Psi_{\mathbf{k}i}(\mathbf{r})|^2$ over the Brillouin zone, but in practice, due to the sampling of the Brillouin zone, this is replaced by a sum:

$$n(\mathbf{r}) = 2\sum_{\mathbf{k}} w_{\mathbf{k}} \sum_{i} f_{\mathbf{k}i}|\Psi_{\mathbf{k}i}(\mathbf{r})|^2 \tag{2.28}$$

where $\mathbf{k}$ goes over a chosen set of points in the first Brillouin zone, the $w_{\mathbf{k}}$ are a suitable set of weights that are inferred from the symmetry of the system, and $f_{\mathbf{k}i}$ is the occupation number of the ith orbital at wavevector $\mathbf{k}$. The self consistent solution of the single

particle equations (2.8), (2.10) and (2.11), or minimisation of the total energy functional F, therefore amounts to evaluating the ground state amplitudes, $C_{\mathbf{k}i\mathbf{G}}$, and associated occupation numbers, $f_{\mathbf{k}i}$.

The electronic wavefunctions at each $\mathbf{k}$ point are now expressed in terms of a discrete plane wave basis set. In principle this Fourier series is infinite. However, the coefficients for the plane waves, $C_{\mathbf{k}i\mathbf{G}}$, each have a kinetic energy $(\hbar^2/2m)|\mathbf{k}+\mathbf{G}|^2$. The plane waves with smaller kinetic energy typically have a more important role than those with a very high kinetic energy (Payne, 1992). Therefore the introduction of a plane wave energy cut-off reduces the basis set to a finite size.

This kinetic energy cut-off will lead to an error in the total energy of the system. However in principle it is possible to make this error arbitrarily small by increasing the size of the basis set by allowing a larger energy cut-off. Convergence of the total energy with respect to plane wave energy cut-off is an integral part of total energy calculations.

2.8 Calculating the total energy

In this section a brief summary is given of how to calculate numerically the total energy in equation (2.14) for given amplitudes $C_{\mathbf{k}i\mathbf{G}}$, occupation numbers $f_{\mathbf{k}i}$ and ionic positions $\mathbf{R}_i$.

First the momentum space representations of the charge density, the inter-electronic Coulombic (or Hartree) potential and the exchange correlation potential are given respectively as:

$$n(\mathbf{r}) = \sum_{\mathbf{G}} n(\mathbf{G}) e^{-i\mathbf{G}.\mathbf{r}} \tag{2.29}$$

$$V_{coul}(\mathbf{r}) = \int \frac{n(\mathbf{r}')}{|\mathbf{r}-\mathbf{r}'|} d\mathbf{r}' = \sum_{\mathbf{G}} V_{coul}(\mathbf{G}) e^{i\mathbf{G}.\mathbf{r}} \tag{2.30}$$

and

$$\mu_{xc}(\mathbf{r}) = \sum_{\mathbf{G}} \mu_{xc}(\mathbf{G}) e^{i\mathbf{G}.\mathbf{r}}. \tag{2.31}$$

The terms entering equation (2.14) are now considered.

2.8.1 Kinetic energy

This term can be evaluated directly as (Gillan, 1989):

$$T[n(\mathbf{r})] = \sum_{\mathbf{k}} w_{\mathbf{k}} \sum_{i} f_{\mathbf{k}i} \sum_{\mathbf{G}} |\mathbf{G}+\mathbf{k}^2||C^2_{\mathbf{k}i\mathbf{G}}|. \tag{2.32}$$

2.8.2 Electron-core energy

Using the Kleinman-Bymander formulation, the energy from the electron-core interaction can be separated down into a local and non-local contribution. For a system consisting of just a single species, the local contribution will be equivalent to:

$$\sum_{i,s} \int f_i \psi_i^*(\mathbf{r}) V_{ion}^{loc}(r-\mathbf{R}_s)\psi_i(\mathbf{r}) d\mathbf{r} = \sum_{s} \int V_{ion}^{loc}(r-\mathbf{R}_s) n(\mathbf{r}) d\mathbf{r} \tag{2.33}$$

$$= \Omega \sum_{\mathbf{G}} S(\mathbf{G}) V_{ion}^{loc}(\mathbf{G}) n(\mathbf{G}), \tag{2.34}$$

where $\mathbf{R}_s$ are the ionic positions of species s and $S(\mathbf{G})$ is the structure factor for species s:

$$S(\mathbf{G}) = \sum_{s} e^{i\mathbf{G}.\mathbf{R}_s}. \tag{2.35}$$

The contribution to the product of the Hamiltonian and the wave function ψ_i at wave vector $\mathbf{k}+\mathbf{G}$ for the Kleinman-Bylander pseudopotential is given by (Ihm, 1988; Payne, 1992)):

$$\sum_{lm}[\chi_{lm,\mathbf{k}+\mathbf{G}}[\sum_{\mathbf{G}'}\chi_{lm,\mathbf{k}+\mathbf{G}'}C_{i,\mathbf{k}+\mathbf{G}'}]], \tag{2.36}$$

where

$$\chi_{lm,\mathbf{k}+\mathbf{G}} = \frac{\int r^2 dr j_1(|\mathbf{k}+\mathbf{G}|r)\delta V_l(r)\phi^0_{lm}(r)}{[<\phi^0_{lm}|\delta V_l|\phi^0_{lm}>]^{1/2}}. \tag{2.37}$$

In equation (2.37), j_l is the spherical Bessel function of order l, ϕ^0_{lm} are pseudo-atomic states (see equation (2.23)) and δV_l is defined in equation (2.24). Equations (2.33) to (2.37) can be easily adapted to accommodate systems with more than one species.

2.8.3 Hartree energy

This contribution is likewise calculated in terms of $n_{\mathbf{G}}$ (Gillan, 1989):

$$\frac{1}{2}\int\int \frac{n(\mathbf{r})n(\mathbf{r}')}{|\mathbf{r}-\mathbf{r}'|}d\mathbf{r}d\mathbf{r}' + = \frac{2\pi}{\Omega}\sum_{\mathbf{G}\neq 0}\frac{n^2_{\mathbf{G}}}{G^2} \tag{2.38}$$

the zero-wavevector term being excluded.

2.8.4 Exchange-correlation energy

This contribution is:

$$E_{xc}[n(\mathbf{r})] = \Omega\sum_{\mathbf{G}}\mu_{xc}(\mathbf{G})n(\mathbf{G}). \tag{2.39}$$

2.8.5 Madelung energy

The Coulomb interaction energy E_{ion} of the ions is calculated using the standard Ewald technique (Ewald, 1917).

2.8.6 Pseudopotential core correction

There is also a contribution to the total energy from the *pseudopotential core correction.* At large distances, the local pseudopotential for a given species approaches that of a pure Coulombic potential of the form Z/r, where Z is the valence of the atom. In a Fourier representation, the pseudopotential diverges as $Z/\mathbf{G}^2$ at small wave vectors. Therefore the total ionic potential at $\mathbf{G} = 0$ is infinite. However there are similar divergences in the Coulombic energies due to the electron-electron interactions and the ion-ion interactions (Ihm, 1988; Payne, 1992). The Coulombic $\mathbf{G} = 0$ contributions to the total energy from the three interactions cancel exactly. This is not surprising because there should be no Coulombic potential at $\mathbf{G} = 0$ in a charge-neutral system, and so there cannot be a contribution to the total energy from the $\mathbf{G} = 0$ component of the Coulombic potential.

However, in the core region, the local part of the pseudopotential is not pure Coulombic but a lot 'softer' to avoid the huge basis set that would be required to represent a wavefunction in this region. Therefore there *is* a contribution to the pseudopotential at zero $\mathbf{G}$, which for atom 'x' is:

$$\nu_{x,core} = \int [Z/r - V^x_{ion,0}] 4\pi r^2 dr \tag{2.40}$$

where $V^x_{ion,0}$ is the pseudopotential for the $l = 0$ angular momentum state, which in

this example represents an arbitrary local pseudopotential. This integral is nonzero only within the core region because the potentials are identical outside this region. Therefore the non-Coulombic part of the pseudopotential at $\mathbf{G} = 0$ does contribute to the total energy. The contribution is:

$$N_{el} \sum_{x} N_x \nu_{x,core} \tag{2.41}$$

where N_{el} is the total number of electrons in the system and N_x is the total number of ions of species 'x'.

It is therefore useful to consider a local pseudopotential, for a given atom, in the form:

$$V_{ion,l}(r) = -Z/r + V_{ion,l}(r) + Z/r \tag{2.42}$$

where the first Z/r on the right hand side represents the Coulombic divergence at $\mathbf{G} = 0$ which is cancelled by the ion-ion and electron-electron terms, and the last two terms of equation (2.42) stay finite as $\mathbf{g} \rightarrow 0$ leading to the core correction contribution to the total energy.

2.8.7 Use of the Fast Fourier Transform

For computational efficiency the evaluation of $n_{\mathbf{G}}$ is done by first calculating the *real* space density coefficients, $n_{\mathbf{i}} = n(\mathbf{r}_{\mathbf{i}})$, on a grid of points $\mathbf{r}_{\mathbf{i}}$ in *real* space which span the supercell, see Figure 2.2.

The $n_{\mathbf{G}}$ are then constructed by Fourier transformation:

$$n_{\mathbf{G}} = w_{\mathbf{i}} \sum_{\mathbf{i}} e^{-\mathbf{G}.\mathbf{r}_{\mathbf{i}}} n_{\mathbf{i}} \tag{2.43}$$

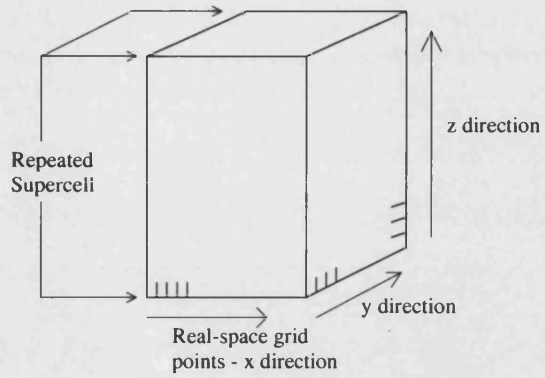

Figure 2.2: Schematic diagram of the 3D supercell. The real-space FFT grid points uniformly span the supercell.

where w_i is the volume per grid point. The n_i are obtained from equation (2.27), after Fourier transformation of the amplitudes.

The number of FFT grid points that span the super cell will depend on the energy cut-off of the plane wave expansion of the wave function, i.e. the number of **G**'s. The plane wave cut-offs and FFT grid sizes used in our calculations will be discussed in chapter 6. Utilising both the real and reciprocal space Fourier representations of the various quantities in total energy pseudopotential calculations is integral to the overall computational efficiency of the method. It will be shown that it continues to play a pivotal role when the analysis of the first principles calculations is developed in chapters 3, 4 and 5.

2.8.8 Minimising the total energy

The self consistent ground state solution to equations (2.8), (2.10) and (2.11) is obtained by direct minimisation of the total energy functional, equation (2.14). The Kohn-Sham energy functional normally has a well-defined energy minimum and searching for this energy minimum *directly* does not lead to instabilities in the evolution of the electronic configuration. The method used in our calculations is the *conjugate-gradients* method

(Payne, 1992). This technique is normally used to locate the minimum of a function $F(\mathbf{x})$, where $\mathbf{x}$ is a vector in multidimensional space, when all that is known is its value and gradient at a set of points. In the case of total energy calculations, the Kohn-Sham energy functional takes the place of the function F and the wavefunctions (with occupancies) take the place of the vector $\mathbf{x}$. The Kohn-Sham Hamiltonian is the relevant gradient operator. In practice the energy convergence achieved by conjugate gradients is excellent and it generally only takes a few tens of iterations to converge total energies for medium-sized systems even though the wavefunctions are expanded with up to 10000 plane waves.

After each iteration in the minimisation algorithm, the total energy is computed as described above. Prior to a calculation a criteria for energy convergence is stipulated; for the calculations in this work the criteria was for successive iterations to differ in total energy by less than 0.001eV.

2.8.9 The dipole correction

The repeated supercell method of calculation will always introduce an electric field across the supercell for systems where either electronegative or electropositive atoms are adsorbed on one side of the surface (Neugebauer, 1992). This artificial field is not negligible, especially for large adsorbates which tend to adsorb further from the surface where the metal electrons are less effective at screening out the induced field. The dipole effect produced from the supercell approach must be fully compensated in order to mimic as closely as possible a real experiment where an adsorbate is adsorbed on a semi-infinite surface. This is conveniently done by adding a periodic external potential across the supercell. The criteria for choosing the external potential are discussed in chapter 6

where the method has been implemented for some of the calculations in this work.

2.9 General remarks

A number of important factors need to be considered to ensure both convergence of the total energy and that the results of the calculation accurately represent an isolated adsorbate on an isolated surface:

- The cut-off energy of the planewave expansion in equation (2.27) has to be high enough;
- The density of special **k** points in the first Brillouin zone has to be high enough;
- The vacuum regions must be wide enough so that faces of adjacent crystal slabs do not interact across the vacuum region;
- The adsorbates in adjacent cells must be sufficiently separated to avoid any mutual interaction;
- The crystal slab must be thick enough so that the two surfaces of each crystal do not interact through the bulk crystal.

In principle, all these factors need to be converged with respect to the critical quantity being measured, whether it be the total energy of a system or an adsorption energy or whatever. This can be achieved by altering the relevant parameters in the calculation - i.e. the number of layers used to represent the surface slab, the size of the 2D surface unit cell, the plane wave energy cut- off or width of the vacuum gap etc.. However, the

memory and speed of the computer will always dictate the size of calculation possible and consequently the quality of the calculation. The particular details for the systems studied in this work are given in chapter 6.

So far in this chapter the basic theory of DFT and the application to total energy pseudopotential calculations of surface systems has been given. In the final section of this chapter we discuss the application of a different basis set within total energy calculations, the so called *mixed basis* set (Gülseren, 1998). The basic theory is given in this chapter, and in chapter 6 some results are presented with respect to some total energy pseudopotential calculations on the H_2/Cu(111) system. The initial reason for testing the mixed basis code during this work is given in the next section, but the particular application towards the analysis of promotion and poisoning is discussed in chapter 5.

2.10 A mixed basis approach to first principles calculations

2.10.1 Introduction

Total energy calculations for large systems (>50 atoms) using a plane-wave basis set are still computationally demanding (despite the fact they are well suited to the pseudopotential approach and the Fourier techniques described in the previous section), if they are to be fully converged with respect to the plane-wave cut-off, k point sampling, supercell size and slab thickness. This provided the impetus to investigate the implementation of a mixed basis approach, which uses pseudo-atomic orbitals (these are

the pseudo-eigenstates which are generated during the construction of a pseudopotential for a given species) and a few low-energy plane waves as the basis set, within a density functional pseudopotential calculation. The initial aim was to establish whether such an approach could provide an efficient way to construct the initial wavefunctions for plane-wave total energy calculations. In a pure plane wave calculation the initial Bloch coefficients are chosen randomly and the search for the global minimum of the energy functional proceeds from that point. If, however, one had a technique for generating initial wavefunctions that were already closer in nature to the true ground state wavefunctions, these could then form the initial wavefunctions for a pure plane wave calculation. The plane wave calculation would then require far less iterations to converge to the ground state wavefunctions. For this to be a clear advantage the time taken to produce the new initial wavefunctions would have to be such that the overall time taken to reach a converged answer is significantly quicker than using a pure plane wave approach.

By carrying out the work it would also be clear whether the mixed basis approach could be used *in its own right* for such calculations. The importance of this will become apparent in chapter 5.

2.10.2 Theoretical issues

Among several different approaches, there are two simple and natural choices of basis set for the expansion of electron wavefunctions: atomic orbitals (and other localised basis sets) and plane waves. On the negative side, atomic orbital methods have difficulties in representing the wavefunctions and potential in interstitial and vacuum regions while plane wave expansions are expensive for representing localised atomic character, for example $3d$ wavefunctions. Nevertheless, plane-wave basis sets are in most common use since they are

simple, independent of atomic positions, fast Fourier transformation (FFT) methods can be applied readily, and accuracy can be systematically improved by including additional plane waves with higher energy cut-offs. Although atomic orbitals are more physical, it is difficult to represent a uniform charge density, as in the vacuum region of a surface, with atom-centred, localised orbitals. On the other hand, plane-wave basis sets are also inefficient in a surface calculation using a slab geometry, since as many plane waves are needed for the vacuum as for the solid region. Therefore a combination of the important properties of plane waves with atomic orbitals in a mixed basis set may give a convenient and efficient representation, especially for systems which include both highly localised (atomic-like) and delocalised (plane wave-like) components.

Also, and most importantly for this work, there is extra interpretability from using a mixed basis set than a pure plane wave approach. For example, it is straightforward to calculate the density of states projected onto orbitals of the individual *atoms*, see section 2.10.4. This is an invaluable tool for investigating promotion and poisoning systems where it might be the case that individual atoms contribute differently to the overall promotion or poisoning effects.

2.10.3 Computational method

The Kohn-Sham eigenfunctions are expanded as:

$$\Psi_{\alpha\mathbf{k}}(\mathbf{r}) = \sum_{\mu} a_{\mu}^{\alpha}(\mathbf{k})\chi_{\mu}(\mathbf{r}) + \frac{1}{\sqrt{\Omega}} \sum_{\mathbf{G}} a_{\mathbf{G}}^{\alpha} e^{i(\mathbf{k}+\mathbf{G}).\mathbf{r}} \tag{2.44}$$

where α is the band index, μ is a combined index which labels the orbitals and atomic sites, a_{μ} and $a_{\mathbf{G}}$ are coefficients of the pseudo-atomic orbitals and plane waves, respectively, and

Ω is the volume of the unit cell. χ_μ is the Bloch sum formed from pseudo-atomic orbitals as:

$$\chi_\mu(\mathbf{r}) = \chi_m^i = \sum_{\mathbf{R}_l} e^{i(\mathbf{R}_l+\tau_i)}\phi_m(\mathbf{r}-\mathbf{R}_l-\tau_i) \tag{2.45}$$

where m labels the orbitals, the $\mathbf{R}_l$ are the lattice vectors, the τ_i are the atomic coordinates, and ϕ_m are pseudo-atomic orbitals. In practice, a plane-wave expansion is used for $\chi_\mu(\mathbf{r})$ with exactly the same FFT grid as in a full plane wave calculation. This makes sense if the wavefunctions from the mixed basis calculation are to be used as the input for a plane wave calculation. Having identical FFT grid sizes makes this transition straightforward. There are therefore two plane wave energy cut-offs to be considered in the mixed basis calculation. The larger one is the cut-off used in the representation of $\chi_\mu(\mathbf{r})$ and is the same as would be used in a full plane wave calculation. The smaller one is the cut-off for the extra, low-energy plane waves which appear in the second term of equation (2.44). This plane wave representation of $\chi_\mu(\mathbf{r})$ makes the calculation of the charge density, the kinetic energy and the contribution from non-local pseudopotentials straightforward (Gülseren, 1998).

Solving the Schrödinger equation then reduces to solving the secular equation:

$$det|H - SE| = 0. \tag{2.46}$$

The overlap matrix elements are given by (Gülseren, 1998) (with reference to the partition of Ψ in equation (2.44)):

$$S_{\mathbf{G}\mathbf{G}'} = \delta_{\mathbf{G},\mathbf{G}'} \tag{2.47}$$

$$S_{\mu\mathbf{G}} = e^{-i\mathbf{G}.\tau_i} I_{\mathbf{G}}^m(\mathbf{k}) \tag{2.48}$$

$$S_{\mu\nu} = \sum_{\mathbf{g}} e^{-i\mathbf{g}.(\tau_i - \tau_j)} I_{\mathbf{g}}^{n*}(\mathbf{k}) I_{\mathbf{g}}^{m}(\mathbf{k}) \tag{2.49}$$

where $\nu = (n, j)$ and $I_{\mathbf{g}}^{m}(\mathbf{k})$ is the Fourier integral of the pseudo-atomic orbital:

$$I_{\mathbf{g}}^{m}(\mathbf{k}) = \frac{1}{\sqrt{\Omega}} \int d\mathbf{r} e^{-i(\mathbf{k}+\mathbf{g}).\mathbf{r}} \phi_m(\mathbf{r}). \tag{2.50}$$

Similarly, the Hamiltonian matrix elements are based on a plane wave representation:

$$H_{\mathbf{G}\mathbf{G}'} = \frac{1}{\sqrt{\Omega}} \int d\mathbf{r} e^{-i(\mathbf{k}+\mathbf{G}').\mathbf{r}} H e^{-i(\mathbf{k}+\mathbf{G}).\mathbf{r}} \tag{2.51}$$

$$= |\mathbf{k}+\mathbf{G}|^2 \delta_{\mathbf{G},\mathbf{G}'} + V_{local}(\mathbf{G}-\mathbf{G}') + V_{NL}((\mathbf{k}+\mathbf{G}),(\mathbf{k}+\mathbf{G}')). \tag{2.52}$$

Then

$$H_{\mu\mathbf{G}} = \sum_{\mathbf{g}} e^{-i\mathbf{g}.\tau_i} I_{\mathbf{g}}^{m}(\mathbf{k}) H_{\mathbf{g}\mathbf{G}} \tag{2.53}$$

and

$$H_{\mu\nu} = \sum_{\mathbf{g}\mathbf{g}'} e^{i\mathbf{g}.\tau_j} e^{-i\mathbf{g}.\tau_i} I_{\mathbf{g}'}^{n*}(\mathbf{k}) I_{\mathbf{g}}^{m}(\mathbf{k}) H_{\mathbf{g}\mathbf{g}'}. \tag{2.54}$$

The local part of the potential in equation (2.52) contains the Hartree and exchange-correlation potentials, as well as the local part of the pseudopotential. In practice, only the Hartree and exchange-correlation contributions need be re-calculated through the self-consistency cycle - the pseudopotential (both local and non-local parts) and kinetic energy matrix elements are calculated only at the first iteration. The Schrödinger equation in equation (2.46) is solved self consistently through iterative diagonalisation, in combination with Kerker charge density mixing and a modified Broyden method (Kerker, 1981; Johnson, 1988). Therefore a direct minimisation through a conjugate gradient minimisation is **not** carried out. The initial charge density is constructed from overlapping, atomic pseudo-charge densities.

Diagonalisation of equation (2.46) is acceptable, since there are at most 9 orbitals (s, p, d) for each atom, and typically 10 to 20 additional waves per atom. This results in a matrix size less than $10^3 \times 10^3$, even for a moderately large system, compared to between 10^4 to 10^5 for a pure plane wave expansion. Tests on the H_2/Cu(111) system show that the mixed basis method is 6 to 8 times faster per iteration than a pure plane wave energy minimisation code. In addition, it typically requires fewer than half as many iterations to converge and so provides a significant improvement in computational speed.

2.10.4 Projected densities of states

The DOS projected onto the basis functions of the mixed basis set is defined by:

$$d^i(\epsilon) = \sum_{\mathbf{k},\alpha} \sum_j a_j^{\alpha *} S_{ji} a_i^{\alpha} \delta(\epsilon - E_{\alpha \mathbf{k}}), \tag{2.55}$$

where i and j label the basis functions. Because the mixed basis set is a non-orthogonal basis set, the normalisation condition for this basis holds:

$$\sum_{ij} a_i^{\alpha} S_{ji} a_j^{\alpha *} = 1. \tag{2.56}$$

With this definition, the total density of states is exactly the sum of $d^i(\epsilon)$ over all basis states, and the total charge associated with any basis function can be defined by:

$$Q_i = \int d^i(\epsilon) d\epsilon. \tag{2.57}$$

In practice, we are mostly interested in projections onto the pseudo-atomic orbitals. As stated in the introduction, this can give insight into the atoms and orbitals that are

significant to the interaction, whether they are surface atoms or adsorbate atoms, see Figure 1.4. In particular changes to the PDOS's before and after adsorption can be examined.

In chapter 5, the incorporation of the mixed basis set into the analysis of promotion and poisoning is discussed.

2.11 The key quantities that can be calculated from first principles calculations of adsorbate systems

Despite the crux of this thesis focusing on a way to improve what can be learnt from first principles calculations on promotion and poisoning, there is still a lot that can be gauged from these calculations alone. As stated in the introduction, the critical quantities are the total energy, the ground state charge density and densities of states. Total energies (extrapolated to 0K) are used to calculate adsorption energies. For example, the following expression is used to calculate the adsorption energy, $\Delta E_{ads,H_2}$, for an H_2 molecule in a given configuration above the Cu surface:

$$\Delta E_{ads,H_2} = E(Cu + H_2) - E(Cu) - E(H_2)_g. \tag{2.58}$$

$E(Cu + H_2)$ is the total 0K energy of a supercell containing a Cu slab (which represents the Cu surface) and an H_2 molecule in a given configuration above the surface, $E(Cu)$ is the total energy of the same size supercell containing just the Cu slab and $E(H_2)_g$ is the total energy of the same size supercell containing just the free H_2 molecule. By altering the configuration of the molecule it is possible to calculate sections of the 6D PES for the

interaction, as in Figure 1.1.

To investigate the possible promotion or poisoning of this process, the adsorption energy at the dissociation barrier on a pre-doped surface would need to be calculated and compared with the size of the barrier on the clean surface. The dissociation barrier on a pre-doped surface would be:

$$\Delta E_{ads,H_2,X} = E(Cu + X + H_2) - E(Cu + X) - E(H_2)_g \tag{2.59}$$

where $E(Cu + X + H_2)$ is the total energy of a supercell containing the slab, the H_2 molecule in the configuration associated with the transition state and a co-adsorbate atom (X).

Plotting the adsorbate induced change to the electronic charge density can provide insight into the formation and breaking of bonds at the surface. For the case of H_2 dissociating on Cu, one would expect to see a shift of electron density away from the single bond between the atoms of the dissociating molecule towards regions between surface and individual H atoms. The quantity plotted, as a function of $\mathbf{r}$, would be:

$$\Delta n^{H_2}(\mathbf{r}) = n(Cu + H_2) - n(Cu) - n(H_2) \tag{2.60}$$

where $n(Cu + H_2)$ is the self consistent ground state charge density of the Cu/H_2 system with H_2 in its transition state, $n(Cu)$ is charge density of the bare Cu system and $n(H_2)$ is the ground state charge density of the bare H_2 molecule in the configuration of the transition state.

2.12 Conclusion

This chapter has given an overview of the theory and computational procedure underpinning the pseudopotential total energy calculations reported in this work. These calculations form the basis for our investigation into the promotion and poisoning of the H_2/Cu(111) interaction, the results of which are reported in chapter 6. In the next three chapters, the theory and computational procedure are developed which enable the analysis of the first principles result to be taken one step further, leading to greater interpretability than is otherwise possible.

Chapter 3

The Frozen Density and Potential Approximation

3.1 Introduction

In this chapter, a theory based on DFT is developed with the aim to extend the interpretability of a first principles investigation into promotion and poisoning. The theory is applicable for two species interacting above a solid surface, for which the promotion or poisoning of diatomic dissociation is one particular example. In the introduction it was stated that for estimating the difference in adsorption energy for an adsorbate in two different surroundings - such as the change in adsorption energy of an atom on two similar metals or the change in adsorption energy on a given metal when another atom or molecule is adsorbed nearby - an expression could be written in terms of the changes in adsorbate-induced one-electron sums between the two different surroundings, plus an

electrostatic term, see equation (1.1):

$$\Delta E = \Delta E_{1el} + \Delta E_{es}. \tag{3.1}$$

Equation (3.1) provides an interpretable means of investigating the origin of ΔE, *provided* the terms can be calculated. The remainder of this chapter therefore focuses on the full DFT derivation of equation (3.1) for the particular case of co-adsorption. The result is an expression of the same form but with the terms written explicitly within a DFT framework. The key difference between this approach and that of previous workers (Hammer 1997; Mortensen 1998), is that before equation (3.1) has only been used as a broad interpretative tool to investigate promotion and poisoning, aiming to justify models based on electrostatics and changes in one-electron sums, as described in the introduction. Although this has met with considerable success, it has never been *proven* thus far in all the systems that have been studied, which part of the interaction - electrostatics or one-electron sums - is producing the dominant effect. For example, by applying the electrostatic model outlined in the introduction and observing a correlation between the dipole-dipole interaction energy and the corresponding first principles interaction energy for a range of systems, does *not* rule out the possibility of substrate mediated mechanisms being important. Previously there has only been strong speculation of the underlying mechanisms in a promotion and poisoning process. This reinforces the justification for our work.

The derivation starts with a schematic view of an adsorbate A and a co-adsorbate B on a surface, Figure 3.1, contained within a supercell repeated over all space.

The quantity of interest is the difference in the adsorption energy of A on the clean surface

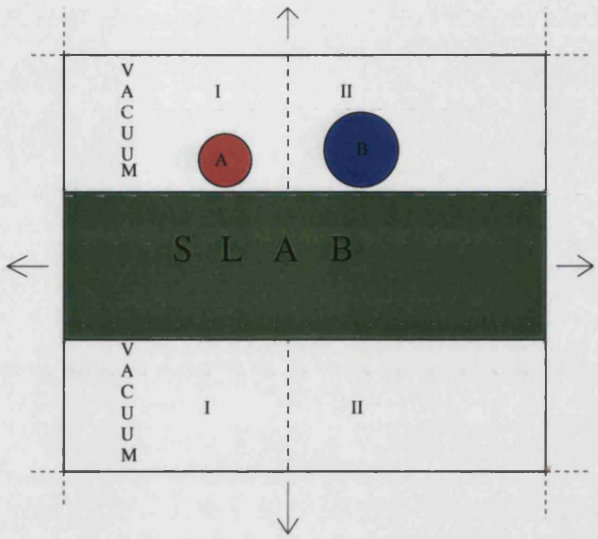

Figure 3.1: Schematic side view of a supercell containing two adsorbates, species A and B, on a surface. For the work in this thesis, species A represents an atomic adsorbate, and species B an H_2 molecule.

relative to the adsorption with B already pre-adsorbed, or vice-versa.

The adsorption energy of A on the clean surface is:

$$E_{ads}(A_{only}) = E(M + A) - E(M) - E(A_{free}) \tag{3.2}$$

where $E(M + A)$, $E(M)$ and $E(A_{free})$ are the self consistent total energies per supercell of the metal plus the adsorbate together, the metal on its own and the adsorbate on its own respectively. The adsorption energy of B is similarly:

$$E_{ads}(B_{only}) = E(M + B) - E(M) - E(B_{free}). \tag{3.3}$$

The adsorption energy of A when B is already present is thus:

$$E_{ads,B}(A) = E(M + A + B) - E(M + B) - E(A_{free}) \tag{3.4}$$

and so the change of adsorption energy of A due to the presence of B is:

$$\begin{aligned} \Delta E_{ads,B}(A) &= E(M+A+B) - E(M+B) - E(A_{free}) \\ &- E(M+A) + E(M) + E(A_{free}) \end{aligned} \tag{3.5}$$

$$= \overbrace{E(M+A+B)}^{\alpha} + \overbrace{E(M)}^{\beta} - \overbrace{E(M+A)}^{\gamma} - \overbrace{E(M+B)}^{\delta}. \tag{3.6}$$

Equation (3.6) is the governing equation used to calculate the self consistent interaction energy for the system displayed in Figure 3.1. It should be noted that there is a clear symmetry in equation (3.6) between A and B. The labels assigned to the four systems are used extensively throughout the derivation.

Equation (3.6) gives the A-B interaction energy in terms of total energies. If $\Delta E_{ads,B}(A)$ turns out to be negative then the presence of B stabilises the adsorption of A, in other words promotes the adsorption; if equation (3.6) is positive then B destabilises the adsorption of A or poisons the adsorption.

3.2 The Frozen density and potential approximation

3.2.1 Introduction

In this section we derive the approximate expression for $\Delta E_{ads,B}(A)$ of the form represented in equation (3.1). A starting point could be to write out all the terms in equation (3.6) using the expression in equation (2.14) for the total (or rather free) energy

F. Although possible, this would undoubtedly lead to a very complex expression, the interpretability of which is probably impossible.

The solution comes in the form of switching the Hohenberg-Kohn energy functional in equation (2.2) for the generalised Harris functional (Harris, 1985), $E[n, V]$, which is stationary about the ground state with respect to *independent* variations of both the electronic density n and the effective one-electron potential V (Methfessel, 1995). The reason for this switch will become apparent throughout the derivation.

$E[n, V]$ is written out in terms of a kinetic energy functional and a potential energy functional:

$$E[n, V] = T[n, V] + F[n] \tag{3.7}$$

with the kinetic energy being a functional of n and V:

$$T[n, V] = \sum_i f_i \epsilon_i[V(\mathbf{r})] - \int n(\mathbf{r}) V(\mathbf{r}) d\mathbf{r} \tag{3.8}$$

and the potential energy a functional of just n:

$$F[n] = \int V_{ion}(\mathbf{r}) n(\mathbf{r}) d\mathbf{r} + \frac{1}{2} \int \int \frac{n(\mathbf{r}) n(\mathbf{r}')}{|\mathbf{r} - \mathbf{r}'|} d\mathbf{r} d\mathbf{r}' + \int n \epsilon_{xc}[n(\mathbf{r})] d\mathbf{r} + E_{ion}. \tag{3.9}$$

Although the Harris functional is stationary with respect to independent variations in charge density and potential, it is equal to the Hohenberg-Kohn functional at the ground state. These are the two key properties of the generalised functional, $E[n, V]$, that the derivation in this chapter is based on. Essentially, substituting the functional, $E[n, V]$, for the Hohenberg-Kohn functional in each of the four systems in equation (3.6) allows an independent variation in the density and the potential around the ground state (the

particular choice of density and potential is discussed later), which will lead to only second and higher order errors in the true Hohenberg-Kohn ground state energies in equation (3.6):

$$E[n_o + \delta n, V_o + \delta V] = E_o + O^2(\delta n, \delta V). \tag{3.10}$$

In the proceeding derivation only local potentials are considered. Including non-local potentials within the Harris functional formalism is discussed in section 3.4 in this chapter.

3.2.2 Frozen densities and potentials

Using the Harris functional there is no one-to-one correspondence between the density and the potential, except at the ground state. Through independent variations of both, it is possible to choose particular densities and potentials (later to be called *frozen* densities and potentials) whereby many of the terms in equations (3.8) and (3.9), when substituted into equation (3.6), cancel to leave a much simpler and, more importantly, interpretable expression. This cancelling of terms through the introduction of frozen densities and potentials within the generalised functional, $E[n, V]$, is key to the frozen density and potential formalism and underpins the following derivation.

Figure 3.1 shows how each supercell in the periodic system can be divided into two regions, one that includes species A (region I) and one that includes species B (region II). Provided the divide is chosen to be far enough away from both adsorbates, the density and one-electron potential in one region will, to a first approximation, be independent of the presence or absence of the adsorbate in the other.

Using this idea the following approximation scheme is developed. The frozen densities and potentials used to approximate the ground state electronic charge density and potential

in each of the four systems in (3.6) are generated from the following three self consistent calculations:

1. The supercell of Figure 3.1 containing just the slab to give (n_M, V_M);
2. The same size supercell containing an identical slab plus *only* adsorbate A which is placed in the same position it would occupy in the co-adsorbed system, to give (n_{M+A}, V_{M+A});
3. The same size supercell containing an identical slab plus *only* adsorbate B which is placed in the same position it would occupy in the co-adsorbed system, to give (n_{M+B}, V_{M+B}).

Then the division of space is applied to each of these three systems to produce six frozen densities and six frozen potentials, which are then used to approximate the four self consistent densities and potentials in equation (3.6). Focusing on charge densities first and using a notation where a semicolon represents the division of space, we have:

$$\begin{aligned} n^{sc}_{M+A+B} &\approx \{n^{I}_{M+A}; n^{II}_{M+B}\} \\ n^{sc}_{M} &= \{n^{I}_{M}; n^{II}_{M}\} \\ n^{sc}_{M+A} &\approx \{n^{I}_{M+A}; n^{II}_{M}\} \\ n^{sc}_{M+B} &\approx \{n^{I}_{M}; n^{II}_{M+B}\}. \end{aligned} \tag{3.11}$$

Taking n^{sc}_{M+A+B} as an example, this is approximated by the frozen density associated with region I of the self consistent calculation (2) added along side the frozen density from region II that is obtained through calculation (3). For n^{sc}_{M}, the approximation in (3.11) is exact.

A similar procedure is adopted to approximate to the self consistent ground state potentials in equation (3.6).

Using the frozen density and potential construction in (3.11), equations (3.8) and (3.9) are substituted into each of the four terms in equation (3.6) which will ultimately produce the desired expression for the interaction energy. Although (3.11) is approximate, the energies based on them should be reasonably accurate.

First we focus on equation (3.8).

3.2.3 The $\int V(\mathbf{r})n(\mathbf{r})d\mathbf{r}$ term

We start with the $\int V(\mathbf{r})n(\mathbf{r})d\mathbf{r}$ term in the kinetic energy expression (3.8). The integral over all space is split into regions I and II and using the approximations in (3.11) (where some of the superscripts have now been dropped), it becomes:

$$\overbrace{\int_I n_{M+A}V_{M+A}}^{\alpha} + \overbrace{\int_I n_M^I V_M^I}^{\beta} - \overbrace{\int_I n_{M+A}V_{M+A}}^{\gamma} - \overbrace{\int_I n_M^I V_M^I}^{\delta}$$

$$+ \overbrace{\int_{II} n_{M+B}V_{M+B}}^{\alpha} + \overbrace{\int_{II} n_M^{II} V_M^{II}}^{\beta} - \overbrace{\int_{II} n_M^{II} V_M^{II}}^{\gamma} - \overbrace{\int_{II} n_{M+B}V_{M+B}}^{\delta} = 0. \qquad (3.12)$$

Each integral in equation (3.12) is with respect to $d\mathbf{r}$. This term therefore vanishes in the approximation for the interaction energy $\Delta E_{ads,B}(A)$. This only happens because of the frozen density and potential approximation.

3.2.4 The electron-ion interaction

The local ionic potential is linear which means, for example:

$$V_{ion}(M+A+B) = V_{ion}(M) + V_{ion}(A) + V_{ion}(B), \quad etc.. \tag{3.13}$$

where $V_{ion}(M+A+B)$ represents the addition of all the pseudopotentials from the ion cores in the α system of equation (3.6), as a function of r.

Using frozen densities, the contribution to terms α, β, $\gamma and \delta$ becomes: (with each integral with respect to $d\mathbf{r}$)

$$\begin{aligned}
\alpha \quad &: \quad \int_I V_{ion}(M+A+B)n_{M+A} + \int_{II} V_{ion}(M+A+B)n_{M+B} \\
\beta \quad &: \quad \int_I V_{ion}(M)n_M + \int_{II} V_{ion}(M)n_M \\
\gamma \quad &: \quad \int_I V_{ion}(M+A)n_{M+A} + \int_{II} V_{ion}(M+A)n_M \\
\delta \quad &: \quad \int_I V_{ion}(M+B)n_M + \int_{II} V_{ion}(M+B)n_{M+B}.
\end{aligned}$$

To evaluate the contribution to the approximate interaction energy, we consider $\alpha + \beta - \gamma - \delta$ which gives:

$$\begin{aligned}
& \int_I V_{ion}(M+A)n_{M+A} + \int_I V_{ion}(B)n_{M+A} \\
+ \; & \int_{II} V_{ion}(M+B)n_{M+B} + \int_{II} V_{ion}(A)n_{M+B} \\
+ \; & \int_I V_{ion}(M)n_M + \int_{II} V_{ion}(M)n_M \\
- \; & \int_I V_{ion}(M+A)n_{M+A} - \int_{II} V_{ion}(M)n_M - \int_{II} V_{ion}(A)n_M \\
- \; & \int_I V_{ion}(M)n_M - \int_I V_{ion}(B)n_M - \int_{II} V_{ion}(M+B)n_{M+B}
\end{aligned}$$

$$= \int_I V_{ion}(B)(r)(n_{M+A} - n_M)d\mathbf{r}$$
$$+ \int_{II} V_{ion}(A)(r)(n_{M+B}) - n_M)d\mathbf{r} \quad (3.14)$$

Equation (3.14) shows there is a contribution to the adsorbate-adsorbate interaction energy involving the local part of the ionic pseudopotentials of the adsorbates. This contribution, therefore, is the sum of the electrostatic energy between the induced charge density from adsorbate A in region I with the tail of $V_{ion}(r)$ from adsorbate B plus the electrostatic energy between the induced charge density from adsorbate B in region II with the tail of $V_{ion}(r)$ from adsorbate A. The induced charge density, $\Delta n^A(\mathbf{r})$, is defined as:

$$\Delta n^A(\mathbf{r}) = n_{M+A}(\mathbf{r}) - n_M(\mathbf{r}), \quad (3.15)$$

which is the induced electronic charge density due to adsorbate A, and similarly for adsorbate B. This is almost a pure Coulombic interaction because for sufficiently separated adsorbates the long range local pseudopotential for species A, for example, will be nearly pure Coulombic in region II.

3.2.5 The pseudopotential core correction contribution

In section 4.3.1, it will be shown that core corrections must be taken into account using the frozen density and potential formalism, just as they do in a normal self consistent approach.

3.2.6 The $\int n\epsilon_{xc}(n)$ term, $E_{xc}[n]$

The exchange-correlation energy is a local function of **r** within the LDA and even for the GGA the functional can be considered local in the sense that the exchange-correlation energy in region I does not depend on the properties of region II (in the sense of the frozen density construction), and likewise for region II.

Using frozen densities the terms α, β, γ and δ become:

$$\alpha \quad : \quad E_{xc}^{I}[n_{M+A}] + E_{xc}^{II}[n_{M+B}] \tag{3.16}$$

$$\beta \quad : \quad E_{xc}^{I}[n_{M}] + E_{xc}^{II}[n_{M}] \tag{3.17}$$

$$\gamma \quad : \quad E_{xc}^{I}[n_{M+A}] + E_{xc}^{II}[n_{M}] \tag{3.18}$$

$$\delta \quad : \quad E_{xc}^{I}[n_{M}] + E_{xc}^{II}[n_{M+B}] \tag{3.19}$$

and $\alpha + \beta - \gamma - \delta = 0$. Again this term has zero contribution to the overall interaction energy. The zero contribution from the $\int V n d\mathbf{r}$ term and the $E_{xc}[n]$ term is to be expected. The frozen densities and potentials are local in the sense that they do not depend on the density and potential outside their region and so by the symmetry of (3.11) and equation (3.6), a zero contribution is expected.

3.2.7 The E_{ion} Term

This term is the Coulombic interaction of all the cores in the periodically repeated supercell and is long ranged. Frozen densities and potentials do not need to be considered. The contribution to the four terms in equation (3.6) becomes:

$$\alpha : \quad E_{ion}(M+A+B) \Rightarrow E_{ion}(M) + E_{ion}(M,A) + E_{ion}(M,B)$$

$$+ E_{ion}(A,B) + E_{ion}(A,A) + E_{ion}(B,B)$$

$$\beta : \quad E_{ion}(M) \Rightarrow E_{ion}(M)$$

$$\gamma : \quad E_{ion}(M+A) \Rightarrow E_{ion}(M) + E_{ion}(M,A) + E_{ion}(A,A)$$

$$\delta : \quad E_{ion}(M+B) \Rightarrow E_{ion}(M) + E_{ion}(M,B) + E_{ion}(B,B)$$

where $E_{ion}(M)$ is the ion-ion interaction energy between the metal atoms alone. $E_{ion}(M+A/B)$ is the ion-ion interaction energy between the metal atoms and adsorbate A or B. $E_{ion}(A,B)$ is the direct A - B ion-ion energy and $E_{ion}(A/B)$ represents the self ion-ion energy for each adsorbate, throughout the periodic system.

Combining the four expressions by $\alpha + \beta - \gamma - \delta$ produces:

$$\alpha + \beta - \gamma - \delta = E_{ion}(A,B). \tag{3.20}$$

Equation (3.20) shows that the contribution to the overall interaction energy from the Coulombic interactions between the ion cores comes only from the direct adsorbate-adsorbate term. This can be determined directly from the self consistent calculations in equation (3.6).

3.2.8 The Hartree term

Before considering the contribution to the approximate interaction energy from the Hartree terms using frozen densities, the Hartree term is first broken down with respect

to the two regions I and II:

$$\frac{1}{2}\int\int \frac{n(\mathbf{r})n(\mathbf{r}')}{|\mathbf{r}-\mathbf{r}'|}d\mathbf{r}d\mathbf{r}' = \frac{1}{2}\int_I d\mathbf{r}\, n(\mathbf{r})\int_{I+II} d\mathbf{r}'\frac{n(\mathbf{r}')}{|\mathbf{r}-\mathbf{r}'|} + \frac{1}{2}\int_{II} d\mathbf{r}\, n(\mathbf{r})\int_{I+II} d\mathbf{r}'\frac{n(\mathbf{r}')}{|\mathbf{r}-\mathbf{r}'|}$$

$$= \frac{1}{2}\int_I d\mathbf{r}\, n(\mathbf{r})\int_I d\mathbf{r}'\frac{n(\mathbf{r}')}{|\mathbf{r}-\mathbf{r}'|} + \frac{1}{2}\int_I d\mathbf{r}\, n(\mathbf{r})\int_{II} d\mathbf{r}'\frac{n(\mathbf{r}')}{|\mathbf{r}-\mathbf{r}'|}$$
$$+ \frac{1}{2}\int_{II} d\mathbf{r}\, n(\mathbf{r})\int_I d\mathbf{r}'\frac{n(\mathbf{r}')}{|\mathbf{r}-\mathbf{r}'|} + \frac{1}{2}\int_{II} d\mathbf{r}\, n(\mathbf{r})\int_{II} d\mathbf{r}'\frac{n(\mathbf{r}')}{|\mathbf{r}-\mathbf{r}'|}$$

$$= \frac{1}{2}\int_I d\mathbf{r}\, n(\mathbf{r})\int_I d\mathbf{r}'\frac{n(\mathbf{r}')}{|\mathbf{r}-\mathbf{r}'|} + \frac{1}{2}\int_{II} d\mathbf{r}\, n(\mathbf{r})\int_{II} d\mathbf{r}'\frac{n(\mathbf{r}')}{|\mathbf{r}-\mathbf{r}'|} \tag{3.21}$$
$$+ \int_I d\mathbf{r}\, n(\mathbf{r})\int_{II} d\mathbf{r}'\frac{n(\mathbf{r}')}{|\mathbf{r}-\mathbf{r}'|}.$$

Each term in equation (3.6) will therefore have three terms involving Hartree energies. The frozen densities can now be substituted in.

The α, β, γ and δ terms then become: (with all integrals with respect to $d\mathbf{r}d\mathbf{r}'$)

$$\alpha \;:\; \frac{1}{2}\int_I\int_I \frac{n_{M+A}n_{M+A}}{|\mathbf{r}-\mathbf{r}'|} + \frac{1}{2}\int_{II}\int_{II} \frac{n_{M+B}n_{M+B}}{|\mathbf{r}-\mathbf{r}'|} + \int_I\int_{II} \frac{n_{M+A}n_{M+B}}{|\mathbf{r}-\mathbf{r}'|}$$

$$\beta \;:\; \frac{1}{2}\int_I\int_I \frac{n_M^I n_M^I}{|\mathbf{r}-\mathbf{r}'|} + \frac{1}{2}\int_{II}\int_{II} \frac{n_M^{II} n_M^{II}}{|\mathbf{r}-\mathbf{r}'|} + \int_I\int_{II} \frac{n_M^I n_M^{II}}{|\mathbf{r}-\mathbf{r}'|}$$

$$\gamma \quad : \quad \frac{1}{2}\int_I\int_I \frac{n_{M+A}n_{M+A}}{|\mathbf{r}-\mathbf{r}'|} + \frac{1}{2}\int_{II}\int_{II} \frac{n_M^{II}n_M^{II}}{|\mathbf{r}-\mathbf{r}'|} + \int_I\int_{II} \frac{n_{M+A}n_M^{II}}{|\mathbf{r}-\mathbf{r}'|}$$

$$\delta \quad : \quad \frac{1}{2}\int_I\int_I \frac{n_M^I n_M^I}{|\mathbf{r}-\mathbf{r}'|} + \frac{1}{2}\int_{II}\int_{II} \frac{n_{M+B}n_{M+B}}{|\mathbf{r}-\mathbf{r}'|} + \int_I\int_{II} \frac{n_M^I n_{M+B}}{|\mathbf{r}-\mathbf{r}'|}$$

and so $\alpha + \beta - \gamma - \delta$ becomes (after much cancellation):

$$\int_I d\mathbf{r}(n_{M+A} - n_M^I)\int_{II} d\mathbf{r}' \frac{n_{M+B}}{|\mathbf{r}-\mathbf{r}'|} \qquad (\alpha,\ \delta) \tag{3.22}$$

$$-\int_I d\mathbf{r}(n_{M+A} - n_M^I)\int_{II} d\mathbf{r}' \frac{n_M^{II}}{|\mathbf{r}-\mathbf{r}'|} \qquad (\beta,\ \gamma) \tag{3.23}$$

$$= \int_I d\mathbf{r}(n_{M+A} - n_M^I)\int_{II} d\mathbf{r}' \frac{(n_{M+B}) - n_M^{II})}{|\mathbf{r}-\mathbf{r}'|}. \tag{3.24}$$

Equation (3.24) gives the final contribution to the overall interaction energy. This term is also electrostatic in nature and is effectively the electrostatic interaction energy between induced charge densities.

3.3 The frozen density expression for the adsorbate-adsorbate interaction energy

Collecting together the expressions (3.14), (3.20) and (3.24) and incorporating the only remaining term from (3.8) and (3.9) not yet considered, i.e., the one-electron sums in the expression for the kinetic energy, the overall result for the adsorbate-adsorbate interaction based on frozen densities and potentials is:

$$\sum_i f_i\epsilon_i[V_{M+A};V_{M+B}] + \sum_i f_i\epsilon_i[V_M;V_M] - \sum_i f_i\epsilon_i[V_{M+A};V_M] - \sum_i f_i\epsilon_i[V_M;V_{M+B}]$$

$$+ \int_{II} d\mathbf{r} V_{ion}(A)(r)(n_{M+B}(\mathbf{r}) - n_M(\mathbf{r})) + \int_I d\mathbf{r} V_{ion}(B)(r)(n_{M+A}(\mathbf{r}) - n_M(\mathbf{r}))$$

$$+E_{ion}(A,B) + \int_I d\mathbf{r}(n_{M+A}(\mathbf{r}) - n_M(\mathbf{r})) \int_{II} d\mathbf{r}' \frac{(n_{M+B}(\mathbf{r}) - n_M(\mathbf{r}))}{|\mathbf{r} - \mathbf{r}'|} + E_{core}. \quad (3.25)$$

where E_{core} is the contribution through the pseudopotential core correction.

3.4 Conclusion

Non-local potentials enter into equation (3.25) through the one-electron sums only and are the same non-local potentials as in the pure self consistent calculations in equation (3.6). A rigorous justification for this is beyond the scope of this thesis, however it has

been shown in a private communication (Trail, 2000) that the Harris functional is both stationary at the ground state, with respect to charge density and one-electron potential, and equal to the Hohenberg-Kohn functional, at the ground state, when the same non-local pseudopotentials are used in both.

Equation (3.25) is the full expression based on DFT for the approximation to equation (3.6) and, as can be seen is of the same form as equation (3.1). The key difference is that the terms in equation (3.25) are written out explicitly. Provided they can be calculated, the contribution to the adsorbate-adsorbate interaction energy from processes based on electrostatics and one-electron sums can be determined. The accuracy of this analysis will depend on the division of space in Figure 3.1, i.e. the condition that to a good approximation the charge density and potential in region I must be insensitive to the presence of the adsorbate in region II and vice versa.

Equation (3.25) shows that one-electron sums do have an interpretative role to play in the analysis of promotion and poisoning provided they are calculated within correctly constructed frozen potentials. Contributions from substrate-mediated processes and direct orbital overlap between adsorbates will be contained within the eigenvalue sums. The next stage is therefore to find a way to calculate the one-electron sums in equation (3.25) in such a way as to determine which atoms and orbitals in the system are significant to the promotion and poisoning. Chapter 5 addresses these issues in the context of the mixed basis set.

The electrostatic terms in equation (3.25) will be significant for strongly electropositive and electronegative adsorbates inducing electrostatic fields across the unit cell.

Calculating the terms in equation (3.25) is addressed in the next two chapters. The

two key challenges that need to be addressed are maintaining charge neutrality within the frozen density construction, to avoid the Coulombic divergences, and establishing a common chemical potential or Fermi level for the four one-electron sums. The latter consideration is crucial for making comparisons and calculating interpretable densities of states.

Although equation (3.25) is only useful if the terms can be calculated, this should not detract from the fact that arriving at an expression that can clearly be separated into one-electron sums and electrostatic parts is an important result.

Chapter 4

Calculating the electrostatic contribution to the approximate interaction energy

4.1 Introduction

In this chapter the computational method for determining the electrostatic contribution in equation (3.25) is discussed. The format for the chapter is the following:

- First we reiterate which of the four self consistent calculations in equation (3.6) are used to generate the frozen densities. Approximating the self consistent charge densities in equation (3.6) with frozen densities will result in the incorrect amount of negative charge in the system, which will not balance the positive charge background from the ion cores. From the discussion in section 2.8.6, in the context of a supercell

calculation, the system must be charge neutral if the Coulombic divergencies are to cancel correctly. Therefore ensuring charge neutrality with the Harris functional approach is essential and implementing this is discussed first.

- Next, having accounted for the inbalance in amount of charge, calculating the terms in equation (3.25) that contain the ionic potentials, V_{ion}, is discussed.
- Then, calculating the term involving the electrostatic interaction energy between the induced charge densities is considered.
- Finally, a summary of what has been achieved so far is given.

4.2 Charge density split-up

From the discussion in section 3.2.2, it is clear that in order to obtain the frozen densities, the full self consistent charge densities from the β, γ and δ terms are required. The division of space in Figure 3.1 can lead to the identification of six frozen densities which are subsequently used to approximate the four self consistent charge densities in equation (3.6). As it stands, the approximation in (3.11) will not contain the right amount of charge because:

$$\int_I (n^{sc}_{M+A}(\mathbf{r}) - n^{sc}_{M}(\mathbf{r}))d\mathbf{r} \neq Z_A \tag{4.1}$$

and

$$\int_{II} (n^{sc}_{M+B}(\mathbf{r}) - n^{sc}_{M}(\mathbf{r}))d\mathbf{r} \neq Z_B \tag{4.2}$$

where the three densities in equations (4.1) and (4.2), i.e. $n^{sc}_{M+A}(\mathbf{r})$, $n^{sc}_{M}(\mathbf{r})$ and $n^{sc}_{M+B}(\mathbf{r})$, are self consistent densities for systems γ, β and δ respectively, and Z_A and Z_B are the valencies of adsorbate A and B respectively.

There are two obvious choices of how to implement this 'needed' charge into the system. The first is where the extra charge is added uniformly over the whole cell. This gives:

$$n^{sc}_{M+A+B} \approx \{n_{M+A} + \delta_1 \; ; \; n_{M+B} + \delta_1\} \tag{4.3}$$

$$n^{sc}_{M} = \{n^{I}_{M} \; ; \; n^{II}_{M}\} \tag{4.4}$$

$$n^{sc}_{M+A} \approx \{n_{M+A} + \delta_2 \; ; \; n^{II}_{M} + \delta_2\} \tag{4.5}$$

$$n^{sc}_{M+B} \approx \{n^{I}_{M} + \delta_3 \; ; \; n_{M+B} + \delta_3\}. \tag{4.6}$$

However, the critical step is to add the extra charge in such a way to keep the $\int nV$ term and the E_{xc} terms cancelling, as they did in the derivation in the last chapter. Ensuring the above criteria are met keeps the interpretability and simplicity of equation (3.25) intact. It can easily be shown that adding the charge in this way does not produce the desired cancellations of equations (3.12) and (3.16).

An alternative way is to add the extra charge that is *specific* to regions I and II only, instead of a uniform charge. So we have:

$$n^{sc}_{M+A+B} \approx \{n_{M+A} + \delta_A \; ; \; n_{M+B} + \delta_B\} \tag{4.7}$$

$$n^{sc}_{M} = \{n^{I}_{M} \; ; \; n^{II}_{M}\} \tag{4.8}$$

$$n^{sc}_{M+A} \approx \{n_{M+A} + \delta_A \; ; \; n^{II}_{M}\} \tag{4.9}$$

$$n^{sc}_{M+B} \approx \{n^{I}_{M} \; ; \; n_{M+B} + \delta_B\} \tag{4.10}$$

where δ_A and δ_B are the neutralising background charges in regions I and II respectively. Adding the extra charge in this way does produce the required cancellations discussed above.

4.2.1 How to calculate the extra charge

In order to calculate the extra charge we introduce two new functions, $S^I(\mathbf{r})$ and $S^{II}(\mathbf{r})$, both of which are continuous periodic functions over the repeated supercell of Figure 3.1. $S^I(\mathbf{r})$ is defined to be 'one' in region I of the supercell and 'zero' outside whereas $S^{II}(\mathbf{r})$ is defined to be 'zero' in region I and 'one' outside in region II. It is through using these two 'shape functions' that the frozen densities are actually implemented. In other words, all the density expressions which follow, i.e. $n_{M+A}(\mathbf{r})$, $n_{M+B}(\mathbf{r})$ and $n_M(\mathbf{r})$ are the **self consistent** densities for the γ, δ and β terms of equation (3.6), but they become localised in the appropriate region, in accordance with (3.11), through multiplication by an appropriate shape function.

Figure 7.2 in chapter 7 displays the surface unit cell in our calculations including the choice of shape function employed in our analysis. The periodic shape function is a cylinder surrounding each atomic adsorbate at the corners of the surface unit cell. Referring to Figure 3.1, region I for our system is the volume enclosed by each cylinder around each atomic adsorbate and region II is the volume outside this containing the H_2 molecule. The choice of shape function was by no means unique, however the cylindrical function was chosen not only because it was a natural choice physically, but also the Fourier representation was trivial to calculate:

$$S(\mathbf{r}) = \sum_{\mathbf{g}} S_{\mathbf{g}} e^{i\mathbf{g}.\mathbf{r}} \tag{4.11}$$

where

$$S_{\mathbf{g}} = \frac{1}{V_c} \int_{cell} d\mathbf{r} S(\mathbf{r}) e^{-i\mathbf{g}.\mathbf{r}}. \tag{4.12}$$

We find that:

$$S_{\mathbf{g}} = \frac{2\pi R_c}{A|\mathbf{g}|} J_1(|\mathbf{g}|R_c) \tag{4.13}$$

where R_c is the cut-off radius for the shape function, A is the area of the surface unit cell, J_1 is the first order Bessel function and $\mathbf{g}$ is a reciprocal lattice vector.

In order to establish the extra charge required in each region, we require that:

$$\int_{cell} \Delta n^A(\mathbf{r}) S^I(\mathbf{r}) d\mathbf{r} = Z_A \tag{4.14}$$

$$\int_{cell} \Delta n^B(\mathbf{r}) S^{II}(\mathbf{r}) d\mathbf{r} = Z_B \tag{4.15}$$

where

$$\Delta n^A(\mathbf{r}) = (n_{M+A}(\mathbf{r}) + \delta_A(\mathbf{r}) - n_M(\mathbf{r})) \tag{4.16}$$

$$\Delta n^B(\mathbf{r}) = (n_{M+B}(\mathbf{r}) + \delta_B(\mathbf{r}) - n_M(\mathbf{r})). \tag{4.17}$$

$\Delta n^A(\mathbf{r})$, $\Delta n^B(\mathbf{r})$ and $S^{I/II}(\mathbf{r})$ are all periodic functions that can be represented in terms of their Fourier components. Equation (4.14) then becomes:

$$\int_{cell} \sum_{\mathbf{hp}} \Delta n^A_{\mathbf{h}} e^{i\mathbf{h}.\mathbf{r}} S^I_{\mathbf{p}} e^{i\mathbf{p}.\mathbf{r}} d\mathbf{r} = V_c \sum_{\mathbf{h}} \Delta n^A_{\mathbf{h}} S^I_{-\mathbf{h}} = Z_A, \tag{4.18}$$

where V_c is the volume of the unit cell. The important step now is to make use of the corresponding real space grid that was discussed in section 2.8.7 in order to calculate $\sum_{\mathbf{h}} \Delta^A_{\mathbf{h}} S^I_{-\mathbf{h}}$. In other words, we represent each reciprocal space Fourier component, $\Delta^A_{\mathbf{h}}$ and $S^I_{-\mathbf{h}}$, in terms of their corresponding real space coefficients:

$$\Delta n^A_{\mathbf{h}} = \frac{1}{N_{FFT}} \sum_{\mathbf{i}} \Delta n^A_{\mathbf{i}} e^{i\mathbf{h}.\mathbf{r}_\mathbf{i}} \tag{4.19}$$

$$S^I_{-\mathbf{h}} = \frac{1}{N_{FFT}} \sum_{\mathbf{j}} S^I_{\mathbf{j}} e^{-i\mathbf{h}.\mathbf{r_j}} \tag{4.20}$$

where $\mathbf{r_i}$ and $\mathbf{r_j}$ are the real space FFT grid points that span the supercell and N_{FFT} is the number of FFT grid points. $\Delta n^A_{\mathbf{i}}$ and $S^I_{\mathbf{j}}$ are FFT's of the corresponding reciprocal-space coefficients. Substituting these real space representations into equation (4.18) then produces a simple expression for fixing the extra charge in region I, $\delta_A(\mathbf{r})$:

$$\frac{V_c}{N_{FFT}} \sum_{\mathbf{i}} \Delta n^A_{\mathbf{i}} S^I_{\mathbf{i}} = Z_A. \tag{4.21}$$

A similar procedure is done for the extra charge required in region II:

$$\frac{V_c}{N_{FFT}} \sum_{\mathbf{i}} \Delta n^B_{\mathbf{i}} S^{II}_{\mathbf{i}} = Z_B \tag{4.22}$$

where the $S_{\mathbf{i}}$'s are analytical FFT's of the $S_{\mathbf{g}}$'s in equation (4.13).

4.3 Calculating the electrostatic terms

In the previous section it was shown how using the appropriate shape function served two useful purposes. Firstly, it enables the frozen densities to be implemented by multiplying together the appropriate self consistent charge density and shape function, and consequently frozen densities need never be saved as units on their own. Secondly, by representing the shape function and the self consistent charge density on the corresponding real space grid (i.e. using S_i's which **must** be calculated directly from the analytic $S_{\mathbf{g}}$'s by FFT), determining the extra charge necessary to achieve charge neutrality across the system is straightforward.

We are now in a position to address the calculation of the electrostatic terms in equation (3.25). The key step is to rewrite the electrostatic terms utilising the appropriate shape functions to create the relevant frozen densities. They become, with the integrals now over all space:

$$\begin{aligned} & \int V_{ion}(B)\Delta n^A(\mathbf{r})S^I(\mathbf{r})d\mathbf{r} \\ + & \int V_{ion}(A)\Delta n^B(\mathbf{r})S^{II}(\mathbf{r})d\mathbf{r} \\ + & \int\int d\mathbf{r}d\mathbf{r}' \frac{\Delta n^A(\mathbf{r})\Delta n^B(\mathbf{r}')S^I(\mathbf{r})S^{II}(\mathbf{r}')}{|\mathbf{r}-\mathbf{r}'|}. \end{aligned} \tag{4.23}$$

4.3.1 The $\int V_{ion}n$ terms

In the same way as calculating the extra charges, the first two integrals in equation (4.23) are expressed in terms of Fourier components. Considering the first integral, this gives:

$$\int \sum_{\mathbf{g}} V_{\mathbf{g}}^{ion}(B)e^{i\mathbf{g}.\mathbf{r}} \sum_{\mathbf{h}} \Delta n_{\mathbf{h}}^A e^{i\mathbf{h}.\mathbf{r}} \sum_{\mathbf{p}} S_{\mathbf{p}}^I e^{i\mathbf{p}.\mathbf{r}} d\mathbf{r}. \tag{4.24}$$

Carrying out the integration gives:

$$V_c \sum_{\mathbf{gh}} V_{\mathbf{g}}^{ion}(B)\Delta n_{\mathbf{h}}^A S_{-\mathbf{h}-\mathbf{g}}^I. \tag{4.25}$$

A similar result is obtained for the second integral in equation (4.23), i.e.:

$$V_c \sum_{\mathbf{gh}} V_{\mathbf{g}}^{ion}(A)\Delta n_{\mathbf{h}}^B S_{-\mathbf{h}-\mathbf{g}}^{II}. \tag{4.26}$$

However, because of the problems discussed in section 2.8.6 involving Coulombic

divergencies within periodic systems, care must be taken in handling the $\mathbf{g} = 0$ term in equations (4.25) and (4.26), ($V_{ion}(\mathbf{g} = 0) \rightarrow \infty$).

In section 2.8.6, the core correction energy for a given atom was defined and the necessity for the correction explained. In the following discussion it will be shown that the core corrections do need to be taken into account in this analysis and that the contribution from the pseudopotential core correction within equations (4.25) and (4.26), is equivalent to the contribution in the full self consistent calculation for the adsorbate-adsorbate interaction energy, equation (3.6).

Focusing on equation (4.25), the $\mathbf{g} = 0$ term becomes:

$$[CD + \nu_{B,core}] \times \sum_{\mathbf{h}} \Delta n^{A}_{\mathbf{h}} S^{I}_{-\mathbf{h}} \tag{4.27}$$

$$= [CD + \nu_{B,core}] \times Z_A, \tag{4.28}$$

see equation (4.18). In equation (4.28), CD is the Coulombic divergent term in equation (2.42) and $\nu_{B,core}$ is the total $\mathbf{g} = 0$ contribution from the local part of the pseudopotential from adsorbate B. Similary for equation (4.26), the $\mathbf{g} = 0$ term becomes:

$$[CD + \nu_{A,core}] \times Z_B. \tag{4.29}$$

It can easily be shown that the contribution in equations (4.28) and (4.29) from the core correction energies is the same as for the full self consistent approach in equation (3.6), i.e.:

$$E_{core} = (\nu_{B,core} \times Z_A) + (\nu_{A,core} \times Z_B). \tag{4.30}$$

The Coulombic divergence terms in equations (4.28) and (4.29) will be discussed a little

later. Having handled the divergent $\mathbf{g} = 0$ term in equations (4.25) and (4.26), the $\mathbf{g} \neq 0$ components are now considered. For equation (4.25), the contribution is:

$$V_c \sum_{\mathbf{g}\neq 0} V_{\mathbf{g}}^{ion}(B) \sum_{\mathbf{h}} \Delta n_{\mathbf{h}}^{A} S_{-\mathbf{h}-\mathbf{g}}^{I}. \tag{4.31}$$

In practice, this can be calculated on the real space grid, where we put:

$$V_{\mathbf{g}}^{ion}(B) = \frac{1}{N_{FFT}} \sum_{\mathbf{i}} V_{\mathbf{i}}^{ion}(B) e^{i\mathbf{g}.\mathbf{r}_{\mathbf{i}}} \tag{4.32}$$

and

$$S_{-\mathbf{h}-\mathbf{g}}^{I} = \frac{1}{N_{FFT}} \sum_{\mathbf{k}} S_{\mathbf{k}}^{I} e^{-i\mathbf{g}.\mathbf{r}_{\mathbf{k}}} e^{-i\mathbf{h}.\mathbf{r}_{\mathbf{k}}}. \tag{4.33}$$

Using this representation, we find the following result:

$$V_c \sum_{\mathbf{g}\neq 0} V_{\mathbf{g}}^{ion}(B) \sum_{\mathbf{h}} \Delta n_{\mathbf{h}}^{A} S_{-\mathbf{h}-\mathbf{g}}^{I} = \frac{V_c}{N_{FFT}} \sum_{\mathbf{i}} \Delta n_{\mathbf{i}}^{A} V_{\mathbf{i}}^{ion}(B) S_{\mathbf{i}}^{I}. \tag{4.34}$$

Comparing equation (4.21) with equation (4.34) shows that both the extra charge δ_A and the quantity in equation (4.34) can be calculated straightforwardly using the real space grid, and in practice they can both be carried out in the same calculation.

Summary

Putting together the two V_{ion} integrals in equation (4.23), we get:

$$\begin{aligned} & (Z_A \times CD) + (Z_A \times \nu_{B,core}) \\ + \; & (Z_B \times CD) + (Z_B \times \nu_{A,core}) \\ + \; & \frac{V_c}{N_{FFT}} \sum_{i} \Delta n_{\mathbf{i}}^{A} V_{\mathbf{i}}^{ion}(B) S_{\mathbf{i}}^{I} + \frac{V_c}{N_{FFT}} \sum_{\mathbf{i}} \Delta n_{\mathbf{i}}^{B} V_{\mathbf{i}}^{ion}(A) S_{\mathbf{i}}^{II} \end{aligned} \tag{4.35}$$

where:

$$\Delta n^A(\mathbf{r}) = n_{M+A}(\mathbf{r}) - n_M(\mathbf{r}) + \delta_A(\mathbf{r}) \; ; \; \frac{V_c}{N_{FFT}} \sum_{\mathbf{i}} \Delta n^A_{\mathbf{i}} S^I_{\mathbf{i}} = Z_A \tag{4.36}$$

$$\Delta n^B(\mathbf{r}) = n_{M+B}(\mathbf{r}) - n_M(\mathbf{r}) + \delta_B(\mathbf{r}) \; ; \; \frac{V_c}{N_{FFT}} \sum_{\mathbf{i}} \Delta n^B_{\mathbf{i}} S^{II}_{\mathbf{i}} = Z_B. \tag{4.37}$$

A key point to note from equations (4.36) and (4.37) is that the sums will produce the correct result because $\Delta n_{\mathbf{h}}$ is represented exactly in equation (4.19).

4.3.2 The Hartree term

It is also efficient to calculate this term on a real space grid using FFTs. Using the shape function approach the Hartree term in equation (4.23) becomes:

$$\int d\mathbf{r} \int d\mathbf{r}' \frac{\Delta n^A(\mathbf{r}) \Delta n^B(\mathbf{r}') S^I(\mathbf{r}) S^{II}(\mathbf{r}')}{|\mathbf{r} - \mathbf{r}'|}. \tag{4.38}$$

Expressing the terms in equation (4.38) in terms of Fourier components gives:

$$\int\int d\mathbf{r} d\mathbf{r}' \sum_{\mathbf{g}\mathbf{g}'\mathbf{h}\mathbf{h}'} \Delta n^A_{\mathbf{g}} e^{i\mathbf{g}.\mathbf{r}} \Delta n^B_{\mathbf{g}'} e^{i\mathbf{g}'.\mathbf{r}'} S^I_{\mathbf{h}} e^{i\mathbf{h}.\mathbf{r}} S^{II}_{\mathbf{h}'} e^{i\mathbf{h}'.\mathbf{r}} \frac{1}{4\pi} \int d\mathbf{q} \frac{e^{i\mathbf{q}.(\mathbf{r}-\mathbf{r}')}}{q^2} \tag{4.39}$$

and after carrying out the integration, equation (4.39) becomes:

$$\frac{V_c}{4\pi} \sum_{\mathbf{p}} \frac{1}{|\mathbf{p}|^2} \sum_{\mathbf{g}} \Delta n^A_{\mathbf{g}} S^I_{\mathbf{p}-\mathbf{g}} \sum_{\mathbf{g}'} \Delta n^B_{\mathbf{g}'} S^{II}_{-\mathbf{p}-\mathbf{g}'}, \tag{4.40}$$

where $\mathbf{p}$ is a reciprocal lattice vector. In practice, the $\mathbf{p} \neq 0$ terms in equatiion (4.40) can be calculated on the real space FFT grid. Consider first the $\mathbf{p} = 0$ term, which becomes

(ignoring the divergent $V_c/4\pi|\mathbf{p}|^2$ term):

$$\sum_{\mathbf{g}} \Delta n^A_{\mathbf{g}} S^I_{-\mathbf{g}} \times \sum_{\mathbf{g}'} \Delta n^B_{\mathbf{g}'} S^{II}_{-\mathbf{g}'} = Z_A \times Z_B. \tag{4.41}$$

This term will cancel correctly with both the Coulombic divergent ion-ion interaction and the divergent V_{ion} terms in equation (4.35).

For the $\mathbf{p} \neq 0$ terms, calculating on the real space grid for the first half of equation (4.40) gives:

$$\begin{aligned} \frac{V_c}{4\pi} \sum_{\mathbf{p}} \frac{1}{|\mathbf{p}|^2} \sum_{\mathbf{g}} \Delta n^A_{\mathbf{g}} S^I_{\mathbf{p}-\mathbf{g}} &= \frac{V_c}{4\pi} \sum_{\mathbf{p}} \frac{1}{|\mathbf{p}|^2} \sum_{\mathbf{g}} \sum_{\mathbf{i}} \Delta n^A_{\mathbf{i}} e^{i\mathbf{g}.\mathbf{r}_\mathbf{i}} \sum_{\mathbf{j}} S^I_{\mathbf{j}} e^{i\mathbf{p}.\mathbf{r}_\mathbf{j}} e^{-i\mathbf{g}.\mathbf{r}_\mathbf{j}} \\ &= \frac{4\pi}{V_c} \sum_{\mathbf{p}} \frac{1}{|\mathbf{p}|^2} \sum_{\mathbf{i}} \Delta n^A_{\mathbf{i}} S^I_{\mathbf{i}} e^{i\mathbf{p}.\mathbf{r}_\mathbf{i}} \end{aligned} \tag{4.42}$$

which is simply $\frac{4\pi}{V_c} \sum_{\mathbf{p}} 1/|\mathbf{p}|^2$ multiplied by the $\mathbf{p}$ component of the FFT of $\Delta n^A \times S^I$.

The whole of equation (4.40) can therefore be calculated if the same method is used for the last two terms in equation (4.40).

4.4 Conclusion

The key points to be taken from this chapter are the following:

- The construction of the frozen densities described in chapter 3 can be conveniently achieved using the appropriate self consistent charge density, corresponding to either the β, γ or δ systems of equation (3.6), multiplied by the appropriate shape function. Therefore all densities n_{M+A}, n_{M+B} or n_M in the above analysis are full

self consistent charge densities.

- Self consistent charge densities generated within total energy calculations are expressed in Fourier components due to the periodic supercell structure, supporting efficient FFT methods to be used throughout the calculations. The local part of the ionic potential, V_{ion}, is also expressed in terms of Fourier components, see equation (2.30), on the same size FFT grid as the densities. Then, by choosing a shape function whose analytic Fourier components, $S_{\mathbf{g}}^{I/II}$, are also calculable, results in all the quantities used to calculate the electronic terms in equation (4.23) being represented on the same FFT grid.

- By applying appropriate FFT's on to the corresponding real space grid, all the terms in equation (4.23) which do not involve Coulombic divergencies or core corrections are straightforward to calculate, including the extra charges needed in both regions to maintain charge neutrality.

- Coulombic divergencies associated with the ion-ion interaction, the local ionic potential and the electron-electron term *will* cancel to zero. The pseudopotential core energy contribution in equation (4.23) is required and is the same as that from the pure self consistent approach in equation (3.6).

Chapter 5

Calculating the eigenvalue sums

5.1 Introduction

The remaining terms in equation (3.25) to be discussed are the eigenvalue sums. Provided they can be calculated, the expression for the approximate interaction energy can then be tested for the purpose for which it was derived.

In order to calculate the eigenvalue sums, the Schrödinger equation must be solved for each of the four systems, α, β, γ and δ, and at the same special $\mathbf{k}$ points as in the self consistent calculations. The frozen potentials are generated in precisely the same way as the frozen densities, of course no consideration is now needed for extra neutralising charge. The three self consistent local potentials associated with the β, γ and δ systems are required. Multiplication by the appropriate shape function will allow the following

approximation scheme to be used:

$$V^{sc}_{M+A+B} \approx \{V^{I}_{M+A}; V^{II}_{M+B}\} \quad (5.1)$$

$$V^{sc}_{M} = \{V^{I}_{M}; V^{II}_{M}\} \quad (5.2)$$

$$V^{sc}_{M+A} \approx \{V^{I}_{M+A}; n^{II}_{M}\} \quad (5.3)$$

$$rV^{sc}_{M+B} \approx \{V^{I}_{M}; n^{II}_{M+B}\}, \quad (5.4)$$

where the semicolon represents the division of space in Figure 3.1, region I to the left and II to the right.

5.2 Theoretical issues

As mentioned at the end of chapter 3, there are a number of theoretical issues that need to be addressed, not only to calculate the eigenvalue sums, but to also maximise the interpretation and understanding that can be gauged from them:

- The time taken to calculate the eigenvalue sums is an important consideration. Calculating what is effectively the band structure for large systems is computationally demanding and so an efficient method must be used.

- As discussed in chapter 2, for metallic systems, it is the free energy functional that is minimised in the total energy calculations, incorporating fractional occupancies for the eigenstates at the Fermi level and an associated electronic entropy. The eigenvalue sums, calculated within the frozen potentials of (5.1), for each of the four systems must, therefore, incorporate fractional occupancies and the associated

entropy function. This will result in three different values for the eigenvalue sums - a 'total', 'free' and 'zero K' contribution.

- The eigenvalue sums are carried out using the mixed basis set. The justification for this is discussed in chapter 6 where it is shown that the mixed basis set can be used in its own right to expand the wavefunctions in total energy calculations, with particular reference to the H_2/Cu(111) system relevant to this work.

- Projecting the wave functions onto this basis set will enable the contribution to the approximate interaction energy from *individual* atoms and orbitals to be calculated.

- Calculating the eigenvalue sums means solving the secular equation (2.46) by incorporating frozen potentials for the local potential in equation (2.52), the same non-local potentials as in the corresponding self consistent calculation and then carrying out a single matrix diagonalisation.

- Analysing the eigenvalue sums in terms of densities of states and densities of states projected onto individual atoms and orbitals has turned out to be an intuitive method of investigating promotion and poisoning systems, indeed adsorbate systems in general. In order to carry this out so as to compare the differences between the four one-electron sums in equation (3.25), a common reference energy is required for each of the four systems. This is generally chosen to be the Fermi level. How to achieve this is also discussed in this chapter.

5.3 Calculating the eigenvalues

Taking the α term as an example, the eigenvalues for each $\mathbf{k}$ point in the first Brillouin zone are calculated by solving the Schrödinger equation within a mixed basis set:

$$[-\frac{1}{2}\nabla^2 + (V^{sc}_{M+A}(\mathbf{r})S^I(\mathbf{r}) + V^{sc}_{M+B}(\mathbf{r})S^{II}(\mathbf{r}) + V_{NL}(\mathbf{r},\mathbf{r}'))]\psi_{i,\mathbf{k}} = \epsilon_{i,\mathbf{k}}\psi_{i,\mathbf{k}}. \tag{5.5}$$

5.3.1 Implementation detail

The shape functions in equation (5.5) localise the relevant local self consistent potential to either region I or II in Figure 3.1. To solve equation (5.5) for the eigenstates and eigenenergies, the Fourier components of a potential of the form $V(\mathbf{r})S(\mathbf{r})$ need to be evaluated. To do this we again use the real space representation of the local potentials and shape functions.

To see this we first write down the $\mathbf{q}$ component of $V(\mathbf{r})S(\mathbf{r})$ (where $\mathbf{q}$ is a reciprocal lattice vector) as:

$$\frac{1}{V_c}\int_{cell} V(\mathbf{r})S(\mathbf{r})e^{-i\mathbf{q}.\mathbf{r}}d\mathbf{r} \tag{5.6}$$

which is equivalent to:

$$\sum_{\mathbf{hp}}\int_{cell} e^{i\mathbf{h}.\mathbf{r}}e^{i\mathbf{p}.\mathbf{r}}S_{\mathbf{h}}V_{\mathbf{p}}e^{-i\mathbf{q}.\mathbf{r}}d\mathbf{r} \tag{5.7}$$

by expressing $V(\mathbf{r})$ and $S(\mathbf{r})$ in terms of their Fourier components. Therefore the $\mathbf{q}$ component in equation (5.7) is:

$$\sum_{\mathbf{p}} S_{\mathbf{q}-\mathbf{p}}V_{\mathbf{p}}. \tag{5.8}$$

In practice, equation (5.8) is easily evaluated by FFT, using the corresponding real space

grid. First we write:

$$S_{\mathbf{h}} = \frac{1}{N_{FFT}} \sum_{\mathbf{i}} S_{\mathbf{i}} e^{i\mathbf{h}.\mathbf{r}_{\mathbf{i}}} \tag{5.9}$$

and

$$V_{\mathbf{p}} = \frac{1}{N_{FFT}} \sum_{\mathbf{j}} V_{\mathbf{j}} e^{i\mathbf{p}.\mathbf{r}_{\mathbf{j}}}. \tag{5.10}$$

Then equation (5.8) becomes:

$$\frac{1}{N_{FFT}^2} \sum_{\mathbf{p}} \sum_{\mathbf{ij}} S_{\mathbf{i}} e^{-i(\mathbf{p}-\mathbf{q}).\mathbf{r}_{\mathbf{i}}} V_{\mathbf{j}} e^{i\mathbf{p}.\mathbf{r}_{\mathbf{k}}} \tag{5.11}$$

$$= \frac{1}{N_{FFT}} \sum_{\mathbf{i}} S_{\mathbf{i}} V_{\mathbf{i}} e^{i\mathbf{q}.\mathbf{r}_{\mathbf{i}}}. \tag{5.12}$$

The result in equation (5.12) shows that the $\mathbf{q}$ component in reciprocal space of $V(\mathbf{r})S(\mathbf{r})$ is just the FFT of $S_{\mathbf{i}}V_{\mathbf{i}}$, provided the $S_{\mathbf{i}}$'s are calculated *exactly* from $S_{\mathbf{h}}$ by FFT. This analysis is very similar to the implementation procedure discussed in chapter 4. Because the $S_{\mathbf{i}}$ are trivial to calculate and the $V_{\mathbf{i}}$ are obtained straight from the relevant self consistent calculation, implementing the two terms in equation (5.5) of the form $S(\mathbf{r})V(\mathbf{r})$ in their Fourier representation is straightforward.

5.4 Analysis of the eigenvalue sums via the DOS

Having calculated the eigenvalues for each of the four systems, α, β, γ and δ, the eigenvalue sum can be evaluated as:

$$\sum_{\mathbf{i},\mathbf{k}} f(\frac{\epsilon_{\mathbf{i},\mathbf{k}} - E_F}{kT}) \epsilon_{\mathbf{i},\mathbf{k}} \tag{5.13}$$

for each of the four systems. The occupancy function, $f(x)$, is defined such that:

$$\sum_{i,\mathbf{k}} f(\frac{\epsilon_{i,\mathbf{k}} - E_F}{kT}) = N, \tag{5.14}$$

where N is the total number of electrons for the particular system. This also defines E_F for the chosen temperature T.

In the same way as in the self consistent calculations, the **free** energy eigenvalue sum contribution can be calculated by writing down an entropy term for each system, $-T\sum_{i,\mathbf{k}} A(f_{i,\mathbf{k}})$, where:

$$A(f_{i,\mathbf{k}}) = \int_{-\infty}^{x(f_{i,\mathbf{k}})} x\frac{df}{dx}dx. \tag{5.15}$$

However, $x(f_{i,\mathbf{k}})$ is the x value required to generate $f_{i,\mathbf{k}}$, which, by definition is just

$$\frac{\epsilon_{i,\mathbf{k}} - E_F}{kT}. \tag{5.16}$$

So, for an **individual** eigenvalue sum, the free energy is:

$$\sum_{i,\mathbf{k}} f(\frac{\epsilon_{i,\mathbf{k}} - E_F}{kT})\epsilon_{i,\mathbf{k}} - T\int_{-\infty}^{\frac{\epsilon_{i,\mathbf{k}}-E_F}{kT}} x\frac{df}{dx}dx. \tag{5.17}$$

So far we have shown how to carry out the standard total energy eignevalue sum and the free energy eigenvalue sum. The average of the two will the zero K energy eigenvalue sum. We now want to look at how this relates to an analysis carried out via a DOS route, i.e. we want to make the link between:

$$\sum \epsilon_i \iff \int_{-\infty}^{E_F} \epsilon d(\epsilon), \tag{5.18}$$

or, more specifically, the link between:

$$\sum_{i,\mathbf{k}} f(\frac{\epsilon_{i,\mathbf{k}} - E_F}{kT})\epsilon_{i,\mathbf{k}} \iff \sum_{i,\mathbf{k}} \int_{-\infty}^{E_F} d\epsilon g(\frac{\epsilon - \epsilon_{i,\mathbf{k}}}{T})\epsilon, \tag{5.19}$$

with $g(x)$ defined such that:

$$\sum_{i,\mathbf{k}} \int_{-\infty}^{E_F} d\epsilon g(\frac{\epsilon - \epsilon_{i\mathbf{k}}}{T}) = N. \tag{5.20}$$

It is shown in Appendix A that by choosing $g(x)$ to be:

$$g(x) = -\frac{1}{kT} f'(x), \tag{5.21}$$

produces the desired result in equation (5.20).

In Appendix A, it is also shown that with this choice of $g(x)$, the eigenvalue sum calculated via the DOS, i.e.:

$$\sum_{i,\mathbf{k}} \int_{-\infty}^{E_F} d\epsilon \; g(\frac{\epsilon - \epsilon_{i,\mathbf{k}}}{kT})\epsilon \tag{5.22}$$

is equivalent to the *free* energy eigenvalue sum in equation (5.17).

This shows that when the analysis of the eigenvalue sums is carried out in terms of the density of states projected onto different atoms and orbitals using the mixed basis set, it is the *free* energy equivalent of the eigenvalue sums in equation (3.25) that is being analysed.

5.5 Determining a common Fermi level, E_F

In this section we consider the choice of the common Fermi energy for each of the four systems. With a common E_F, it is possible to make meaningful comparisons between the DOS projected onto different atoms and orbitals for each of the four systems in equation (3.25), which could give insight into the origin of the interaction energy from particular atoms and orbitals.

The first step in achieving a common Fermi level across each of the four systems, α, β, γ and δ, is to *align* the local potential for each system (formed from two 'spliced' frozen potentials) to a high degree of accuracy. To do this the local potential in the centre of the slab was chosen to be the same across all four systems and equal to that of the β system, i.e. the bare slab calculation. The result of this is that the eigenvalues across all four systems are already aligned.

The important step now is not to alter this alignment between different systems otherwise $\sum \epsilon_i$ will be wrong. However, we need to define an E_F for each system otherwise $\sum \epsilon_i$ can't be defined. Therefore a *common* E_F must be chosen across *all* four systems together, at the expense of altering the true occupancies of each system by a small amount. However, by then setting this common E_F to specifically zero, the eigenvalue sum differences around E_F can be made very small.

The overall result is a reference energy common to each of the four systems, which is a common Fermi level, E_{F_c}, the zero of energy. Although the overall occupancy of each of the four systems will now be slightly different to their true values, the effect on the eigenvalue sum differences in equation (3.25) will be negligible.

5.6 The link to promotion and poisoning

So far in this section it has been shown that calculating and interpreting the eigenvalue sums is possible. The key considerations were the identification of a common Fermi level across each of the four systems and the link between the basic eigenvalue sums and those calculated through the density of states. In this section, we clarify further the interpretability that is possible for promotion and poisoning using a DOS analysis, within a basis set of pseudo-atomic orbitals and low-energy plane waves.

Looking at each of the four systems, α, β, γ and δ, separately, the DOS projected onto the basis functions of the mixed basis set is defined by:

$$d^m(\epsilon) = \sum_{\mathbf{k},i} \sum_j a_j^{i*} S_{jm} a_m^i \frac{1}{kT} f'(\epsilon - \epsilon_{i\mathbf{k}}), \tag{5.23}$$

where j and m label the basis functions. From the density of states projected onto individual basis functions it is then possible to determine the contribution each makes to the **free** eigenvalue sums of equation (3.25) by:

$$\begin{aligned} \Delta\epsilon_x^m &= \int_{-\infty}^{E_F} \overbrace{\epsilon d_x^m(\epsilon)}^{\alpha} + \int_{-\infty}^{E_F} \overbrace{\epsilon d_x^m(\epsilon)}^{\beta} \\ &- \int_{-\infty}^{E_F} \overbrace{\epsilon d_x^m(\epsilon)}^{\gamma} - \int_{-\infty}^{E_F} \overbrace{\epsilon d_x^m(\epsilon)}^{\delta}, \end{aligned} \tag{5.24}$$

where $d_x^m(\epsilon)$ is the DOS projected onto the mth basis function of atom x. Equation (5.24) is the pivotal expression that is used in the analysis of the eigenvalue sums in chapter 7. Summing $\Delta\epsilon_x^m$ over all the basis states of each atom in the α, β, γ and δ systems will equal the free energy equivalent of the eigenvalue sums in equation (3.25).

5.7 Conclusion

In this chapter and in chapter 4, it has been shown how to calculate the terms in equation (3.25). The electrostatic terms in chapter 4 are easy to calculate using the relevant output quantities from the self consistent calculations. To calculate the eigenvalue sums using the mixed basis set requires a single matrix diagonalisation. Although straightforward in principle, for the size of systems used in our calculations, the diagonalisation takes between 3 and 4 hours per **k** point on an Origin 2000 node.

The work presented so far in this thesis has shown a methodology for interpreting, quantitatively, a self consistent DFT investigation of the interaction of two species above a solid surface.

Chapter 6

Results of self consistent calculations

6.1 Introduction

In this chapter the self consistent DFT total energy calculations carried out for this work are discussed. Firstly, the results of testing the mixed basis set, discussed in section 2.10, within a total energy pseudopotential calculation for the H_2/Cu(111) system are presented. The results from these tests are crucial and, as will be shown, fully justify the use of the mixed basis set to calculate the eigenvalue sums in equation (3.25).

Then, the self consistent results using CETEP for the promotion and poisoning of the H_2/Cu(111) system are given together will full details of the supercell and associated parameters used in the calculations. These calculations were carried out in order to determine the magnitude of any change in the dissociation barrier caused by either pre-adsorbed H, K or O atoms, plus any changes to the PES for the reaction.

In chapter 7, the Harris functional analysis is applied to the self consistent results in this

chapter.

6.2 Results of the mixed basis total energy calculations on H_2/Cu(111)

To test the mixed basis approach, calculations were carried out on the H_2/Cu(111) system, each time increasing the number of additional low-energy plane waves and comparing the results with an exactly equivalent calculation based on plane waves **only**. This shows the convergence properties with respect to this low energy cut-off. The cut-off for the Bloch sums which represent the pseudo-atomic part of the basis set is fixed at the cut-off of the Bloch states in the pure plane wave calculations. A semi-relativistic Trouiller-Martins pseudopotential, with associated $4s$, $4p$ and $3d$ pseudo atomic orbitals, was used to describe the Cu atoms and each H atom was described by the full Coulombic potential, with localised $1s$ and $2p$ orbitals.

6.2.1 Computational details

Technical details of the full H_2/Cu(111) calculation are as follows. The substrate was modelled by a 5 layer, rigid Cu slab with the experimental lattice parameter of 3.61Å. There are 3 Cu atoms per layer within a $(\sqrt{3} \times \sqrt{3})$ geometry and 4 layers of vacuum separate the slabs, see Figure 6.1. An H_2 molecule was placed on only one side of the slab. The surface Brillouin zone was sampled by 54 special $\mathbf{k}$ points, and the Fermi surface is broadened with a kT of 0.25eV, with the total energy being extrapolated to zero temperature (see section 2.4). A cut-off of 800eV was used for the pure plane

wave calculation, and for representing the localised orbitals in the mixed basis method. These parameters were expected to provide well converged results for the energy barrier (Hammer, 1994), although this was not a critical issue as these calculations were primarily only interested in testing whether the mixed basis set could accurately represent the wavefunctions as compared with a full plane wave pseudopotential calculation. Exchange and correlation effects are described using the PW91 GGA approximation (Perdew, 1992).

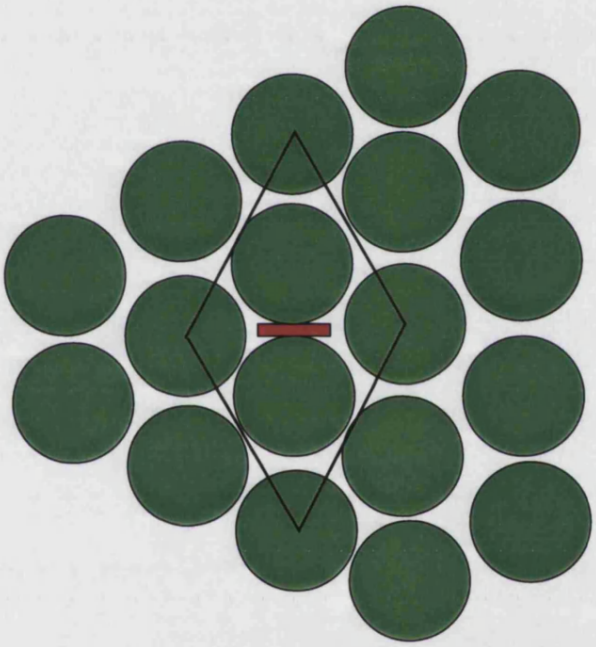

Figure 6.1: Plan view of the Cu(111). Solid line indicates the $(\sqrt{3} \times \sqrt{3})$ in-plane supercell. The position of the H_2 is marked as red. The scale of the plot can be taken from the H-H bondlength of 1.1Å, represented by the length of the red rectangle.

Six values of the minimum barrier were calculated using:

$$E_b = E(Cu(111) + H_2) - E(Cu(111)) - E(H_2)_g \tag{6.1}$$

with the same calculation parameters used in the evaluation of each of the three terms in equation (6.1). The free H_2 molecule was at its theoretical equilibrium bond length of

0.74Å and for the adsorbed system the molecule was at the transition state configuration of $(d, Z) = (1.1\mathring{A}\ ,\ 1.2\mathring{A})$, i.e. with the bond length extended to 1.1Å and the centre of the molecule 1.2Å above the top layer of Cu atoms. Five calculations used the mixed basis approach with different numbers of additional plane waves, corresponding to energy cut-offs of 0eV (i.e. pseudo-atomic orbitals only), 20eV, 40eV, 60eV and 80V. The number of additional plane waves were 0, 65, 180, 330 and 520 respectively for these cut-offs. The PW cut-off for the Bloch sums of the pseudo-atomic orbitals was 800eV. The sixth calculation was a full plane wave calculation at 800eV cut-off. Computed values of the minimum energy barrier are given in Table 6.1. The value of the pure plane wave barrier value is within 50meV of the fully converged value calculated in Hammer (1994), which actually shows the parameters in our calculation are not fully converged. It can be seen that the mixed basis method provides an accurate value for the barrier height (within 10meV) once plane waves with energies of at least 40eV are included.

Energy Cutoff(eV)	Barrier Height (eV)
AO	-0.854
20	0.520
40	0.606
60	0.614
80	0.613
PW	0.612

Table 6.1: GGA minimum barrier for H_2 dissociation on Cu(111). AO represents the pure atomic orbital limit (i.e. 0eV cut-off) and PW the full plane wave limit (with plane waves up to 800eV).

6.2.2 Conclusion

The mixed basis method we have presented has the potential, therefore, to provide an accurate and computationally cheap alternative to full plane wave methods for first principles calculations of surface systems. Although only a single system has been tested here, tests on a variety of systems have confirmed the generality of this approach, with structural parameters being accurate to of order 0.01Å and energy differences accurate to within a few meV. If required, the calculation can then be 'finished off' using a full plane wave expansion, in which case the mixed basis method will provide an accurate starting structure and highly optimised wavefunctions.

Calculating the one-electron sums using the mixed basis set, in its own right, was now justified.

6.3 CETEP calculations on the promotion and poisoning of H_2/Cu(111)

6.3.1 The supercell

The supercell contains five Cu(111) layers, separated by either five or seven equivalent layers of vacuum. The seven layer system was used for the K investigation. Due to its larger size than O or H and the fact it adsorbs further from the surface (Padilla-Campos, 1997), a seven layer vacuum was required to limit the interaction with the opposite 'clean' side of the slab. The experimental lattice parameter of 3.61Å was used. An important feature of the calculations is that we have used a relatively large in-plane supercell (3×3),

in order to separate the adsorbed atoms as far as possible. It also provides a number of inequivalent impact sites, B1 - B6, at in-plane distances of 4.10, 2.66, 3.68, 1.95, 3.21 and 0.74 Å from the atomic adsorbates respectively. We have singled out bridge sites once again because previous calculations have shown these to be the most favourable sites for H_2 dissociation over Cu(111), see Figure 1.1. A plan of the surface is shown in Figure 6.2.

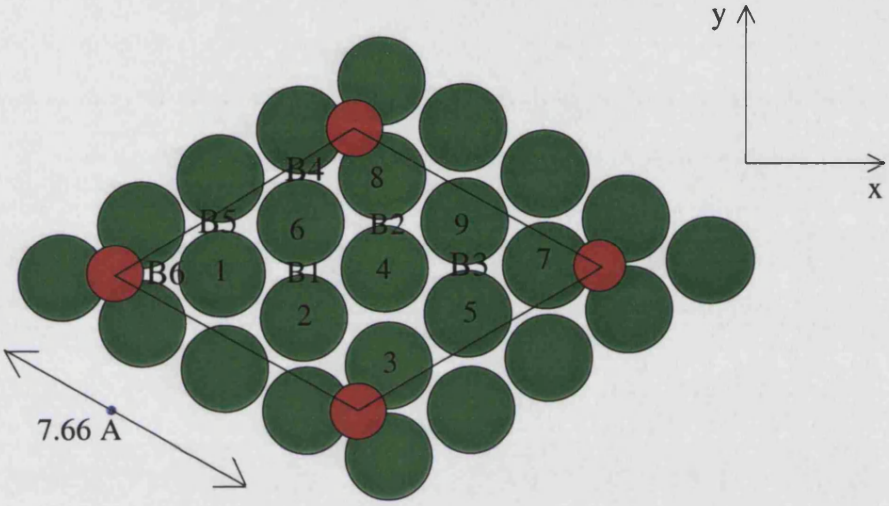

Figure 6.2: Plan view of the Cu(111) surface. Solid line indicates the 3×3 in-plane supercell. The atomic adsorbates are marked as red circles and the six inequivalent bridge sites as B1 to B6.

For this coverage of $\theta=\frac{1}{9}$ the atomic adsorbates are separated by 7.66Å. The entire system with both adsorbates present therefore consists of 45 Cu atoms, 1 atomic adsorbate (either H, O or K) and 1 H_2 molecule in each supercell. The calculations were performed with a plane wave cut-off of 800eV and 18 special **k** points in the surface Brillouin zone. With reference to the fully converged results for the energy barrier for H_2 dissociation on clean Cu(111) (Hammer, 1994), these calculations should be well converged with respect to the above parameters of the calculation. The co-ordinates of the Cu atoms were held fixed in their bulk positions in all the calculations for simplicity. The size mismatch between H_2 and a Cu metal surface would prevent any displacement of the Cu atoms during

dissociation. It is straightforward to include more realistic situations where surface atoms would not be modelled in their bulk positions, i.e. for steps, terraces or for general thermal fluctuations, using first principles calculations and could have been included here with subsequent Harris functional analysis. However for this work, we were primarily interested in testing the Harris functional analysis and to this end we kept the systems tested as simple as possible.

In the calculations the generalised gradient correction (PW91) is used to calculate the exchange-correlation energy (Perdew, 1992). The PW91 approximation has been used to study a wide variety of adsorption systems and has become one of the standard approximations used.

In Figure 6.2, the two inequivalent bridge sites, B1 and B2, were selected out for the investigation into the promotion and poisoning of H_2 using the Harris functional approach described in the previous chapters. By doing so it was possible to make a comparison between longer range and shorter range interaction.

H, O or K atoms were placed at the sites marked by red circles.

The results of the plane wave self consistent calculations will be reported in the following order:

- First, the results of the calculations used to determine the equilibrium adsorption heights of the H, O and K atoms above the Cu(111) surface will be given.
- Second, the determination of the dipole correction function will be discussed.
- Thirdly, the calculation of the barrier height and PES on the clean Cu(111) surface is presented to confirm our calculation is in agreement with previously converged

results (Hammer, 1994).

- The next set of results will be the change in the H_2 dissociation barrier at bridge sites B1-B5 for each of the three atomic adsorbates.
- The final set of results will be the PES's for the H_2 molecule dissociating at sites B1 and B2 on the pre-doped surface.

6.4 Determining the H, O and K equilibrium adsorption heights

The expression for the adsorption energy of an adatom on a surface in terms of total energies is:

$$\Delta E_{ads} = E(slab + X) - E(slab) - E(X) \tag{6.2}$$

where $E(slab+X)$ is the total energy of the system with the adsorbate 'X' on the surface, $E(slab)$ is the total energy of the bare slab and $E(X)$ is the total energy of just the adsorbate. In all three calculations the supercell size and calculation parameters are kept the same. For the K adsorbate the vacuum gap was 7 layers of equivalent Cu layers whereas for the O and H adsorbate only 5 layers of vacuum gap were used. By determining the adsorption (which is the negative of the binding) energy of each atom as a function of height above the surface, the equilibrium adsorption height could be deduced from the minimum in the adsorption energy.

We find that the most favourable adsorption site for the O atom is in a fcc, three-fold hollow site as depicted by the red circles in Figure 6.2. The next most favourable site is

the hcp hollow, but this has a binding energy 0.13eV lower than the fcc site. The fcc site was chosen for all three adsorbates. Choosing between the fcc site and the hcp site was not a critical issue. Previous calculations for the K/Cu(111) system (Padilla-Campos, 1997) showed that in fact adsorption directly on top of a Cu atom was more stable than above the hollow sites. To maintain consistency in all the calculations, although this again is not critical, the adsorption site was kept the same for all three adsorbates. The important issue was being able to test the analysis in chapters 3, 4 and 5 on various promotion and poisoning systems; and particular systems was less important. The calculated adsorption heights were 0.97Å, 1.18Å and 3.00Å for the H, O and K atoms respectively. These calculations were carried out without the dipole correction.

6.5 The dipole correction

In section 2.8.9 it was discussed how for supercell calculations of adsorbate systems, an intrinsic electric field is set up across the cell when electronegative or electropositive atoms are adsorbed due to the adsorbate-induced dipole moment at the surface. This can be seen in Figure 6.3 which plots the local part of the self consistent potential averaged in planes across the length of the supercell for both the bare Cu(111) slab and K/Cu(111) calculations. (Referring to Figure 6.3, for the K/Cu(111) system, the length of the supercell was 25.01Å. The Cu layers are at -4.17Å, - 2.08Å, 0.0Å, 16.67Å and 18.76Å. The seven layers of vacuum are therefore contained within the central region of the supercell.) For the bare Cu(111) system the steep rise in the potential which constitutes the surface barrier can be clearly seen which levels off in the vacuum region. The potential level in the vacuum essentially defines the work function of the metal surface, the work function

being the difference between the Fermi energy and the potential energy in the vacuum.

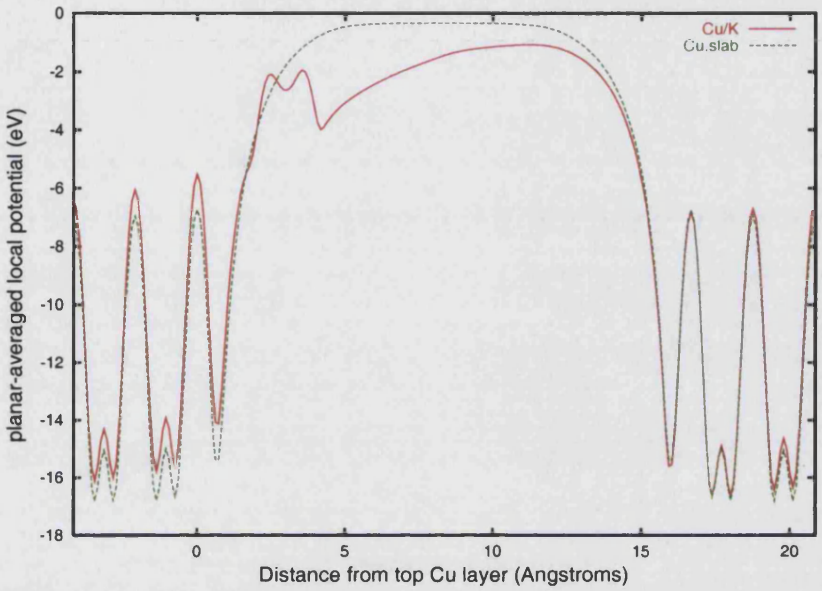

Figure 6.3: Planar-averaged local potential across the length of the supercell for the Cu/K system.

For the K/Cu(111) system, the presence of the K adsorbate on the surface has produced a potential gradient, i.e. an electric field, across the length of the supercell and it is this electric field that must be compensated for. An external potential is therefore added across the supercell such that a level planar-averaged local potential is restored in the vacuum region, as would be the case for an experimental situation of an isolated K atom on a semi-infinite surface. The appropriate function is displayed in Figure 6.4(a) and the resultant self consistent local potential for the K/Cu(111) system, after inclusion of this dipole correction into the minimisation of the total energy, is displayed in Figure 6.4(b). Two important things can be seen from Figure 6.4(b). First, the potential on the

non-adsorbate side of the slab is level and second, the presence of the K atom has clearly lowered the work function of the surface by approximately 4eV. This would be expected from alkali-metal adsorption (Zangwill, 1988).

For the O and H systems a similar analysis showed that the induced electric fields were negligible as was the effect on the calculated total energy with or without the dipole correction. Although O is a strongly electronegative atom, its small size coupled with the effective screening of the Cu(111) surface and the smaller adsorption height compared with K, prevented the need for inclusion of the dipole correction (see Figures 6.5, 6.9 and 6.10 (a) and (b)). The dipole correction is therefore unique for a given system.

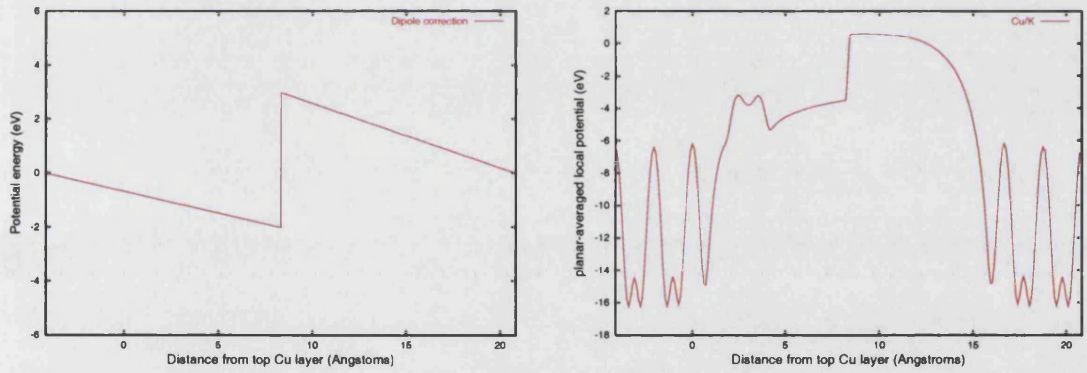

(a) (b)

Figure 6.4: (a) Added external potential and (b) Planar-averaged local potential for Cu/K system with added dipole correction.

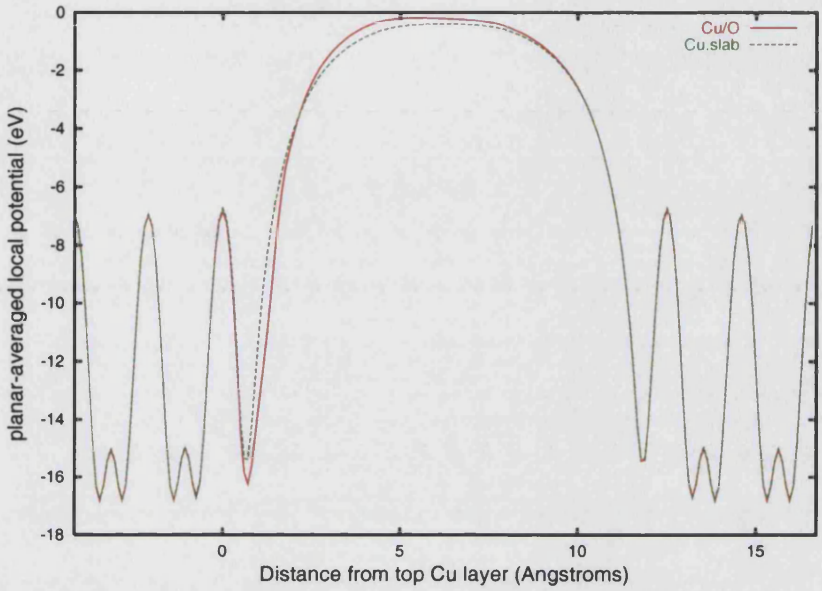

Figure 6.5: Planar-averaged local potential for the Cu/O system.

6.6 Calculation of the barrier for H_2 dissociation over Cu(111)

The transition state for the clean surface was investigated by placing the H atoms at a bridge site equivalent to those labelled in Figure 6.2, such that the H-H bond is parallel to the surface and the H atoms pointing towards the nearest hollow sites. Exactly the same calculation parameters were used as described above, except of course the omission of the atomic adsorbates at the corners of the cell. The expression for the barrier height for H_2 dissociation is given in equation (6.1), with the H_2 molecule in its transition state geometry above the bridge site. In order to calculate the PES for H_2 dissociation, the

molecule was placed at nine different points on a $Z - d$ grid around the (predicted) transition state on the clean surface, see Figure 6.7. Then using equation (6.1) for each point on the grid and applying a simple interpolation formula, the PES in Figure 6.6 was generated. Referring back to Figure 1.1 which displays the same PES for H_2 dissociating

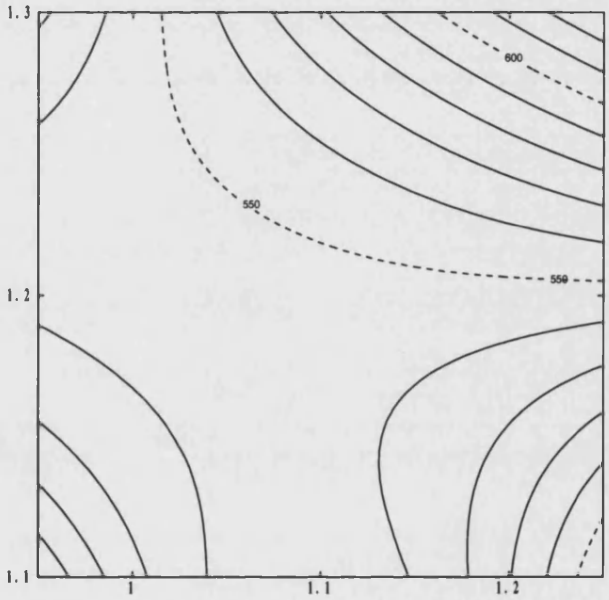

Figure 6.6: Section of the PES in the vicinity of the transition state for H_2 on clean Cu(111). Contour values are in meV and are the values taken directly from equation (6.1). The horizontal axis is the H-H bond length, d, in Å and the vertical axis is the height, Z, of the centre of the H_2 molecule above the top Cu layer in Å.

in the energetically most favourable orientation, it can be seen that the transition state (or saddle point) in our calculations is very similar, with the transition state at (Z, d) co-ordinates of (1.2Å , 1.1Å). The transition state was confirmed in our calculations by studying the forces on the two H atoms in this configuration after full minimisation of the total energy. The forces were zero to 3dp, indicative of a flat region in the PES associated with an energy barrier, in this case the minimum barrier configuration on the Cu(111) surface.

In equation (6.1) the term $E(H_2^{gas})$ refers to the total energy of an H_2 molecule in the gas phase, i.e. with an equilibrium bond length of 0.74Å. The molecule is not stretched to 1.1Å for this calculation because the barrier height to dissociation is defined as the energy barrier encountered by an approaching molecule *from the gas phase.*

The barrier calculated was 0.55eV, in agreement with the fully converged results in Hammer (1994). Although the GGA value is 0.73eV in Figure 1.1, which is from the same reference, it was concluded that this was not a fully converged answer with respect to slab thickness and the number of Cu atoms per layer in the supercell.

6.7 Adsorbate-induced barrier changes across the unitcell

The promotion and poisoning effect of each of the three atomic adsorbates was calculated with the H_2 molecule at each bridge site B1 to B5. Site B6 was not included as it was too close to an adsorbate atom to be meaningful. The configuration of the H_2 molecule was that of the transition state over the clean surface, i.e. d =1.1Å and Z =1.2Å. With the aim of keeping comparisons between different sites as simple as possible we used this configuration for all the bridge sites. Results for the dissociation barrier and the change in the barrier relative to the clean surface are presented in Table 6.2.

For the oxygen-covered system, Table 6.2 shows that site B4 is strongly poisoned by the presence of O, B2 is more weakly poisoned and sites B3 and B1 show a weak, but distinct promoting effect.

For the K covered system, Table 6.2 shows that all the bridge sites are poisoned and the

Bridge site	Distance from O/Å	Barrier/meV	ΔE/meV
B4	1.95	1175	+625
B2	2.66	725	+175
B5	3.21	570	+20
B3	3.68	495	-55
B1	4.10	500	-50

Bridge site	Distance from K/Å	Barrier/meV	ΔE/meV
B4	1.95	1070	+520
B2	2.66	749	+199
B5	3.21	721	+171
B3	3.68	704	+154
B1	4.10	698	+148

Bridge site	Distance from H/Å	Barrier/meV	ΔE/meV
B4	1.95	658	+108
B2	2.66	610	+60
B5	3.21	602	+52
B3	3.68	597	+47
B1	4.10	592	+42

Table 6.2: Values of the energy barrier to dissociation for H_2/Cu(111) with oxygen co-adsorbed, top Table, potassium co-adsorbed, middle Table and hydrogen co-adsorbed, bottom Table. Sites B1 to B5 are shown in Figure 6.2, and ΔE is the change relative to the barrier on clean Cu(111). In all cases the transition state has been assumed to have a bond length of 1.1Å and to be 1.2Å above the top layer Cu atoms.

effect increases as the adsorbate-molecule distance decreases.

For the H covered system, there is a poisoning effect similar to the K system, although not as strong.

These results show that the promoting and poisoning effect from each adsorbate is very much dependent on the particular site over which the H_2 molecule is dissociating. Intuitively, it would be expected that O would poison the H_2 dissociation and K promote

it. As stated in section 1.6.2, electronegative adsorbates tend to raise the work function of a metal surface whilst electropositive adsorbates decrease the work function. Dissociation of molecules at surfaces is normally accompanied by transfer of electrons from surface to molecule and so raising the work function of the surface would hinder this whereas lowering it would promote this process. This argument has been used previously to explain the electrostatic promoting effect of K on N_2 dissociation over Fe, e.g. in ammonia synthesis. Therefore the long range promoting effect of O and the poisoning of K is somewhat unexpected and is discussed in more detail in chapter 7.

Without calculating the actual PES for each bridge site, it is not possible to know whether the position of the transition state has changed from that of the clean surface. This was the next thing we investigated through first principles calculations. Two bridge sites were selected for this, B1 and B2. These two sites were focused on as they represent a comparison of shorter and longer range interaction and for the O covered system in particular, the difference in the promoting and poisoning effect could be investigated. The Harris functional analysis was carried out for these two bridge sites in order to try and explain the difference in short range and long range interaction shown by the self consistent calculations. The Harris functional analysis is presented in chapter 7.

6.8 Adsorbate-induced changes in the PES for H_2/Cu(111)

In this section we present the results of the self consistent calculations of the PES for H_2, at sites B1 and B2, on the adsorbate covered Cu(111) surface. The expression for the

barrier in the presence of the co-adsorbate is:

$$E(Cu + H_2 + X) - E(Cu + X) - E(H_2^{gas}) \tag{6.3}$$

where $E(Cu + H_2 + X)$ is the total energy of the combined system with both H_2 and an adsorbate on the surface. In order to gauge the change in the PES for H_2 dissociation, the molecule was again placed at nine different points on a $Z - d$ grid around the transition state on the clean surface, see Figure 6.7. Then using the expression in (6.3) for each point on the grid, the following PES's were generated, see Figure 6.8.

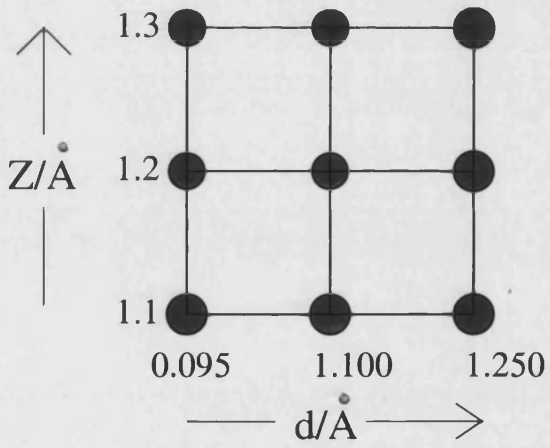

Figure 6.7: Grid showing nine different H_2 configurations, represented by the blue circles, used to calculate sections of the PES around the transition state configuration for the clean Cu(111) surface, i.e. (1.1Å, 1.2Å).

Induced changes to the PES over the clean surface due to the presence of H, K or O can now be gauged. To reiterate what has been said above, it can be seen that for bridge B2, which is 2.66Å from the atomic adsorbate, all three adsorbates are acting as poisons, whereas for B1, which is 4.10Å from the atomic adsorbate, the O is acting now as a promoter and the H and K still poisons. Table 6.3 summarises the results. For the K system the presence of the atomic adsorbate has resulted in a clear shift in the transition

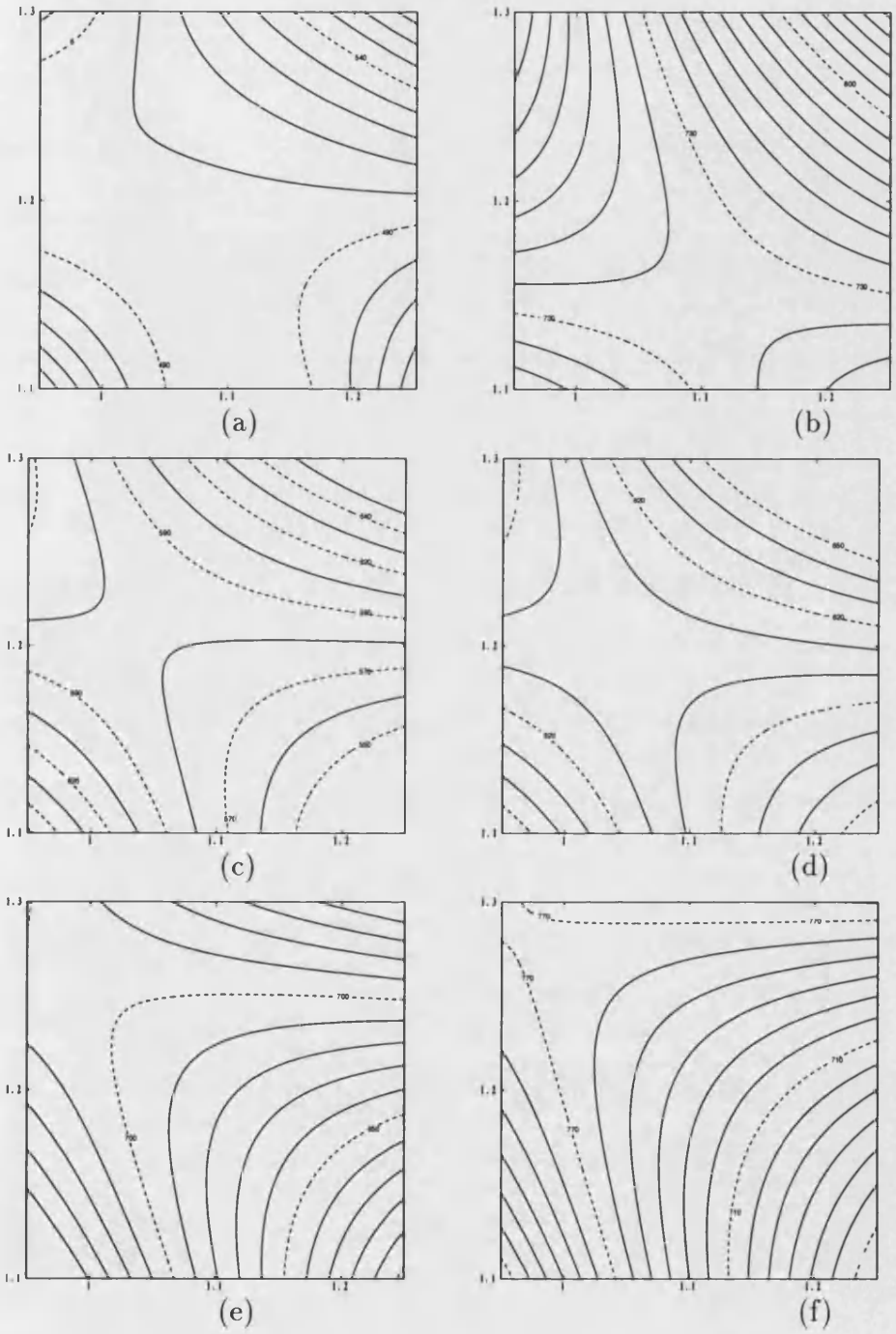

Figure 6.8: Sections of the PES in the vicinity of the transition state for H_2 on (a) oxygen-covered surface with H_2 at B1, (b) oxygen-covered surface with H_2 at B2, (c) hydrogen-covered surface with H_2 at B1, (d) hydrogen-covered surface with H_2 at B2, (e) potassium-covered surface with H_2 at B1 and (f) potassium-covered surface with H_2 at B2. The axis are the same as in Figure 6.6.

state. The shift is in the direction of the entrance channel and is more pronounced for B2 than B1. For the O-covered surface, the poisoning effect for B2 has coupled with a shift of the transition state to a region slightly, but not insignificantly, closer to the surface whereas for B1 the transition state position essentially has not changed from that of the clean surface. On the H-covered surface the poisoning effect seen at both bridges is not accompanied by a significant shift in the transition state position.

Adsorbate	B1 Δ E (eV)	Z (Å)	d (Å)	B2 Δ E (eV)	Z (Å)	d (Å)
O	-0.033	1.20	1.10	0.179	1.15	1.10
H	0.042	1.20	1.06	0.060	1.20	1.06
K	0.140	1.27	1.00	0.220	1.30	1.00

Table 6.3: Summary of the self consistent results for the promotion and poisoning from each of the three atomic adsorbates, with H_2 at either B1 or B2. ΔE refers to the change in the dissociation barrier caused by the atomic adsorbate and columns headed Z and d refer to the position of the 'new' transition state.

For the potassium systems, the increase in the barrier height and the shift in its position away from the surface is not surprising when the large size and electropositivity of the K atom is considered. Figure 6.9 shows the charge transfer induced by K adsorption on the clean Cu(111) surface, $\Delta n^K(\mathbf{r})$, where:

$$\Delta n^K(\mathbf{r}) = n[Cu(111) + K](\mathbf{r}) - n[Cu(111)](\mathbf{r}). \tag{6.4}$$

Here $n[Cu(111)+K](\mathbf{r})$ is the self consistent ground state charge density of the Cu surface with K adsorbed and $n[Cu(111)](\mathbf{r})$ is the charge density of the clean surface. Figure 6.9 reveals a noticeable enhancement of electron density in the surface region, away from the K atom. It can be seen that there is some mutual interaction between the K atoms across the unit cell. Given that the height of the transition state on the clean surface is 1.2Å, this

enhancement occurs in the vicinity of the transition state and could lead to an increase in the Pauli repulsion and hence the overall barrier. However without any quantitative analysis to back this up, the arguments are speculative.

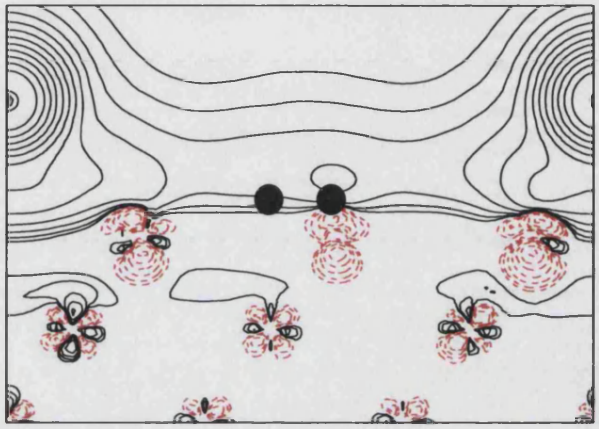

Figure 6.9: Change of electron density induced by K adsorption on Cu(111). Plane shown is perpendicular to the surface and runs through the K atoms and bridge B1. The small black circles mark the position of the H atoms at B1. Full (dashed) contours enclose regions of enhanced (depleted) electron density. The scale of the plot can be deduced from the H-H bond length of 1.1Å. Contours are at $\pm 0.94 \times 10^{-3}|e|\mathring{A}^{-3}$, $\pm 1.88 \times 10^{-3}|e|\mathring{A}^{-3}$, $\pm 3.76 \times 10^{-3}|e|\mathring{A}^{-3}$, $\pm 7.52 \times 10^{-3}|e|\mathring{A}^{-3}$,...

Figure 6.10(a) shows the change of electron density induced by O adsorption and a noticeable depletion of electron density in the surface region away from the adsorbate is revealed. This would suggest a decrease in the Pauli repulsion for an approaching H_2 molecule and a resultant lowering of the barrier. However this argument may work for B1 dissociation, but for B2 the effect was to raise the barrier.

Figure 6.10(b) shows the change of electron density induced by the H adsorbate. As with oxygen, the hydrogen atoms are drawing electrons towards them from neighbouring Cu atoms, although the effect appears to be less long ranged than for the O-covered system. However, for bridge B1, both the electronegative adsorbates (O and H) are producing opposing effects on the barrier height.

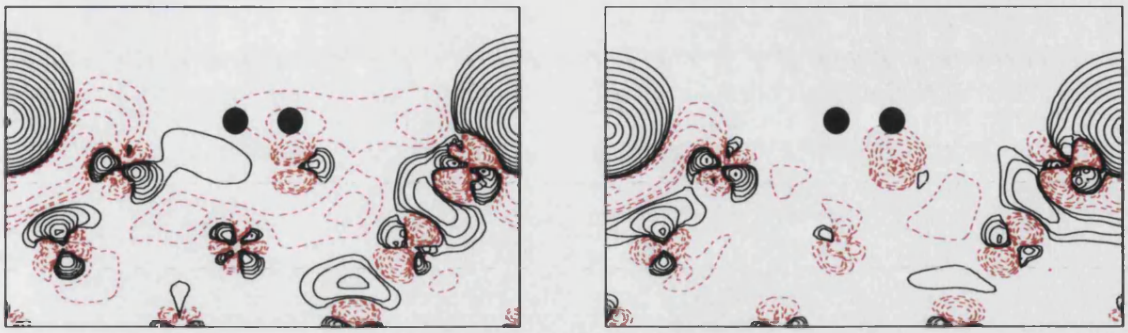

(a) (b)

Figure 6.10: Change of electron density induced by (a) : O adsorption on Cu(111) and (b) : H adsorption. Plane shown is perpendicular to the surface and runs through the O/H atoms and bridge B1. The small black circles mark the position of the H atoms at B1. Full (dashed) contours enclose regions of enhanced (depleted) electron density. The scale of the plot can be deduced from the H-H bond length of 1.1Å. Contours are at $\pm 0.94 \times 10^{-3}|e|\mathring{A}^{-3}$, $\pm 1.88 \times 10^{-3}|e|\mathring{A}^{-3}$, $\pm 3.76 \times 10^{-3}|e|\mathring{A}^{-3}$, $\pm 7.52 \times 10^{-3}|e|\mathring{A}^{-3}$,...

6.9 Conclusion

The discussion of the adsorbate-induced changes in the PES for H_2 dissociation on Cu(111) shows there are two clear avenues in the study of molecule-surface interaction - namely that of describing the motion and explaining the motion of a molecule as it interacts with a surface. The PES's above show changes in the position and height of the dissociation barrier and might also, if a larger region of phase space was sampled, reveal other changes in the topology of the H_2/Cu(111) PES. This *ab initio* data is the basis on which quantum dynamic simulations can be done to calculate, for example, the adsorbate-induced changes in the sticking coefficient for H_2. However, the question still remains as to why the energy barrier has changed in magnitude and position. The charge density plots seem to correlate with the changes in transition state position, i.e. the depletion (enhancement) of electron density due to O (K) adsorption allows (prevents) the H_2 molecule to come in closer compared to the clean surface before feeling the same Pauli repulsion from the metal *sp* electrons. However this analysis does not provide enough information to explain the changes in the barrier heights. This is a clear limitation of the first principles method

and shows the need for more analytical tools to aid the investigation.

In this section the first principles results have been stated for the effect of pre-adsorbed H, O and K on the dissociation of H_2 on Cu(111). The changes in position and magnitude of the barrier have been determined.

In the next chapter the analysis is extended using the frozen density and potential formalism discussed in chapters 3, 4 and 5. The aim is to understand the origin of Table 6.3.

Chapter 7

Analysis of the first principles results using the Harris functional

7.1 Introduction

In the last chapter, the promotion and poisoning effect of H_2 on Cu(111) was investigated via first principles, self consistent, calculations. Two bridge sites were selected for subsequent analysis using the Harris functional analysis developed in chapters 3, 4 and 5. These bridge sites are displayed in Figure 7.1, including the positions of the atomic adsorbates - H, K or O atoms. The analysis is presented in the following format:

- First, the one independent parameter in the Harris functional analysis, i.e. the cut-off radius of the shape function, is discussed. The focus is choosing the optimum radius for each of the six systems studied (three different atomic adsorbates with H_2 at either B1 or B2).

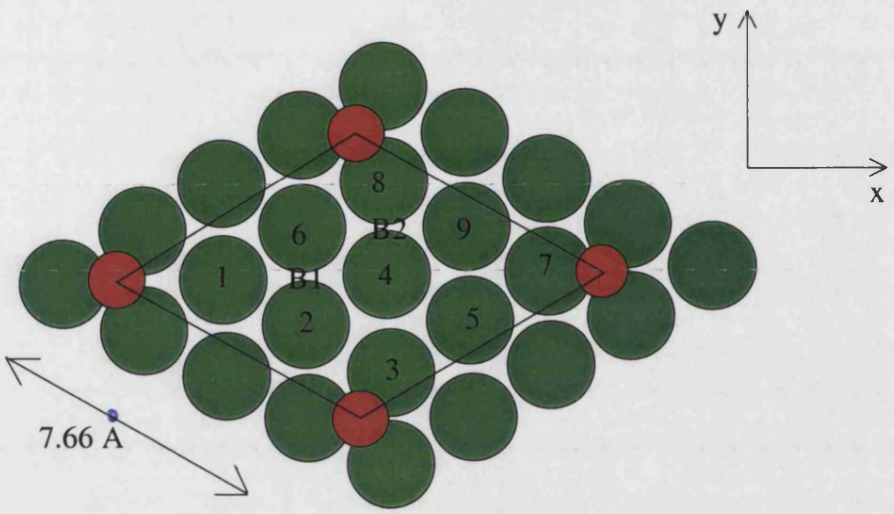

Figure 7.1: Plan view of the Cu(111). Solid line indicates the 3×3 in-plane supercell. The atomic adsorbates are marked as red circles and the two bridge sites as B1 and B2.

- Then, the overall conclusions across all six systems are given. The breakdown of the first principles results into the electrostatic component and the contribution through one-electron sums is compared for each of the systems.
- Next, the electrostatic contribution for all six systems is discussed, including the sign and magnitude of the interaction.
- Finally, the contribution through the one-electron sums for each of the six systems is presented.

7.2 Choice of shape function radius

The in-plane supercell is shown again in Figure 7.2 together with the shape function used. The shape function is a cylinder of radius R_c surrounding each atomic adsorbate which penetrates down into the slab. Three different radii are shown in Figure 7.2. Region I, in

Figure 3.1, corresponds to the volume enclosed by the cylinders and region II, the volume outside it. The one parameter that can be varied, therefore, is the radius of the shape function.

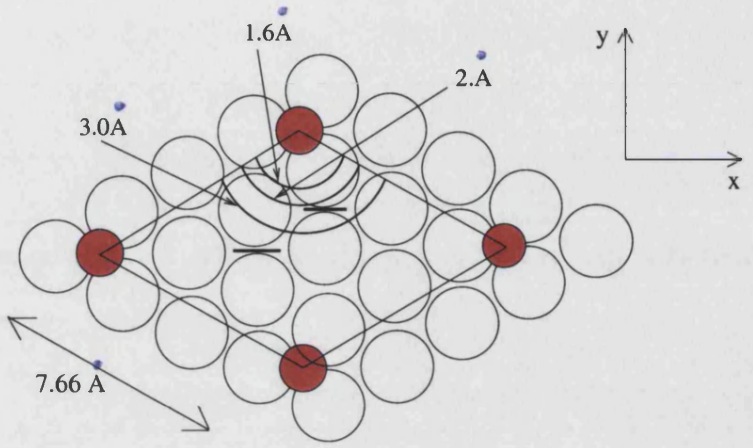

Figure 7.2: Unit cell showing the shape function, $S(\mathbf{r})$, for three different radii. For each radius there is a similar function around the other three atomic adsorbates, the total enclosed area constituting region I, with region II outside.

If, for example, the Harris functional result calculated using equation (3.25) yielded precisely (or was very close to) the self consistent interaction energy for a given cut-off radius, then it might be assumed that for that particular radius, the frozen density approximation, and the resultant analysis, was justified. However, the *conclusive* test is to repeat the analysis over a range of cut-offs close to the original cut-off. If the frozen density and potential result does not vary significantly with cut-off radius, using the approximation in equation (3.25) is justified. The reason for this is that the underlying assumption behind the division of space is that the charge density and potential in one region is insensitive to the presence of an adsorbate in the other region. A direct signature for this would be a result that was insensitive to a *range* of cut-off radii. If, for example, the Harris functional result is sensitive to cut-off radii and yet for one particular radius the agreement with the self consistent result is good, it would be unclear whether such a result was valid, perhaps other factors (such as inherent cancellations in the calculation,

for example) had conspired to produce the result.

A method of 'homing in' on the range of cut-off radii to use in a calculation would be to analyse the electronic charge density induced by the adorption of the atomic species or the H_2 molecule. The division of space should be such that the excess charge from the atomic adsorbate in region I should mostly be contained within the cut-off radius and likewise most of the excess charge induced by the H_2 molecule should be contained in region II. Figure 7.3 shows plots of the total induced charge density $\Delta n(r)$ as a function of the cut-off radius r. For the atomic adsorbates this is the total induced charge within the cut-off radius whereas for the H_2 adsorbate the line represents the induced charge outside the cut-off radius. The result for H_2 at B2 is also shown.

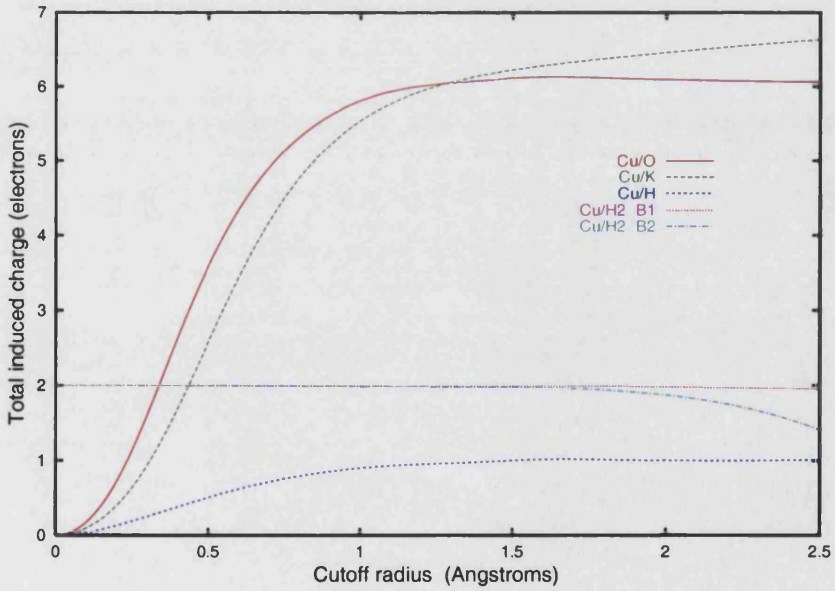

Figure 7.3: Induced charge contained within region I for the atomic adsorbates and region II for the H_2 adsorbate at both B1 and B2.

For the O-covered system, for example with the H_2 at B1, we would expect the optimum range of radii to be large enough to enclose the 6 valence electrons from the atomic adsorbate, but not so large as to reduce the excess charge from the H_2 molecule in region II to significantly less than 2 electrons. Between 1.0 and 2.0Å would seem a suitable range, for which the excess induced charges for region I and II are 5.82 and 2.00 electrons for the 1.0Å radius and 6.10 and 1.99 electrons for the 2.0Å radius.

For the K-covered system the large size of the K adsorbate prevents a division of space where close to 7 electrons are enclosed in region I and 2 electrons in region II (see also Figure 6.9). For this system, the optimum range of radii would most likely be between 2.0 and 3.0Å for B1 and between 1.5 and 2.0Å for B2. For B1, the K-induced and H_2-induced valence charge densities being 6.46 and 1.99 electrons for the 2.0Å radius and 6.76 and 1.90 electrons for the 3.0Å radius.

For the H-covered system, the optimum range of radii is between 1.0 and 2.0Å for both bridge sites.

Referring to Figure 7.3, the radius of the shape function cannot go beyond 2.0Å for H_2 at B2, otherwise region I would contain *both* adsorbates.

The six tables that follow show for each system the stability of the total Harris functional result in equation (3.25) with respect to the shape function radius. Also shown is the balance of terms between the electrostatic term and one-electron sums.

Cutoff(Å)	Electrostatic (eV)	$\Sigma\epsilon_i$ (eV)	Total(eV)	S.C (eV)
1.0	0.000	-0.050	-0.050	-0.033
1.2	-0.004	-0.035	-0.039	-0.033
1.4	-0.010	-0.027	-0.037	-0.033
1.6	-0.015	-0.023	-0.038	-0.033
1.8	-0.017	-0.021	-0.038	-0.033
2.0	-0.019	-0.022	-0.041	-0.033
2.2	-0.017	-0.029	-0.046	-0.033

Cutoff(Å)	Electrostatic (eV)	$\Sigma\epsilon_i$ (eV)	Total(eV)	S.C (eV)
1.5	0.096	0.011	0.107	0.140
1.8	0.101	0.016	0.117	0.140
2.0	0.103	0.020	0.123	0.140
2.2	0.095	0.024	0.119	0.140
2.5	0.080	0.031	0.111	0.140
3.0	0.047	0.029	0.076	0.140

Cutoff(Å)	Electrostatic (eV)	$\Sigma\epsilon_i$ (eV)	Total(eV)	S.C (eV)
1.6	-0.001	0.039	0.038	0.042
2.1	0.001	0.038	0.039	0.042

Table 7.1: Breakdown of the approximate interaction energy (calculated within the Harris functional, equation (3.25)) for H_2 with either O, K or H atomic adsorbates, into electrostatic and one-electron components. The top Table refers to the oxygen-covered system, the middle Table the potassium-covered system and the bottom Table the hydrogen-covered system. H_2 is at bridge B1. The third column shows the total interaction energy using equation (3.25) and column 4 is the self consistent result.

for for

Although from Figure 6.8 the position of the H_2 transition state has changed from that over the clean surface, the results in Tables 7.1 and 7.2 all refer to the H_2 molecule in a configuration of the *clean* surface transition state. When investigating promotion and poisoning systems, see equation (3.6), the H_2 molecule in the α system is at the transition state on the adsorbate-covered surface. However, because of the way the Harris functional

Cutoff(Å)	Electrostatic (eV)	$\Sigma\epsilon_i$ (eV)	Total(eV)	S.C (eV)
1.2	-0.002	0.181	0.179	0.179
1.3	-0.018	0.193	0.175	0.179
1.5	-0.034	0.206	0.172	0.179
1.8	-0.074	0.233	0.159	0.179

Cutoff(Å)	Electrostatic (eV)	$\Sigma\epsilon_i$ (eV)	Total(eV)	S.C (eV)
1.5	0.204	-0.027	0.177	0.199
1.6	0.215	-0.030	0.185	0.199
1.8	0.247	-0.039	0.208	0.199
2.1	0.347	-0.084	0.263	0.199

Cutoff(Å)	Electrostatic (eV)	$\Sigma\epsilon_i$ (eV)	Total(eV)	S.C (eV)
1.2	0.006	0.046	0.052	0.060
1.4	0.006	0.045	0.051	0.060
1.7	0.008	0.042	0.050	0.060
2.0	0.009	0.040	0.049	0.060

Table 7.2: Breakdown of the approximate interaction energy (calculated within the Harris functional, equation (3.25)) for H_2 with either O, K or H atomic adsorbates, into electrostatic and one-electron components. The top Table refers to the oxygen-covered system, the middle Table the potassium-covered system and the bottom table the hydrogen-covered system. H_2 is at bridge B2. The third column shows the total interaction energy using equation (3.25) and column 4 is the self consistent result.

analysis is constructed, the configuration of the H_2 molecule for both the α and δ systems must be the same. Strictly speaking, we are analysing, in this chapter, the change in adsorption energy of an H_2 molecule in the configuration $Z = 1.2$Å and $d = 1.1$Å on the clean Cu(111) surface compared with that on an adsorbate-covered surface with the molecule in the same configuration.

7.2.1 Conclusion

Tables 7.1 and 7.2 shows that the (total) Harris functional approximation works strongly for the O and H-covered systems and less so for the K-covered systems. This is to be expected due to the large size of the K atom preventing the charge separation shown in Figure 7.3 from being as clean as the O and H atoms. For the oxygen and hydrogen-covered systems, the range of cut-off radii which show good stability with respect to the self consistent result are shown in bold. Selecting a particular radius for further analysis with respect to the DOS's projected onto various atoms and orbitals is therefore straightforward for these four systems. For the K-covered system at the short range B2 site, the only option is to choose the radius which gives the closest agreement with the self consistent result. However, this is not ideal in light of the discussion earlier, and the conclusion here is that probably this system is not particularly suited to the Harris functional analysis.

The next thing to study is the stability of the electrostatic and one-electron contributions as a function of the shape function radius. At the longer range B1, both contributions are showing good stability within the selected ranges shown in bold in the Tables. For B2, the H-covered system is very stable, however the O-covered system is becoming slightly less stable than it was with the H_2 at B1. The K-covered system at B2 is again unstable.

Overall, this means that the long range systems are well suited to the Harris functional analysis, whereas at short range only the small H adsorbate provides a system with good stability as a function of the shape function radius.

For the O-covered system at B2, the instability is not that significant. First , the total Harris functional result is in good agreement with the self consistent result over a range of

radii and second, the conclusion that the one-electron contribution is dominating is still clear across the range.

The results for the K system at short range are not that convincing; however there is still something to be learnt from the result for this system in Table 7.2, i.e. the electrostatic terms are dominant.

The particular cut-off radii chosen are given in the next section.

7.3 Summary of the Harris functional analysis

The following table collates the results from Tables 7.1 and 7.2 at the optimum radius chosen for each of the six systems. This enables an overall comparison between the six systems to be gauged before going into the detailed arguments for particular systems.

System	Cutoff(Å)	Electrostatic (eV)	$\Sigma\epsilon_i$ (eV)	Total(eV)	S.C (eV)
B1 O	1.6	-0.015	-0.023	-0.038	-0.033
B1 H	1.6	-0.001	0.039	-0.038	-0.042
B1 K	2.0	0.103	0.020	0.123	0.140
B2 O	1.3	-0.018	0.193	0.175	0.179
B2 H	1.2	0.006	0.046	0.052	0.060
B2 K	1.8	0.247	-0.039	0.208	0.199

Table 7.3: The Harris functional approximation, equation (3.25), to the self consistent interaction energies across all six systems. Also included is the contribution through the electrostatic term and the one-electron sums. For the H-covered system, the dominant interaction comes through the one-electron sums. For K, the poisoning effect is a result of the strong electrostatic interaction between the H_2 molecule and the large electropositive atom. On the O-covered system, the long range promotion is a result of both electrostatics and electronic effects through the one-electron sums and the short range poisoning comes predominantly through the calculated one-electron sums.

Table 7.3 shows the results for each system at an optimum cut-off radius. These radii

were subsequently used for the one-electron sum analysis through the density of states projected onto individual atoms and orbitals. The broad conclusions that can be drawn from Table 7.3 are the following:

- For the K-covered systems at both bridge sites, the dominant poisoning effect is coming as a result of a strong electrostatic interaction between the H_2 molecule and K atom. Despite the instabilities in the Harris functional result discussed earlier in this chapter, this is still a rather convincing conclusion, although it is difficult to be quantitative and give an accurate magnitude for this effect. It can be said, however, that the interaction is of the order 0.1eV for B1 and 0.2eV for B2. (In contrast, electropositive adsorbates, such as Na and Cs, have been argued to *promote* N_2 dissociation through strong electrostatic interactions (Mortensen, 1998)).

- The poisoning effect from H comes predominantly through the one-electron sums. This is to be expected from the small size of atomic H yielding negligible electrostatic effects.

- The O-covered surface is more interesting due to both the promoting and poisoning effects that have been calculated. At both bridge sites the electrostatic effect from O is both small and promoting and the effect larger for B2 than B1. It is therefore the contribution through the one-electron sums that governs whether the overall interaction is promoting or poisoning. At short range the one-electron sum contribution is dominant, whereas at the long range B1 site, the magnitude of this interaction is similar to that of the electrostatic contribution.

The results in Table 7.3 could not have been derived from the first principles calculations alone. For the O and H-covered systems, we have some reliable quantitative interpretation

to the promoting and poisoning effects reported in the previous chapter. Even for the K system, the results suggest a strong electrostatic interaction as expected. However, more questions are raised than answered from Table 7.3. For example, why is the effect through the one-electron sums from oxygen promoting at long range and yet poisoning at short range, and why does hydrogen poison at long range through the one-electron sums whereas oxygen promotes.

This is clearly the more detailed interpretation that it was hoped at the outset the Harris functional analysis would provide. The one-electron sums were therefore analysed in terms of the DOS, as discussed in chapter 5, and the results are presented later in this chapter in an attempt to provide the answers to these and other questions. First, though, a little more is said about the electrostatic results in Table 7.3.

7.4 The electrostatic contribution

The magnitude and sign of the electrostatic contributions given in Table 7.3 are correct for the particular cut-off radius chosen. They are certainly the most reliable values that can be obtained. Their accuracy, i.e. how close they are to the true electrostatic contribution to the self consistent results, depends on the success of the frozen density and potential approximation for a particular system. The O-covered systems are better suited than the two K-covered systems but even here the best accuracy we can hope for is to 10meV. For the oxygen B1 system, the overall interaction is only -33meV and having been able to show, using the Harris functional analysis, that there is a small but significant electrostatic contribution is an important result in itself. For the potassium B1 system, the contribution is of the order 100meV and for the B2 system of the order 200meV, although the confidence

in the frozen density and potential approximation is considerably less for the latter system.

Despite the limitations in determining the magnitudes of the electrostatic interactions accurately, the values calculated, particularly for the oxygen systems are still more reliable than similar values calculated using the dipole-dipole model discussed in chapter 1. However, it is interesting to calculate and compare with values obtained using this model and, in particular, it can help us to understand the *sign* of the electrostatic interaction.

7.4.1 Comparison with the dipole-dipole model

The expression for the dipole-dipole interaction energy is:

$$\Delta E = -\epsilon\mu \tag{7.1}$$

where ϵ is the electric field induced by the atomic adsorbate at the position of the dissociating H_2 molecule and μ is the induced dipole moment of the dissociating H_2 molecule. The dipole moment μ has been calculated for the H_2 transition state on the clean Cu(111) surface:

$$\mu = \int d^3\mathbf{r} z \Delta^R n(\mathbf{r}) = +0.067 e\mathring{A} \tag{7.2}$$

where z is the co-ordinate perpendicular to the surface and $\Delta^R n(\mathbf{r})$ is the induced charge density redistribution caused by the H_2 molecule in its transition state, i.e.:

$$\Delta^R n(\mathbf{r}) = n[Cu(111) + H_2] - n[Cu(111)] - n[H_2] \tag{7.3}$$

where $n[Cu(111) + H_2]$ is the charge density of the full Cu(111)/H_2 system, with H_2 in its transition state, n[Cu(111)] is the density of the clean surface and $n[H_2]$ is the density

of an H_2 molecule without the Cu slab but in a geometry corresponding to the transition state. A plot of $\Delta^R n(\mathbf{r})$ is given in Figure 7.4 which shows there is a depletion of electrons from the H-H bond and an enhancement between the H_2 and the surrounding Cu atoms. This is as expected, since the H-H bond is being broken by the filling of anti-bonding states while surface-H bonds are being formed. The positive sign of the H_2 molecule dipole moment can now be justified: - normally adsorption or dissociation of molecules at surfaces is accompanied by a transfer of electrons from metal to molecule. This would normally lead to a negative dipole moment, as in the case of N_2 in its transition state over an Fe surface. However, for H_2 dissociation, the distribution of $\Delta^R n$ is less straightforward and it is the depletion of electron density furthest from the surface which, in this case, ultimately decides the sign of μ.

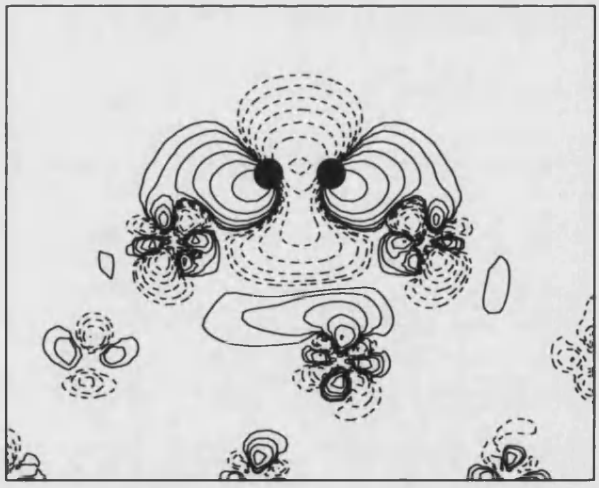

Figure 7.4: $\Delta^R n(\mathbf{r})$, defined in equation (7.3), for H_2 in its transition state above a clean Cu(111) surface. The plane shown passes through the hydrogen nuclei. Full (dashed) contours enclose regions of enhanced (depleted) electron density. Contours are at $\pm 1.89 \times 10^{-3} e\text{Å}^{-3}$, $\pm 7.56 \times 10^{-3} e\text{Å}^{-3}$, $\pm 15.11 \times 10^{-3} e\text{Å}^{-3}$,...The scale of the plot can be determined from the H-H bond length of 1.1Å.

We determine ϵ in equation (7.1) from the O or K-induced change in the local part of the

self-consistent potential:

$$\delta\phi = \phi[Cu(111) + K/O] - \phi[Cu(111)]. \tag{7.4}$$

A plot of $\delta\phi$ as a function of distance normal to the surface for both bridge sites is shown in Figure 7.5. It can be seen that both the electronegative and electropositive adsorbate have induced an electric field outside the surface, of *opposite* sign. We take the value of ϵ $(d\Delta\phi_{K/O}/dz)$ where its absolute magnitude has a maximum, and combine this with the calculated value of $\mu = +0.067$eÅ. The results are shown in Table 7.4.

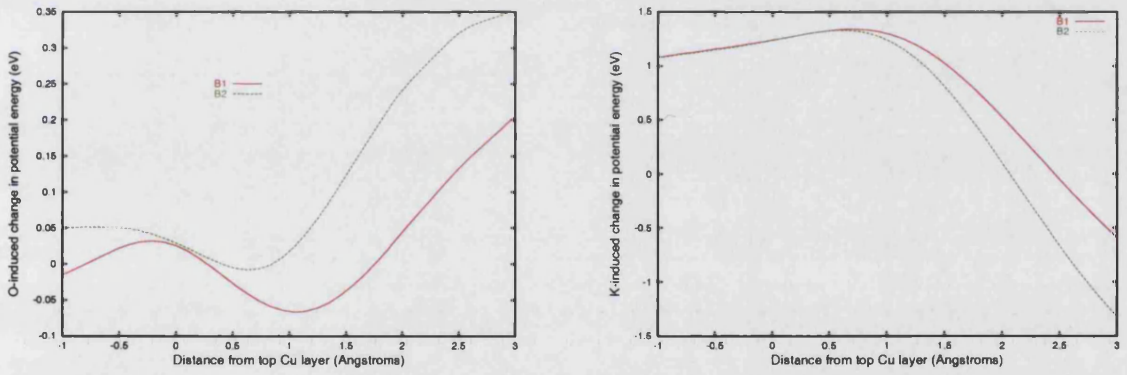

(a) (b)

Figure 7.5: $\delta\phi$, defined in equation (7.4), above B1 and B2 as a function of distance from the top Cu plane. Graph (a) is for the O-covered system and (b) for the K-covered system.

Table 7.4 shows that for the oxygen systems the simple dipole-dipole model describes well the electrostatic contribution, whereas for the K-covered systems the model is not producing values comparable to the results from the Harris functional analysis. The results above and those in the literature suggest that the model can be applied to longer range interaction where both adsorbates are well separated. At closer range, the model is just too simple too expect accurate results. However, the sign of the electrostatic interactions

System	Dipole-dipole energy (meV)	Harris electrostatic interaction (meV)
B1 O	-13	-15
B1 K	73	103
B2 O	-19	-18
B2 K	100	247

Table 7.4: Table comparing the electrostatic contributions in Table 7.3 to the corresponding values calculated using the simple dipole-dipole model.

in Table 7.3 can be understood using the dipole-dipole model.

7.5 One-electron sum breakdown

The results in Table 7.3 show that the contribution to the interaction energy through the eigenvalue sums is significant for both the O and H-covered systems. For potassium, the conclusion to be drawn is that the dominant process causing the poisoning is electrostatic in nature. In this section, therefore, we focus on analysing the one-electron sums for the oxygen and hydrogen systems.

The expression in (5.24) gave the contribution to the (free energy) eigenvalue sums from a particular basis function of the mixed basis set. Tables 7.5 and 7.6 show the eigenvalue sums for the O and H-covered systems, for sites B1 and B2, respectively, broken down into contributions from individual atoms and orbitals. The Cu atoms numbered 1-9 refer to the labels in Figure 7.1, i.e. the top layer of Cu atoms. The contributions from the Cu atoms in the four layers beneath the surface layer have been ignored as their contribution to the interaction energy was 0meV for all four systems. Hydrogen labelled H1 refers to the left-most hydrogen of the H_2 molecule of Figure 7.1 and H2 the right most hydrogen.

The localised pseudo-atomic orbitals were, for Cu: 4*s* 4*p* and 3*d*, for oyxgen: 2*s* and 2*p* and for H 1*s* and 2*p*.

	Oxygen B1			Hydrogen B1		
Cu Atom	4*s* (eV)	4*p* (eV)	3*d* (eV)	4*s* (eV)	4*p* (eV)	3*d* (eV)
1	0.000	-0.008	-0.001	0.001	-0.002	0.000
2	-0.006	0.007	-0.003	-0.002	0.004	0.000
3	0.000	-0.014	-0.001	0.001	0.000	0.001
4	-0.004	0.000	-0.004	-0.001	0.007	-0.001
5	-0.001	-0.002	-0.001	0.000	0.001	0.001
6	-0.006	0.007	-0.003	-0.002	0.004	0.000
7	0.002	-0.012	-0.003	0.002	0.003	-0.001
8	0.000	-0.014	-0.001	0.001	0.000	0.001
9	-0.001	-0.002	-0.001	0.000	0.001	0.001
Total	**-0.021**	**-0.023**	**0.016**	**0.004**	**0.020**	**0.003**
Orbitals	1*s*			1*s*		
H1	0.002	0.000	0.000	0.001	0.000	0.000
H2	-0.001	0.000	0.000	-0.001	0.000	0.000
Orbitals	2*s*	2*p*		1*s*		
O or H	0.002	-0.001	0.000	0.003	0.000	0.000
PW	0.037			0.007		

Table 7.5: Breakdown of the eigenvalue-sum for the oxygen and hydrogen-covered systems with H_2 at B1. Contributions from individual atoms and orbitals are shown. The row labelled 'Total' gives the total contribution to the eigenvalue sum from the top Cu layer for each of the orbitals 4*s*, 4*p* and 3*d*. The contribution from the plane wave component is also shown.

7.5.1 Long range promotion and poisoning

Focusing on the long range interaction first, with H_2 at bridge B1, it can be seen that the promotion due to the oxygen is strongest through the *sp* band, with a small effect coming through the *d* band. The poisoning on the H-covered surface is through the *p* band, with the *s* and *d* band showing a negligible contribution. The main conclusion to be drawn here is that for the long range bridge site, the interaction between the dissociating H_2

	Oxygen B2			Hydrogen B2		
Atom	4*s* (eV)	4*p* (eV)	3*d* (eV)	4*s* (eV)	4*p* (eV)	3*d* (eV)
1	0.003	-0.002	-0.001	0.001	-0.002	-0.001
2	-0.002	-0.021	0.002	-0.001	0.001	0.000
3	0.001	-0.031	0.010	-0.001	0.001	-0.001
4	-0.008	-0.003	-0.004	0.000	0.001	-0.001
5	-0.003	-0.001	-0.002	-0.002	0.005	0.000
6	-0.006	0.042	-0.003	0.000	0.024	-0.002
7	0.000	-0.003	0.001	0.004	0.011	-0.001
8	0.015	0.096	0.046	0.005	-0.044	0.027
9	0.002	-0.002	-0.004	0.003	-0.003	-0.001
Total	**0.004**	**0.076**	**0.042**	**0.016**	**0.011**	**0.022**
Orbitals	1*s*			1*s*		
H1	0.057	0.000	0.000	0.000	0.000	0.000
H2	0.018	0.000	0.000	0.000	0.000	0.000
Orbitals	2*s*	2*p*		1*s*		
O	-0.003	0.000	0.000	0.000	0.000	0.000
PW	-0.050			-0.010		

Table 7.6: Breakdown of the eigenvalue-sum for the oxygen and hydrogen-covered systems at B2. Contributions from individual atoms and orbitals are shown.

molecule and atomic adsorbate is substrate mediated, with the *sp* bands playing a more pivotal role than the *d* bands. This would be expected from the more localised nature of the *d* bands around each Cu atom.

In order to try and understand why the oxygen promotes and the hydrogen poisons, we have plotted in Figures 7.6 and 7.7 the following expressions:

$$S(\epsilon) = \overbrace{d^{sp}_{Cu}(\epsilon)}^{\alpha} + \overbrace{d^{sp}_{Cu}(\epsilon)}^{\beta} \tag{7.5}$$

and

$$T(\epsilon) = \overbrace{d^{sp}_{Cu}(\epsilon)}^{\gamma} + \overbrace{d^{sp}_{Cu}(\epsilon)}^{\delta} \tag{7.6}$$

where α, β, γ and δ refer to the four systems in equation (3.6), i.e.:

$$\overbrace{E(Cu + H_2 + H/O)}^{\alpha} \quad \overbrace{E(Cu(111))}^{\beta} \quad \overbrace{E(Cu + H/O)}^{\gamma} \quad \overbrace{E(Cu + H_2)}^{\delta}. \tag{7.7}$$

$d^{sp}_{Cu}(\epsilon)$ is the sp DOS projected onto all nine surface Cu atoms. The overall expression for the promotion and poisoning in equation (3.6) is a balance between the properties of the α, β systems and those of the γ, δ systems. Plotting and comparing $S(\epsilon)$ with $T(\epsilon)$ could therefore give insight into the origin of the promotion or poisoning. Also plotted

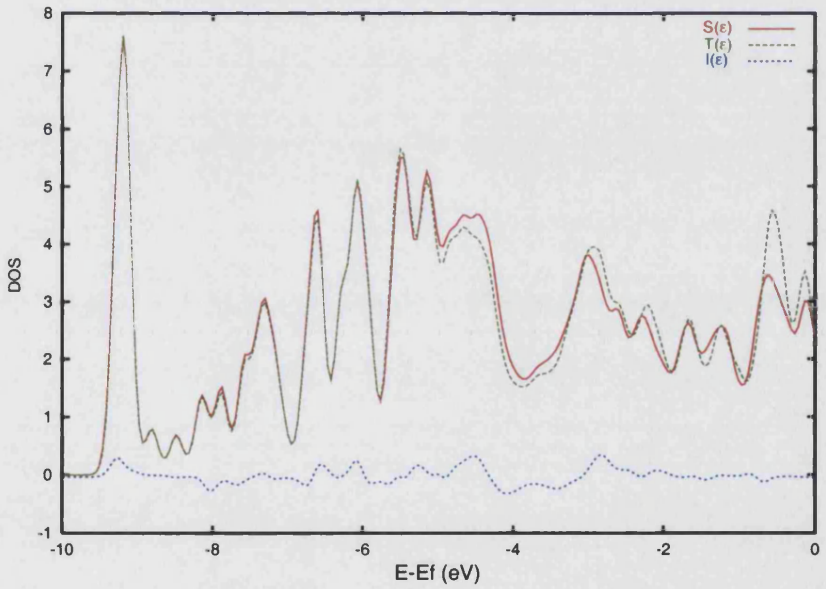

Figure 7.6: $S(\epsilon)$ and $T(\epsilon)$ for the O-covered system with H_2 at B1. Also plotted is the running integral of $(S(\epsilon) - T(\epsilon))$ across the band.

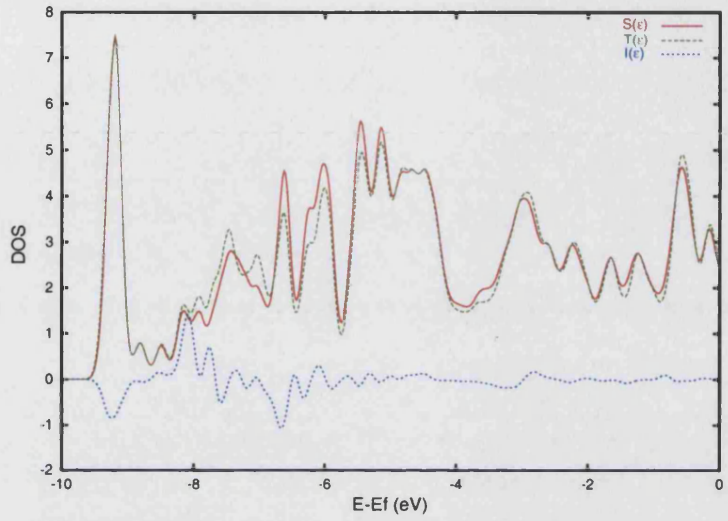

Figure 7.7: $S(\epsilon)$ and $T(\epsilon)$ for the H-covered system with H_2 at B1. Also plotted is the running integral of $(S(\epsilon) - T(\epsilon))$ across the band.

in Figures 7.6 and 7.7 is the following expression:

$$I(\epsilon) = \int_{-\infty}^{\epsilon} \epsilon(S(\epsilon) - T(\epsilon))d\epsilon. \tag{7.8}$$

In Figure 7.6, $I(\epsilon)$ is -0.044eV at the Fermi level which is equal to the total *sp* promotion in Table 7.5 for the oxygen system, and in Figure 7.7, $I(\epsilon)$ is 0.024eV at the Fermi level.

The onset of the promotion and poisoning in Figures 7.6 and 7.7 is unclear and no picture emerges to explain the role of the *sp* band in the overall interaction. What can be said is the effect appears to come from the entire band, as seen from the $I(\epsilon)$ curves. As stated in the previous chapter, the depletion of electron density shown in Figure 6.10(a) could result in a depletion in Pauli repulsion experienced by an approaching H_2 molecule leading to a lower barrier to dissociation. However, without a more quantitative model

linking the role of the *sp* band to a reduction in Pauli repulsion, interpreting Table 7.5 is difficult.

7.5.2 Short range promotion and poisoning

Table 7.6 shows the contributions to the eigenvalue sums from individual atoms and orbitals. For both systems, the key difference for this bridge site is the significant contribution through the *d* band, especially Cu atom 8 which is *shared* by the H_2 molecule and the atomic adsorbate. For the oxygen system, one of the hydrogen atoms is also contributing significantly.

Focusing on the O-covered system first, it is once again difficult to interpret the effect through the surface Cu *p* band, despite the magnitude of this substrate-mediated interaction. However, it is possible to understand the effect through the *d* band of Cu atom 8. Figure 7.8 shows $S(\epsilon)$ and $T(\epsilon)$ for the DOS projected onto the *d* orbitals of Cu atom 8. The relative positions of the two plots account for the poisoning in Table 7.6 and shows the model of Hammer and Nørskov relating to *d* band shifts within surface metal atoms, described in the introduction, to be applicable.

An equivalent analysis to explain the poisoning through the *d* states of Cu atom 8 for the H-covered system is shown in Figure 7.9. The effect is less pronounced but can still be observed.

In Table 7.6, there is a significant poisoning effect through the hydrogen *s* orbitals on the O-covered system. The origin of this effect can be seen by by projecting out the *s* states on, for example, the hydrogen atom labelled H1, for both the Cu+H_2 and Cu+H_2+O systems (the β and γ systems do not need to be considered here as they do not contain

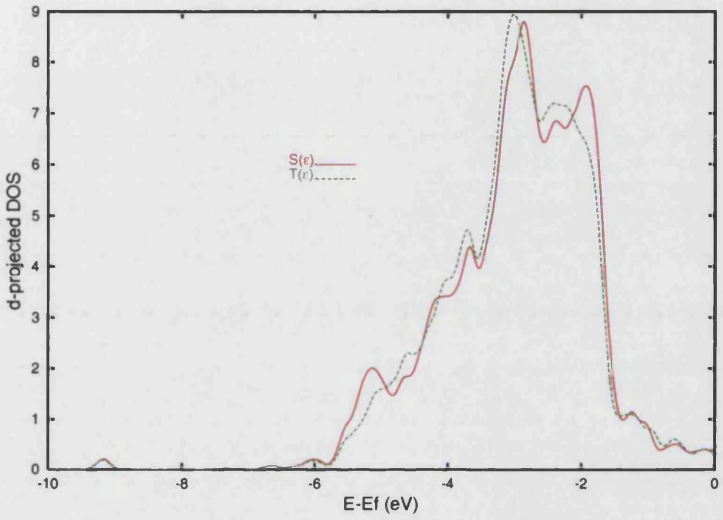

Figure 7.8: d DOS projected onto Cu atom 8 for $(\alpha + \beta)$ $(S(\epsilon))$ and $(\gamma + \delta)$ $(T(\epsilon))$ combinations.

the H_2 molecule). Figure 7.10 shows the projections and the shift upwards in energy for the H s state in the Cu+H_2+O system is clearly visible, which produces the poisoning effect.

7.6 Conclusion

The long range promotion and poisoning of H_2 at site B1, due to the presence of either H or O, has been shown to be a system particularly suited to an analysis based on the Harris functional within the frozen density and potential approximation. However, the atom and orbital breakdown of the eigenvalue sums, although interesting, did not prove to be very useful. For potassium, there is evidence of the approximation breaking down,

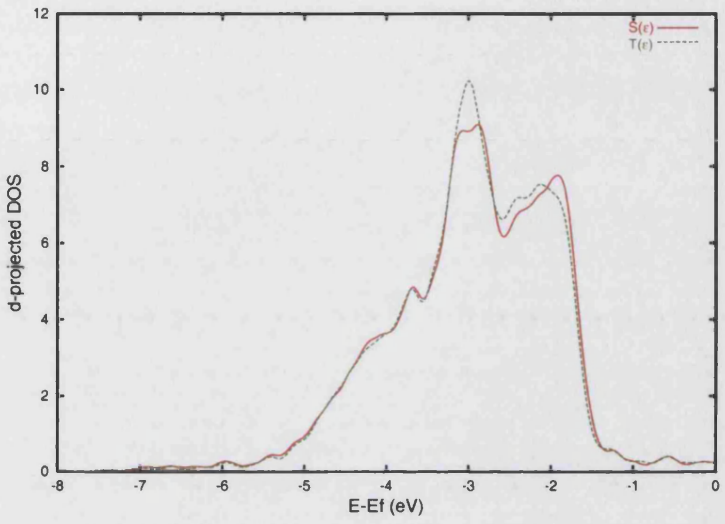

Figure 7.9: d DOS projected onto Cu atom 8 for $(\alpha + \beta)$ $(S(\epsilon))$ and $(\gamma + \delta)$ $(T(\epsilon))$ combinations.

although it can be seen from the results that an electrostatic interaction is dominant.

The short range promotion and poisoning of H_2 is less suited to the Harris functional analysis. With the exception of the H-covered system, the frozen density and potential approximation is starting to break down due, to the charge separation being less complete. For the potassium system, it can again be argued that the interaction is dominated by electrostatics. The atom and orbital breakdown for the O and H-covered systems again fell short of providing a full interpretation for the poisoning calculated through the one-electron sums. However, for Cu atom 8, the d band poisoning could be explained in terms of the Hammer and Nørskov model.

In general, the one-electron sum breakdown, using the mixed basis set, can provide *relative* contributions to the overall interaction from different atoms and orbitals, but interpreting

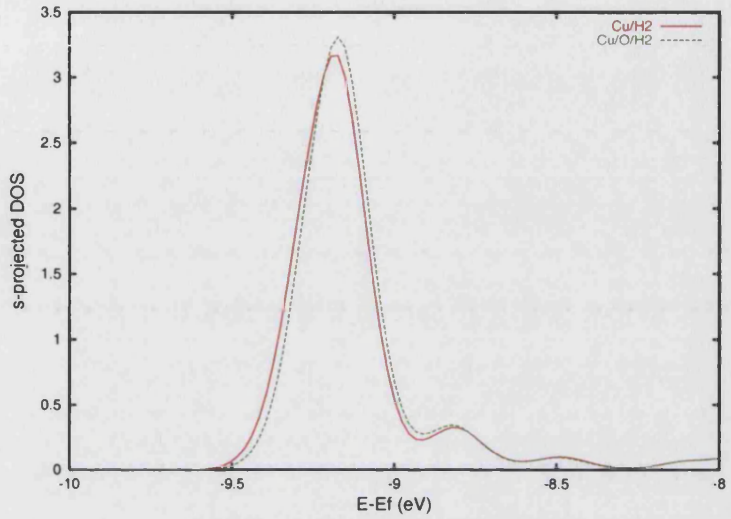

Figure 7.10: s DOS projected onto onto the H1 atom of the α and δ systems for the oxygen B2 system.

the answers is difficult.

Regarding the electrostatic contributions, the answers reported above are correct and can be used to test models such as the simple dipole-dipole model. For the potassium B2 system, it could be argued that the result is misleading, due to the Harris functional analysis breaking down, but even for this system the order of magnitude obtained is probably meaningful.

Chapter 8

Conclusions

8.1 Introduction

In this chapter we present the conclusions from this project, in particular:

- Why we chose this particular route as a possible solution to the problems posed in the introduction;
- What the main difficulties and obstacles were that had to be overcome;
- Whether the original objectives were actually met;
- Where we go from here for future work.

8.2 Harris functional DFT

The aim of the project was to enhance the ability to understand simple promotion and poisoning systems studied through first principles calculations. Although the energetics of these systems can be calculated to an accuracy comparable to experiment through first principles calculations, the subsequent interpretation is limited to applying simple models that fit or correlate with the first principles results. Although this has met with some success, a method that can actually substantiate these models quantitatively is a far more powerful tool, leading to greater confidence in knowing the underlying mechanisms of a particular process.

Any method posed would clearly have to start with a first principles approach and the DFT expressions it is based on. By manipulating these expressions for a co-adsorption system using the Harris functional, as described in chapter 3, we were able to reduce a complex expression to a simpler and more importantly interpretable expression. The Harris functional approach had been suggested previously (Hammer, 1997), as a method of achieving this. However, it had never been tested computationally, only used as a broad interpretative tool for using arguments based on electrostatic interactions and one-electron sums.

The derivation in chapter 3 was straightforward and provided a full DFT justification for reducing the interaction of two species on a surface to a purely electrostatic component plus a contribution through properly calculated one-electron sums. The only physical condition to the approximation was having the adsorbates sufficiently separated, so that the electron density and potential in the surrounding region was, to a good approximation, insensitive to the presence of the neighbouring adsorbate. Choosing a cylindrical shape

function to describe the division of space seemed a natural choice, especially since the analytic Fourier components were trivial to calculate.

8.3 Calculating the terms in the approximate interaction expression

8.3.1 The electrostatic terms

Chapter 4 described how to calculate the electrostatic component to the approximate interaction energy. The key points here were the addition of the extra charge to maintain charge neutrality within the periodic system and the use of real space coefficients by FFT of the relevant periodic quantities, i.e. the self consistent charge densities, the local ionic pseudopotential for each adsorbate and the shape functions.

Inclusion of the pseudopotential core correction was also necessary and was equal to the contribution in a purely self consistent approach.

8.3.2 The one-electron sums

The mixed basis set provided a computationally efficient method of calculating the eigenvalues for each of the four systems in equation (3.25). The Fourier components of the frozen potentials, represented as full self consistent local potentials multiplied by the appropriate shape function, were trivial to calculate and incorporate into the mixed basis code. The time taken to diagonalise the Hamiltonian matrix was approximately

4 hours per **k** point, with each **k** point calculation being carried out simultaneously on parallel nodes of an Origin 2000 workstation.

Aligning the potentials in each of the four one-electron sums was critical in order to identify a common Fermi energy.

Projecting the DOS onto different atoms and orbitals was straightforward. The overall contribution to the eigenvalue sums, calculated via the DOS route, was equivalent to the free energy. The contribution from individual atoms and orbitals could be determined to assess those which were significant to the overall promotion and poisoning effect.

The recipe outlined here would, in principle, meet the objective of interpreting a first principles investigation into promotion and poisoning. The theory is general in the sense that it can be applied to any system, as in Figure 3.1, containing two species near a solid surface. The context for our work was the interaction of an atomic adsorbate with an H_2 molecule, which had been placed in the configuration corresponding to the transition state on the clean surface.

8.4 First principles investigation into promotion and poisoning of H_2/Cu(111)

Table 6.2 showed the promotion and poisoning effect of each of the atomic adsorbates for five different bridge sites within the surface unit cell. For the K and H adsorbate, the poisoning effect decreased as the molecule-adsorbate distance increased, whereas for the O adsorbate the interaction went from that of poisoning to promoting.

The first principles results also illustrate the complexity of studying promotion and poisoning systems and the range of effects that can occur across a surface. The PES's in Figure 6.8 showed whether the atomic adsorbates are causing a shift in the H_2/Cu(111) transition state at the two bridge sites chosen (these bridge sites were subsequently chosen for the Harris functional analysis. For K, the shift in the transition state away from the surface is expected for a large electropositive adsorbate, as is shown in the calculated PES. For the O adsorbate the shift for B2 is towards the surface as would be expected from a strongly electronegative atom, however due to its small size this effect is not seen at B6 for the longer range interaction. The small H atom, adsorbed closer to the surface than the O or K, is not causing a significant shift in the position of the barrier at either bridge site.

Despite the lack of interpretability, the first principles calculations have provided a lot of information about these systems which would be difficult to infer from experiment alone.

8.5 Harris functional analysis, long range interaction - B1

The long range promotion and poisoning of H_2 at bridge B1 has shown to be a system particularly suited to the frozen density and potential analysis and was one of the reasons for choosing it. This was illustrated by the stability of the Harris functional analysis as a function of the cut-off radius of the shape function.

For the H and O-covered systems, the overall interaction is quite small, although still significant. This did not necessarily imply that tracing the origin of the interaction

would be difficult, although this did prove to be the case. The interaction through the one-electron sums was primarily through the metal *sp* band, with a small electrostatic contribution for the O-covered system, which was comparable to a value obtained via the dipole-dipole model. Any role surface states might be playing in the interaction is difficult to gauge from a first principles method based on a slab approach, due to the splitting of the surface state band into a symmetric and anti-symmetric combination (Bird, 1998).

For the K-covered system, the Harris functional analysis was stable over a range of cut-off radii, but overall was less stable than the O and H-covered systems. The analysis showed that the dominant contribution to the interaction was electrostatic in nature, in agreement with previous work on alkali metals.

Although the frozen density and potential analysis did provide further interpretation to the first principles result, determining precisely how the interaction manifests itself through the *sp* band was not possible.

8.6 Harris functional analysis, short range interaction - B2

The results show that bridge B2 is less suited to the Harris functional analysis, in particular for the K-covered system. The poisoning from the H and O for this bridge site has a significant contribution through the *d* band, especially from Cu atom 8, which is shared by both adsorbates. Projecting the DOS onto the *d* band for this Cu atom showed that the poisoning effect can be described by the model proposed by Hammer and Nørskov involving *d* band shifts. This result in particular gives confidence in the

Harris functional analysis. The *d* band model has been used extensively throughout the literature to describe the reactivity of transition metal surfaces, including promotion and poisoning systems where both species share a surface atom.

Using the Harris functional analysis for the K-covered system should be carried out with caution. The system is not stable with respect to cut-off radius, despite the close agreement at approximately 1.8Å. However, to infer a dominant electrostatic contribution is probably justified, the precise magnitude of which is unclear.

8.7 General remarks

The model system investigated in this work illustrated that the frozen density and potential analysis can be successfully applied to a promotion and poisoning system. The terms in the approximate interaction expression, equation (3.25) can be calculated to give a result in good agreement with the first principles result. The stability observed as a function of the one independent parameter in the analysis, the division of space, is a necessary condition to implement the method. The result of this is that the Harris function analysis is a tool more suited to long range interaction, where the induced charge densities from either adsorbate do not interact significantly.

The use of the Harris functional analysis to investigate other co-adsorbate systems is encouraged for future studies. The challenge is to increase the interpretability from the one-electron sum analysis, in particular the role of *sp* electrons in promotion and poisoning systems.

Appendix A

Appendix

Using this choice of $g(x)$ we find:

$$\sum_i \int_{-\infty}^{E_F} d\epsilon(-\frac{1}{kT}) f'(\frac{\epsilon - \epsilon_i}{kT}) \tag{A.1}$$

as the expression for the total number of electrons in the system. By letting

$$y = \frac{\epsilon - \epsilon_i}{kT} \Rightarrow kT dy = d\epsilon, \tag{A.2}$$

we find:

$$-(\frac{kT}{kT}) \sum_i \int_{-\infty}^{\frac{\epsilon_F - \epsilon_i}{kT}} dy f'(y) = -\sum_i [f(\frac{\epsilon_F - \epsilon_i}{kT}) - 1]. \tag{A.3}$$

But $f(-x) = 1 - f(x)$ and $f(x) = 1 - f(-x)$, which gives the result:

$$\sum_i f(\frac{\epsilon_i - \epsilon_F}{kT}) = N \tag{A.4}$$

which suggests that the relevant function is indeed $-\frac{1}{kT}f'(x)$. We now begin to work with the eigenvalue sums. We have:

$$\sum_i \int_{-\infty}^{E_F} d\epsilon\ \epsilon g(\frac{\epsilon - \epsilon_i}{kT}) = \sum_i \int_{-\infty}^{E_F} d\epsilon\epsilon(-\frac{1}{kT})f'(\frac{\epsilon - \epsilon_i}{kT}). \tag{A.5}$$

We let:

$$\frac{\epsilon - \epsilon_i}{kT} = y, \quad d\epsilon = kTdy \tag{A.6}$$

$$\epsilon = kTy + \epsilon_i. \tag{A.7}$$

The eigenvalue sum (A.5) becomes:

$$\begin{aligned}
&\Sigma_i \int_{-\infty}^{\frac{\epsilon_F - \epsilon_i}{kT}} Tdy(kTy + \epsilon_i)f'(y) \times (-\frac{1}{kT}) \\
&= -\frac{1}{kT}[kT\sum_i \epsilon_i \int_{-\infty}^{\frac{\epsilon_F - \epsilon_i}{T}} f'(y)dy + (kT)^2 \int_{-\infty}^{\frac{\epsilon_F - \epsilon_i}{kT}} dyyf'(y)] \\
&= -\sum_i \epsilon_i[f(\frac{\epsilon_F - \epsilon_i}{kT}) - 1] - kT\int_{-\infty}^{\frac{\epsilon_F - \epsilon_i}{kT}} dyyf'(y).
\end{aligned} \tag{A.8}$$

The first term in (A.8) is the total energy part of the eigenvalue sums and the second term is the entropy term of equation (5.15). This shows that the expression:

$$\sum_i \int_{-\infty}^{E_F} d\epsilon\epsilon g(\frac{\epsilon - \epsilon_i}{kT}), \tag{A.9}$$

gives the *free energy* of the eigenvalue sum, where

$$g(x) = -\frac{1}{kT} f'(x). \tag{A.10}$$

Therefore if the eigenvalue sums are evaluated using the DOS route, the overall contribution to equation (3.25) will be the free energy contribution, equation (5.17).

Appendix B

References

Anger G, Winkler A and Rendulic K D 1989 *Surface Science* **220** 1

Bachelet G B, Hamann D R and Schlüter 1982 *Phys. Rev. B* **26** 8 4199

Becke A D 1988 *Phys. Rev. A* **38** 3098

Berger H F, Leisch M, Winkler A and Rendulic K D 1990 *Chem. Phys. Lett* **175** 425

Bertel E and Lehmann J 1995 *Phys. Rev. B* **52** 384

Bertel E and Memmel N 1996 *Appl. Phys. A*

Bird D M and Gravil P A 1996 *Surface Science* **421** L121

Bird D M 1998 *Faraday Discuss.* **110** 335

Bonzel H P, Bradshaw A M and Ertl G 1989 *Physics and Chemistry of Alkali Metal Adsorption* (Elsevier)

Born M and Oppenheimer R 1927 *Ann. Phys.* **84** 457

Brivio G P and Trioni M I 1999 *Reviews of Moderm Physics* **71** 231

Brown J K, Luntz A C and Schultz P A 1991 *J. Chem. Phys.* **95** 3767

Ceperley D M and Alder B J 1980 *Phys. Rev. Lett.* **45** 566

Cohen M L and Heine V 1970 *Solid State Physics* Vol. 24 37

Darling G R and Holloway S 1995 *Rep. Prog. Phys.* **58** 1595

Davidson S G 1992 *Basic theory of Surface States* (Clarendon Press, Oxford)

Dreizler R M and Gross E K U 1990 *Density Functional Theory* (Springer - Verlag, Berlin)

Ertel G, Lee S B and Weiss M 1981 *Surface Science* **111** L711

Ewald P P 1917 *Ann. Phys.* **54** 519

Gillan M 1989 *Condens. Matter* **1** 689

Gross A, Wilke S and Scheffler M 1995 *Phys. Rev. Lett.* **75** 2718

Gülseren O, Bird D M and Humphreys S E 1998 *Surf.Sci.* **402** 827

Häkkinen H and Manninen M 1989 *Condens. Matter* **1** 9765

Hammer B, Jacobsen K W and Nørskov J K 1993 *Phys. Rev. Lett.* **70** 3971

Hammer B, Scheffler M, Jacobsen K W and Nørskov J K 1994 *Phys. Rev. Lett.* **73** 1400

Hammer B and Nørskov J K 1995 *Surface Science* **343** 211

Hammer B and Nørskov J K 1997 *Chemisorption and Reactivity on Supported Clusters and Thin Films* ed. Lambert R M and Pacchioni G, Dordrecht.

Harris J 1985 *Phys. Rev.* **31** 1770

Hayden B E and Lamont C L A 1991 *Faraday Diss. Chem. Soc.* **91** 415

Hoffman R 1988 *Rev. Mod. Phys.* Vol. 60 No. 3

Hohenberg P and Kohn W 1964 *Phys. Rev.* **136** B864

Ihm J 1988 *Rep. Prog. Phys.* **51** 105

Jacobsen K W, Nørskov J K and Puska M 1987 *Comments Condens. Matter Phys.* **14** 129

Jacobsen K W, Stoltze P and Nørskov J K 1996 *Surface Science* **366** 394

Johnson D D 1988 *Phys. Rev. B* **38** 12807

Kerker G P 1981 *Phys. Rev. B* **23** 3082

King D A and Woodruff D P 1993 *The Chemical Physics of Solid Surfaces* (Elsevier, Amsterdam)

Kinnersley A D, Darling G R, Holloway S and Hammer B 1996 *Surface Science* **364** 219

Kiskinova M P 1992 *Stud. Surf. Sci. Catal.* **70**

Kleinman L and Bylander D M 1982 *Phys. Rev. Lett.* **48** 1425

Kohn W and Sham L J 1965 *Phys. Rev.* **140** A1133

Li Z Y, Lamb R N, Allison W and Willis R F 1989 *Surface Science* **211** 931

Methfessel M 1995 *Phys. Rev. B* **52** 8074

Monkhorst H J and Pack J D 1976 *Phys. Rev. B* **13** 12 5188

Mortensen J J, Hammer B and Nørskov J K 1998 *Phys. Rev. B*

Neugebauer J and Scheffler M 1992 *Surface Science* **287** 572

Newns D M 1969 *Phys. Rev.* **178** 1123

Nørskov J K and Lang N D 1980 *Phys. Rev. B* B 21 2131

Padilla-Campos L, Toro-Labbé A and Maruani J 1997 *Surface Science* **385** 24

Parr R G and Yang W 1989 *Density-Functional Theory of Atoms and Molecules* (Oxford University Press, New York)

Passek F and Donath M 1993 *Phys. Rev. Lett* **71** 2122

Payne M C, Teter M P, Allan D C, Arias T A and Joannopoulos J D 1992 *Rev. Modern Physics* **64** 4 1045

Perdew J P and Zunger A 1981 *Phys. Rev. B* **23** 5048

Perdew J P, Chevary J A, Vosko S H, Jackson K A, Pederson M R, Singh D J and Fiolhais C 1992 *Phys. Rev B* **46** 6671

Perdew J P and Wang Y 1992 *Phys. Rev. B* B **45** 13244

Resch C, Zhukov V, Lugstein A, Berger H F, Winkler A and Rendulic K D 1993 *Chem. Phys.* **177** 421

Resch C, Berger H F, Rendulic K D and Bertel E 1994 *Surf.Sci.* **316** L1105

Rettner C T, Auerbach D J and Michelsen H A 1992 *Phys. Rev. Lett.* **68** 1164

Scheffler M and Stampfli C 1999 *Handbook of Surface Science* Vol 2: Electronic Structure

Schiff L I 1955 *Quantum Mechanics* (New York: McGraw-Hill)

Somorjai G A 1994 *Introduction to Surface Chemistry and Catalysis* (Wiley, New York)

Trouiller N and Martins J L 1991 *Phys. Rev. B* **43** 1993

Vosko S H, Wilk L and Nusair M 1980 *Can. J. Phys.* **58** 1200

White J A, Bird D M and Payne M C 1995 *Phys. Rev. B* **53** 1667

Wilke S and Scheffler M 1995 *Phys. Rev. B* **53** 4926

Wilke S and Scheffler M 1995 *Surface Science* **329** L605

Zangwill A 1988 *Physics at Surfaces* (Cambridge University Press)